Master's thesis

NTNU
Norwegian University of Science and Technology
Faculty of Natural Sciences
Department of Geography

Danielle A. M. Hallé

Predicting Runoff for a Drinking Water Catchment in Southwest Greenland

Master's thesis in Natural Resource Management, Geography

Supervisor: Irina Rogozhina, Signe H. Larsen and Andreas P. Ahlstrøm

May 2020

NTNU
Norwegian University of
Science and Technology

Abstract

As meltwater runoff increases from local glaciers and ice caps in Greenland, there is motivation to better quantify this runoff to improve the understanding and more accurately estimate its contribution to global sea level rise, dynamics of seawater freshening on ocean currents and gauging the potential for natural resource exploitation. Twelve percent of the world's glaciers and ice caps are contained around the periphery of Greenland and the vast majority lies in partially glaciated basins that are ungauged and without weather stations, thereby, resulting in a gap of available data required to calculate meltwater runoff in these catchment areas. This then leaves climate models as the key method to simulate and predict the amount of future runoff produced. Currently, calculating meltwater discharge with coarse resolution general circulation models or even regional climate models, does not completely capture the intricacies of the terrain in a partially glaciated basin and can create large potential for error. This study highlights these errors by presenting the strengths and shortcomings of several global and regional climate models on local scales on glacier catchments, with the aim to predict runoff more accurately. This evaluation has shown that none of the climate models adequately captures either spatial or temporal variability in air temperature and meltwater production. *Statistical* downscaling of climate grids, from 11 kms to 30 m, was applied as a tool to better resolve air temperature and precipitation in partially glaciated basins but was unable to counteract inaccuracies leaking from climate models into local estimates. The total monthly runoff was predicted, out to 2060, using a *positive degree day* model that focused on one drinking water catchment in Southwest Greenland, with a discharged peak in 2040. The catchment is therefore assessed as being able to provide a continuous source of drinking water for export throughout the next 40 years.

Abstrakt

Efterhånden som smeltevandsafstrømningen fra Grønlands gletsjere og iskapper stiger, er der et øget behov for at kvantificere denne afstrømning, for at forbedre forståelsen og give et mere nøjagtigt estimat af bidraget til den globale havniveaustigning, ændringer i havstrømme på grund af en faldende saltkoncentration og potentialet for udnyttelse af naturressourcer.
12 % af verdens gletsjere og iskapper findes langs Grønlands periferi, hvor langt størstedelen ligger i oplande med delvist isdække, uden målinger og vejrstationer til at kunne beregne smeltevandsafstrømningen. Klimamodeller har derfor en nøglerolle i at simulere og estimere mængden af smeltevand i fremtiden. Generelle cirkulationsmodeller og regionale klimamodeller har for lav opløsning til at fange terrænvariationerne i oplande med delvist isdække og kan resultere unøjagtigheder ved beregning af smeltevandsafstrømninger
Denne undersøgelse fremhæver disse unøjagtigheder ved at præsentere styrker og svagheder ved flere klimamodeller; undersøgelsen validerer regionale klimamodeller på lokal skala, for at opnå afstrømning af smeltevand i mindre afvandingsområder i Grønland. Statistisk nedskalering fra 11 km til 30 m blev anvendt som et værktøj til at forbedre opløsningen på lufttemperatur og nedbørsdata i oplande med delvist isdække. Den samlede månedlige afstrømning i et afvandingsområde, i Vestgrønland, blev forudsagt frem til 2060 ved hjælp af en positiv gradedagsmodel. Med en beregnet smeltevandsafstrømning, der topper i 2040, konkluderer denne undersøgelse, at mængden af smeltevand er tilstrækkelig til kommerciel udnyttelse i de næste 40 år.

Acknowledgements

I knew this was not going to be easy, but it would have been significantly more difficult had it not been for the support of the many people who helped me throughout this thesis. I want to personally thank several of them who patiently guided me through this process and who provided support that allowed me to produce the result reflected in this paper.

I would like to extend my deepest appreciation and thanks to my academic supervisor at NTNU, Dr. Irina Rogozhina, who provided me with the much-needed direction and insight during the many steps of this thesis. She was there to encourage me throughout my work, all while providing me with the much-needed humor interspersed between the more serious talks that focused on climate modeling, runoff, and glaciers. I will be forever grateful to her for everything she has done for me.

I cannot begin to express my thanks and gratitude to my supervisors at the Geological Survey of Denmark and Greenland, Dr. Andreas Peter Ahlstrøm and Dr. Signe Hillerup Larsen, who have given me the opportunity to work on these pertinent topics in advancing my understanding of the subject matter. Many thanks to Dr. Ahlstrøm for working with me in helping to develop the concepts of the project and providing me the opportunity of a lifetime to join the team on field work in Greenland, undoubtedly one of the most beautiful places on earth. Signe who also availed of her time assisting me with all my technical questions and played a huge part in developing the runoff modeling for this thesis.

I could not leave NTNU without giving a huge note of thanks to my classmates from the Natural Resource Management Program for providing the supportive and social environment that is necessary for any master student to grow, thrive and integrate into a unique academic community. I would also like to acknowledge and thank my father, Marcel Hallé, who sat down with me for hours virtually editing the contents of the thesis from the UK, where he would patiently listen as I explained all the natural science concepts that were, for the most part, foreign to him. Furthermore, I extend a big note of thanks to my mother, Elaine, my sister, Reneé and brother, Matthieu who all provided moral support throughout my thesis.

I am also grateful to my partner, Mikkel Baastrup Hovgaard, who assisted me with most of the technical aspects of programming, translation of the abstract and was always available for in depth discussions on this project.

Table of Contents

List of Figures

List of Tables

List of Equations

List of Abbreviations

AMOC	Atlantic Meridional Overturning Circulation
ArcGIS	Arc Geographic Information System
AWS	Automatic Weather Station
CEN	Centre d'Etudes de la Neige
CM	Climate Model
DEM	Digital Elevation Model
DMI	Danish Meteorological Institute
ECHAM	European Centre HAMburg
ECMWF	European Centre for Medium Range Weather Forecasts
ERA	ECMWF Re-Analysis
GCM	General Circulation Model
GC-NET	Greenland Climate NETwork
GEM	Greenland Ecosystem Monitoring
GEUS	Geological Survey of Denmark and Greenland
GIMP	Greenland Ice Mapping Project
GRIB	GRIdded Binary
GrIS	Greenland Ice Sheet
Gt	Gigatonne
HadGEM	Hadley Centre Global Environment Model version 2
HIRHAM	HIRLAM ECHAM
HIRLAM	High Resolution Limited Area Model
ICEsat	Ice, Cloud, and land Elevation Satellite
IMAU	Institute for Marine and Atmospheric Research
KNMI	Royal Netherlands Meteorological Institute
LGM	Last Glacial Maximum
LIA	Little Ice Age
m.a.s.l.	Meters above sea level
MAR	Modèle Atmospérique Régional
MATLAB	MATrix LABoratory
NetCDF	Network Common Data Form
PDD	Positive Degree Day
PGIC	Periphery Glacier and Ice Caps
PROMICE	Program for Monitoring of the Greenland Ice Sheet
RACMO	Regional Atmospheric Climate Model
$RACMO_H$	Regional Atmospheric Climate Model HadGEM
$RACMO_E$	Regional Atmospheric Climate Model ERA
RCM	Regional Climate Model
RGI	Randolph Glacier Inventory
RMSE	Root Mean Square Error
SEB	Surface Energy Balance
SISVAT	Soil Ice Snow Vegetation Atmosphere Transfer
SLR	Slope Lapse Rate
SMB	Surface Mass Balance
w.e.	water equivalent

1 Introduction

Glaciers are vital resources to many human populations across the planet. They provide a natural source of potable water, contribute to energy production, and provide tourism opportunities for many countries. As an example of their importance, in parts of South America, 50 % of the drinking water derives from glacial runoff (Oerlemans., 2010, pp.6). The economic and social benefits that accrue from glaciers have varied over time within countries that possess them. In the last few decades, advances in technology, coupled with the impact of a warming climate not only provide several opportunities for nations that have glaciers, but are cause for significant concerns for those lower laying ones threatened with territorial displacement due to the rise in sea level. In Greenland, it is becoming more frequent to see hydro plants being used to provide power to settlement communities, which are also dependent on glacial runoff as its source (Ahlstrøm et al., 2018). Although the main supply of drinking water in Greenland is from surface water, in other parts of the world, the runoff from glaciers is increasingly becoming an important resource. As a result, future opportunities exist for glacial runoff to be used in aid of those countries that are currently in need or those that could soon suffer from severe water shortages and/or a growing rate of water sources being polluted.

More pressingly, as global temperatures continue to rise, the world is likely to turn more of its attention towards Greenland. This unique continent contains one of the largest ice sheets in the world. It is abundant in natural resources and it has a stunning landscape with large open wilderness areas to enjoy. Of significance, the largest reserve of freshwater in the Northern Hemisphere is located here. Impressively, its holdings are equivalent to approximately seven meters in sea level rise (Ettema et al., 2010) and with its glaciers, ice caps and the ice sheet melting, the freshwater it will discharge could be made readily available as a common good. The ability to harvest this abundant source of potential freshwater for commercial means remains a question as to how glaciers and ice caps will continue to react in a changing climate. Of equal importance is understanding what a warming planet is doing to the melting of glaciers and ice caps and its follow-on effect to positive climate feedback loops, future weather patterns, sea level rise and the impact on marine ecosystems. An example is understanding the dynamics from seawater freshening on ocean currents and the strength of the thermohaline circulation.

From a scientific perspective, there has been a lack of observational data at the periphery of the Greenland continent in the mountain valley catchments. To that end, the challenge is to fully understand and to quantify the amount of runoff being produced from these specific catchment areas. The aim of this paper will be to study glacial runoff from small scale catchments that are of interest to both industry, in support of their efforts in assessing the commercial viability of exporting the freshwater being produced, while also contributing to the glaciological community's understanding of glacier dynamics at these smaller scale catchments situated within Greenland's Periphery Glaciers and Ice Caps (PGIC).

Where observational data has been absent, Regional Climate Models (RCM) are used as one of the primary tools for determining climate data. Over the years, these have become more reliable as their accuracy and precision improves. Previous studies have compared the data from various weather stations with that obtained through climate model outputs and have highlighted certain biases within the interannual cycle across the Greenland Ice Sheet (GrIS). When Box and Rinke compared the interannual variability, it was determined to be greater in the climate model than that of the observational data (Box and Rinke, 2003). Comparing climate model performance with observational data is an initial step to better understand how the models perform in the specific areas being studied. When calculating the performance of RCMs, correlation coefficients and the root mean square error (RMSE) are commonly used methods to evaluate them (Noel et al., 2019, Andersson and Erikson, 2018, Ettema et al., 2010).

In addition to RCMs, when assessing catchments, another pertinent necessity is the need for high resolution climate data, particularly in remote places. In compensating for the lack of high resolution data, downscaling of climate data outputs is a method that has been used for some time. There are several different downscaling methods to obtain the data to achieve the desired climate model resolution. Three downscaling methods that are used within the climatological-glaciological community are: (1) *statistical*, (2) *dynamical*, and (3) *hybrid* (Machguth et al., 2013, Jarosch et al., 2012). The simplest form of downscaling utilizes a fixed relationship between the coarser resolution of the climate model grids and subgrid surfaces, which are further described by higher resolution grids of elevation and topography (Fiddes and Gruber, 2014). This study uses a simple *statistical downscaling* method that requires the calculation of slope lapse rates as the transfer function between the two scales. The background on these downscaling techniques are further explained in Section 2.1.5. Regardless of the downscaling

method used, after producing a downscaled product, *surface mass balance* models can then be used to calculate the runoff of a specific glacier at the catchment scale.

There are several types of *surface mass balance* (SMB) models with the main categories falling under: (1) *surface energy balance (SEB),* and (2) *temperature index* modeling such as *positive degree day (PDD)*. In defining it, *SMB* is the overall sum of what is accumulated versus what is lost over a period (Hanna et al., 2011). Throughout the history of *SMB* modeling of glaciers, several schemes over the last century have been developed and tested, proving to be a valuable method when studying glaciers (Reeh., 1991, Arnold et al., 1996 Calov and Greve., 2005). Employing either of the two models comes with both benefits and limitations when simulating the *SMB*. These will be discussed in more detail later in the paper, but for the purposes of this study, the *PDD* model is used to calculate meltwater runoff using air temperature as the input parameter. Finsterwalder and Schunk first applied the concept of the *positive degree day model* in 1887. Over time, slight improvements and minor changes to the model have occurred, but overall, it has remained relatively unchanged.

1.1 Thesis Objective

As the overall mean temperature of the Earth continues to rise, the knock-on effects are elevated levels of greenhouse gases and an increasing rate at which glaciers and ice caps are melting (Edward et al., 2019). As a result, predicting runoff from catchments in Greenland is important in being able to estimate the effect that this will have on the planet and the well-being of its inhabitants. Obvious effects are the sea level rise and freshening of oceans from melting glaciers and ice caps, with global impacts on coastal lines, thermohaline circulation and marine ecosystems, to name but a few. To that end, the principle aim of my thesis is about better understanding climate dynamics that are necessary to predict meltwater runoff from small scale catchments in Greenland and to which extent these are captured by climate models used to make regional predictions of future climate conditions. In addition, aspects of this study are being done in collaboration with the Geological Survey of Denmark and Greenland (GEUS) who are investigating the natural resource potential from several small catchments for the purposes of determining the feasibility of exporting potable water. In support of their decision-making process, it will provide specific insight emanating from my work that will better inform the debate on the viability of exporting drinking water from this Arctic nation; a motivational aspect that has been a driver for me to undertake this work. The sub-objectives that underpin this study's main aim are:

- *How well do the climate models simulate climate in Greenland on local scales?*

- *Do regional climate models and their downscaled products replicate observations from weather stations more accurately than the output from coarse resolution global climate models?*

- *Is the selected drinking water site viable for a consistent long-term extraction of this resource?*

1.2 Problem Statement

The focus of this study is on Greenland's small catchments, including a catchment located in South West Greenland. The challenge is that these areas do not contain any observational data, ergo making climate models the main tool for providing climate data in these catchments. Given that the scale of these study sites is smaller than the typical size of grid cells in climate models, it is necessary to use downscaling methods to attain higher resolution of the climate variables and calculate glacial runoff from each catchment.

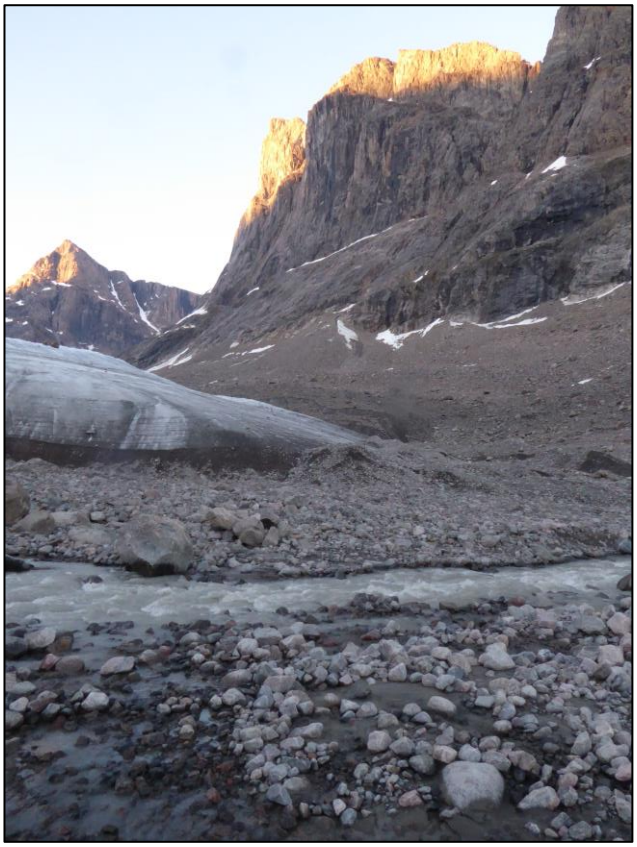

Figure 1: Picture from June 2019 at the drinking water catchments. Top photo (on previous page) is at the glacier tongue with melt water channel in the foreground. Bottom photo is the melt water channel flowing through the valley.

2 Background

This section introduces the importance of quantifying runoff in small glacial catchments. It will elaborate on previous work that has been done by other experts in this field. It will also describe the intricacies of the climate dynamics that exist within the valley system.

2.1 Periphery Glaciers and Ice Caps in Greenland

Glaciers and ice caps on the periphery (PGIC) of Greenland compromise less than 5 % of the area of the Greenland Ice Sheet (Bjørk et al., 2018) as shown at Figure 2. Of importance, in the first part of this century (2003-2008), PGIC accounted for 20 % of glacier loss in Greenland and the global rise in sea level (Bolch et al., 2013). The hypsometry, seasonal dynamics, and location of PGIC in Greenland make them more sensitive to atmospheric changes than that of the GrIS and marine terminating glaciers. In their work, Bjørk and others studied PGIC lengths for almost 350 Greenlandic glaciers from when the Little Ice Age (LIA) ended, 1890 on the West Coast and 1910 on the East Coast, until 2015. On the West Coast of Greenland, they discovered that the PGIC retreat rate was substantially greater (16.6 m yr^{-1}) over the last five decades as compared to the entirety of the time period covered by their study (Bjørk et al., 2018). Contrasting this to the East Coast of Greenland, in the same study, Bjork et al documented that a steady rate of warming had been observed from 1972 to 2012 that

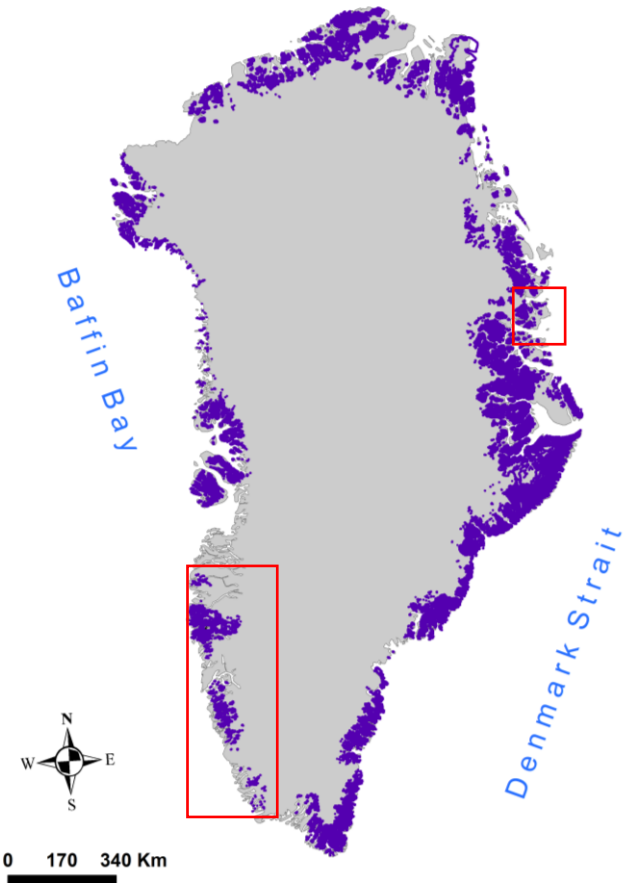

Figure 2: Location of periphery glaciers (in purple) in Greenland and the sites of the drinking water catchments in the SW and the observational validation study site in the NE at Zackenberg (in the red boxes).

reflected a constant PGIC retreat rate of 6.7 m yr^{-1}. The difference between east and west retreat rates is as a result of a higher snow accumulation rate in Eastern Greenland, which is an important factor that explains the reduced rate of change in the length of these glaciers. From a holistic perspective, again based on Bjork et al.'s study, the overall result concludes that all 350 PGICs studied had a greater rate of retreat over the last five decades. Of note, they determined that the rate of deglaciation on the East Coast over a 20-year period, centered on 1920, to be more severe than the other PGICs.

From a global perspective, Jacob and others (2012) looked at the individual mass loss of glaciers and ice caps (GIC) for all glaciated regions, except for Greenland and the Antarctic. Their study was unable to accurately capture the mass loss of ice from the PGIC in Greenland and Antarctic due to the low resolution of the Gravity Recovery and Climate Experiment (GRACE) satellite. This study went on to highlight the importance of sea level contribution from GICs over a seven-year period (2003 to 2010) that concluded a 0.41 +/-0.08 mm yr^{-1} increase in sea level rise, excluding the PGIC of Greenland and Antarctica (Jacob et al. 2012).

A different approach was used by Machguth and others to predict sea level rise emanating from PGIC in Greenland. By inputting the data obtained from three regional climate models through a simplified *surface energy balance* model, they ascertained the rise in sea level out to 2098. The data from the three RCM's used (HIRHAM, RACMO and MAR) produced the respective projections of 5.8, 7.4 and 11.2 mm when inputted into the *surface energy balance* model. Their study showed that the contribution from sea level rise from the north-east regions of Greenland would be less in contrast to the southern half of Greenland due to increase in precipitation rates and a more stable hypsometry (Machguth et al. 2013).
PGIC are an important contributor to global rise in sea level. Though the GrIS is extensively studied and as global warming is a significant potential source of sea level rise, it is somewhat surprising that the PGIC in Greenland have not had the same level of scientific attention. According to Abermann et al. (2019), only six out of the 20,300 PGICs are monitored in Greenland, of which three of them are located on the West Coast. From their study, it was reported that between 1985 and 2014, there was a volume loss of 25 % from mountain PGIC in the western part of Greenland (Abermann et al., 2019). As PGIC continue to retreat, it will be important to better understand their dynamics through a changing climate, so a more reliable means can be developed to project glacier losses into the future. This could be the continued development of models and monitoring networks, improving the use of existing

methods through novel approaches or a combination of both. The approach for my study will be to use differing methods, by utilizing existing climate and glacier models, with a focus on the lesser studied field of PGIC in Greenland.

2.1.1 Drinking Water Catchments

As mentioned earlier, this study is part of a collaborative effort with GEUS. The results of this work will inform them of the viability of sustainable drinking water sources for those catchments analyzed within this thesis. In fulfillment of this requirement, the location of the study areas was determined by GEUS. Of the several potential sites they have listed, the six selected are the ones that I assisted in the fieldwork conducted by GEUS, during the summer and fall of 2019. These six catchments were selected due to them being readily accessible, as well as, the abundance and quality of the water at the glacial runoff areas. Of the six catchments of interest, one was selected for further study and analysis in determining downscaled runoff.

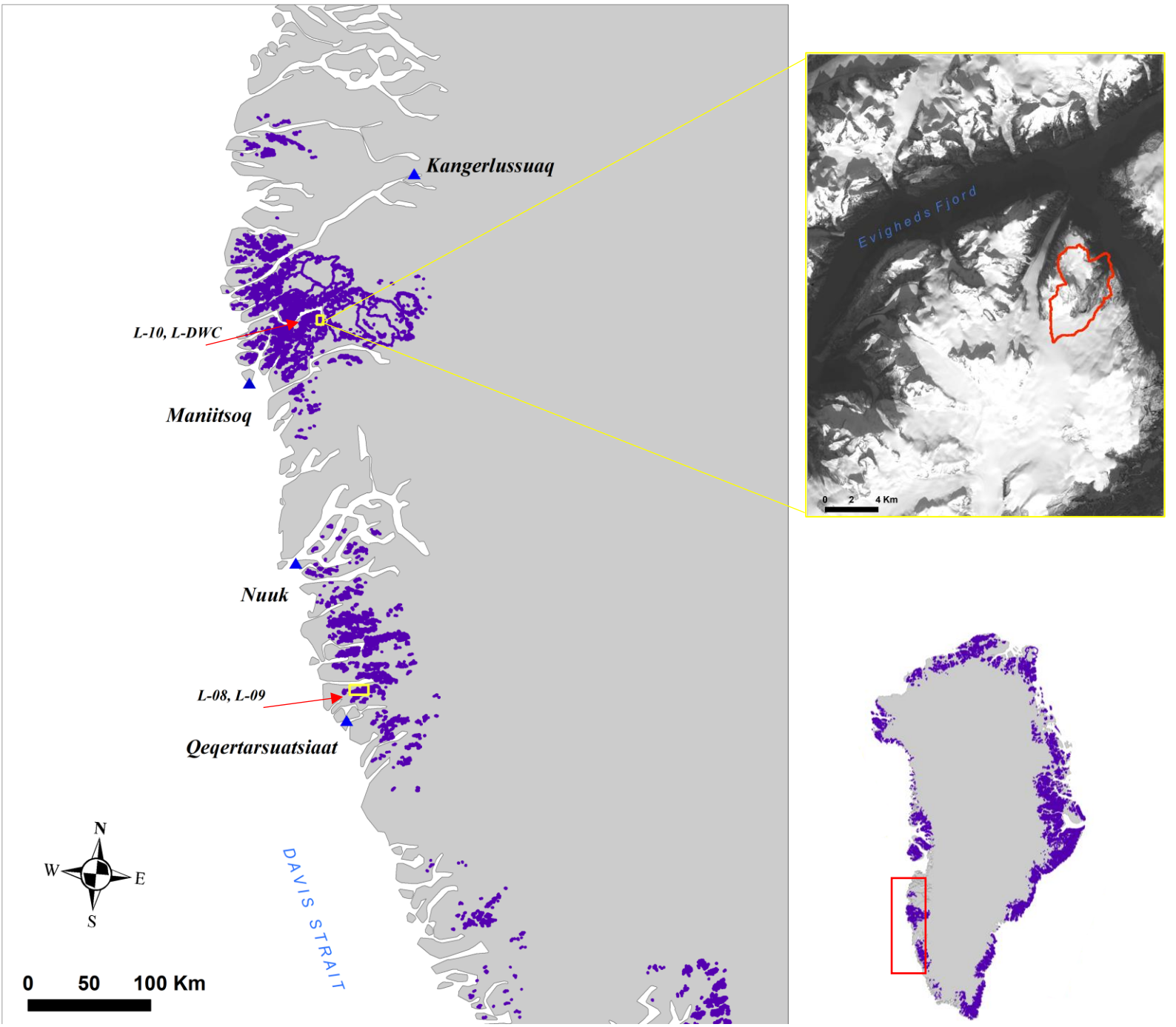

Figure 3: Southwest coast of Greenland place names and location of the drinking water catchments, where L-DWC is the catchment downscaled and modelled in this study. With an inset map of Greenland in the bottom right of the study area. Top right map shows the fjord system with the L-10 catchment outlined.

The drinking water catchment studied is in South West Greenland where the climate is low Arctic continental (Cappelen, 2019). The mean annual air temperature in these areas average -6 ^{o}C, with summer daytime temperatures periodically exceeding 15 ^{o}C. In the winter months, the temperatures can dip as low as -40 ^{o}C. The catchments are in maritime climates, close to the coastline and therefore, experience less fluctuation in temperature extremes and have typical precipitation rates of 300 to 400 mm yr^{-1}.

Of the six selected catchments by GEUS, three of them are found in Evighedsfjord, where L-10 is depicted in Figure 3 and the two other catchments are in proximity to L-10. They are situated approximately 50 kms north of Maniitsoq. These catchments are all partially glaciated and drain from a larger ice cap, noting that neither are connected to the GrIS. The other three catchments are located at L-08, L-09, and one other in the same region and situated approximately 40 kms north of Qeqertarsuatsiaat (Fiskenæsset). These last three catchments drain from local glaciers that are similarly disconnected from the GrIS. All six of these catchments are embedded within mountain valley systems and each grouping respectively drains into their deep fjord systems (Ahlstrøm et al., 2019).

Appreciating that there are several potential catchment areas that can be investigated for commercial means, for this study, showing the feasibility of the meltwater runoff modeling developed does not necessitate all catchment areas being calculated, but rather selecting only one to demonstrate its utility. The catchment area selected for this purpose is one located near L-10 and will be referred to as the drinking water catchment (L-DWC). Referring to it as location L-DWC is due to the commercial sensitivity of its position as well as the location of the other two undisclosed sites mentioned earlier.

2.1.2 Validation Site: Zackenberg

Zackenberg is in North Eastern Greenland and is host to the Zackenberg Research Station. This region is characterized as being a continental climate even though it is located near the coast. The nearby sea is frozen most of the year creating cold winters and generally dry conditions (Stendel et al., 2008). It is situated in a valley surrounded by relatively high mountains that creates a drainage basin for the surrounding glaciers and the A.P. Olsen Ice Cap. This well-known Ice Cap is the headwaters for the river basin which includes St. Sødal Valley, Lindeman Valley and Zackenberg Valley. The basin covers an area of approximately 514 km^2 where 106 km^2 of it is covered by glaciers and the A.P. Olsen Ice Cap. Again, none of these are connected to the GrIS. The annual mean air temperature for this area is -9 ^{o}C and

it is only in June, July, August, and September that the average monthly air temperature increases above 0 °C. Its mean annual precipitation is 211 mm yr^{-1}, which predominantly falls as snow during the eight to nine months of winter (Søndergaard et al., 2015). In the summer months, the slope lapse rate averages -0.5 °C/100m (Stendal et al., 2008).

Although the location of Zackenberg is at a considerable distance from the catchments of interest, this area was used as part of the validation process for the climate and glacier models used in this study as it is a partially glaciated catchment. In addition, it also benefits from having extensive monitoring programs, which makes the much-needed observational data available.

2.1.3 Climate in Greenland

It is well known that Greenland has seen an increased level of warming since the early 1990s. The increasing temperatures being experienced on this continent are attributed to *Arctic Amplification* (Stendel et al., 2008). This phenomenon results from an accelerated climate change induced warming in the Arctic that comes from a wavier jet stream caused by a reduced poleward temperature gradient (Ahlstrøm et al., 2017). In turn, this is coupled with the positive feedback cycle of snow-ice albedo. The obvious effect from rising temperatures is an increase in glacier runoff. As a follow on, this creates a densification of the firn layer (snow that is older than a year), thereby reducing the storage capacity of these layers, which contributes to increased meltwater production (van Angelen et al., 2013). The climate in South West Greenland is typically subjected to high atmospheric pressure, which in turn reduces the amount of cloud cover that enhances the absorption of solar radiation, with the effect being increased runoff. Conversely, in the northern part of Greenland, it has experienced significant mass loss of its glaciers since the 1990's, resulting in enhanced meltwater runoff. This is due to rising temperatures and increased cloud cover. This combination has led to an increased summertime rainfall of approximately 42 % (Noel et al., 2019). The climate in Eastern Greenland is colder compared to that of the western region for similar latitudes (Steffen and Box, 2001). Despite these similarities, it is considerably wetter than that experienced on the west side, with nearly 1000 mm/year of precipitation, mostly in the form of snow, on the south east coast (near Tasiilaq/Ammassalik) (Stendel et al., 2008).

2.1.4 Mountain Valley Microclimates

The climate where glaciers exist typically exhibit differences between those observed at a large atmospheric scale versus those mountain valley areas in proximity to coastlines. Conversely, these mountain valley areas are often referred to as microclimates and are also

more susceptible to inversions. Inversions occur when a warmer upper layer traps cold air underneath it (Zhang et al., 2011). The occurrence rate of inversions varies in the different coastal areas, but when they happen, it influences lapse rate calculations in the respective mountain valley systems. This is further discussed in the downscaling section that follows in Section 7.2.2.

In addition to the effect that inversions have on a glacier, other attributes such as varying slope lapse rates, the glacier's aspect and katabatic winds also have an impact on the climate of the glacier. The air temperature of the surrounding environment varies, whereas, the temperature at the surface of the glacier is for the most part fixed at 0 ^{o}C. However, this variation in air temperature is less so in the winter months because the surrounding environment is covered in snow. Valley winds are generated at the lower end of the glacier and flow upwards driven by the vertical differences in temperature. This then creates a mixing of the warmer and cooler air masses in the valley. Over the glacier's surface, the cooler air creates a downward katabatic wind that causes turbulence to occur, which impacts the exchange of mass and energy from the atmosphere to the glacier. Oelermanns' observations noted these winds to be shallow and can be as much as 20 m above the glacier's surface (Oelermanns., 2010, p.20).

2.1.5 Downscaling Background

As part of the background, the theory behind the two general downscaling categories, nested models, and empirical approaches (Raju and Kumar, 2018), will be explained. In comparing the two types, the nested models apply a more process-based technique, whereas the empirical approach uses a transfer function between the two scales (Hewitson and Craine, 1996). From these two categories emerge three different types of downscaling methods: (1) dynamical, (2) hybrid and (3) statistical. Other downscaling methods, such as weather generators and weather typing, are used when long term observation data exists, which is not the case for this study; ergo, these methods were not factored into the assessment.

2.1.6 Dynamical Downscaling

The first of the three methods to be discussed is d*ynamical* downscaling which comes from *nested* models. This downscaling method is typically how regional climate models are produced from GCM, where the RCM is *nested* within the GCM. The RCM is integrated into the GCM along the boundaries at each time step and at each vertical profile. The RCM then simulates the atmospheric conditions within the boundaries resulting in a process that can replicate the important synoptic and mesoscale atmospheric circulations that captures the

features of the region. Although RCMs improve the output of the GCMs, in areas with more complex terrain, the dynamical method can bring with it the biases and internal errors of the GCM used. Flowing from this, the RCMs will also reflect the errors inherent in the GCMs climate simulation (Hostetler et al., 2011). Of note, the complexity in producing nested models and the high computational processing subsequently required (Raju and Kumar, 2018) were limiters.

2.1.7 Hybrid Downscaling

The *hybrid* method uses both the *statistical* and *dynamical* downscaling methods and according to Jarosch et al. (2010) is computationally a more efficient approach. A study by Jarosch et al. (2010) describes the benefits of using the *hybrid* method which was used to model glacier dynamics with high resolution air temperature and precipitation data. They set out to create a method that established four criteria: (1) a method that captures climate variations and patterns that replicate alpine glacier climate, (2) it must work in an area without in situ data, (3) it must perform well with little or no calibration, and (4) it must be computationally efficient. In adhering to these criteria, the result obtained is a method that sits between *dynamical* and *statistical* downscaling methods. It uses a linear model of orographic precipitation to simulate the saturated air that is driven by prevailing winds when approaching mountain slopes. It uses Fourier transform for the wave numbers of the topography and air parcels that downscale the precipitation to the high resolution 90 m digital elevation model (DEM). The air temperature downscaling is an extension of previous studies that have applied similar methods to modeling alpine snowpack (Durand et al., 1993) and the mass balance of individual glaciers (Rasmussen and Conway, 2001). In their study, they use a piecewise function that is linearly fit to the vertical air temperature column. The use of this function makes it possible to identify inversions that can often occur from Arctic air masses in winter or inversions that can occur during the nights in summer. Although this approach would have been ideal to use for this thesis, based on its criteria, the complexity required in building a Fourier transformational model was beyond the capability and timeframe to develop for this thesis.

2.1.8 *Statistical* Downscaling

Statistical downscaling, an *empirical* approach, is a simple method for resolving air temperature data at finer spatial resolutions. Methods for *statistical* downscaling involve using a transfer function between the predictor and predictand (Raju and Kumar, 2018). An example of this would be the *empirical* relationship between air temperature and elevation

calculated to downscale air temperature. A study by Machguth et al. (2013) used a downscaling procedure based on the *statistical* downscaling method. Their approach applied a two-step process. The first step consisted of interpolating the climate model topography grids to the resolution of the DEM by inverse distance weighting, followed by making adjustments to the air temperature relative to the elevation of the DEM using a lapse rate that was derived by the parameterization work done by Fausto et al. (2009). This was also the same method that they used for precipitation.

The *statistical* method was the one selected for this thesis, as it represented the most feasible approach for the scope and format of the present study. In particular, the way it effectively downscales for air temperature at given elevations, which is a pertinent aspect of my work. Of note, it follows a similar process, the exception being that the SLR is derived from AWS data by way of PROMICE and GC-NET for the nine respective regions in Greenland, as opposed to the parameterization used by Machguth et al. (2013).

3 Methods

There are different methods that exist for assessing glacial melt. As each method varies, the challenge is to select the ones that best fits the specific research being done and available data. The description of the methods used in this paper are divided into four sections: (1) the datasets in Section 3.1 to 3.3, (2) comparing climate models to AWS in Section 3.4, (3) downscaling in Section 3.5 and (4) *positive degree day* modeling in Section 3.6. This chapter begins with describing the spatial datasets in Section 3.1 to 3.3 that provides information on all the data used for the methods. This is followed by the weather station datasets in Section 3.4 that will compare climate data obtained by automatic weather stations and those generated by the climate model, assessing the differences in performance between them. Section 3.5 describes the method and workflow for downscaling the climate model dataset selected from the previous section. The last section, Section 3.6 on *positive degree day* modeling, goes on to describe both the melt modeling process and the parameters that are required as inputs.

3.1 Spatial Datasets

3.1.1 Ice Mask from Randolph Glacier Inventory

Glacier outlines from the Randolph Glacier Inventory (RGI) were used as binary ice masks formulating the inputs for the *positive degree day* model. This model distinguishes ice from bare ground within the catchments. The RGI is a collection of outlines across the globe, noting that they exclude the Greenland and Antarctica ice sheets. Several institutions worked together to produce these outlines through various satellite imagery acquired from 1999 onward. RGI uses semi-autonomous or autonomous routines to map the glaciers from satellite imagery based on the distinctive spectral reflectance signatures of snow and ice (Pfeffer et al., 2014).

3.1.2 Catchment Shapefiles

The catchment Shapefiles outline the area where the surface water drains. Dr. Ken Mankoff, from GEUS, produced Shapefiles for these catchment areas. As these Shapefiles are still under consideration for commercial licensing, they cannot be disclosed to the public at this time. These files were imported into ArcGIS and rectangle polygons were drawn around the catchments and exported as a raster for easier manipulation in MATLAB. The catchment

rasters are used as binary masks to indicate whether the climate model cell is located within the catchments.

3.1.3 GIMP 30m DEM

The Greenland Ice Mapping Project (GIMP) produced a 30 m resolution digital elevation model that is used for the downscaling aspect in this thesis. The GIMP DEM is created from two satellite image series, Landsat-7, and RADARSAT-1, with imagery acquired for the time period between 1999 to 2002. It covers the entirety of Greenland. The DEM is projected in polar stereographic, positioned over Greenland. It is centered at 90◦ N, 45◦ W and referenced to the WGS84 ellipsoid (Howat et al. 2014). The GIMP DEM was clipped specifically to study area catchments in ArcGIS using the clip tool. The tiles 1.1 and 1.2 were downloaded for the South West Greenland study area, while tiles 4.3 and 5.3 were downloaded for the Zackenberg area in North East Greenland. These tiles were downloaded from the National Snow and Ice Data Center (NSIDC) from the following link: https://nsidc.org/data/nsidc-0645/versions/1.

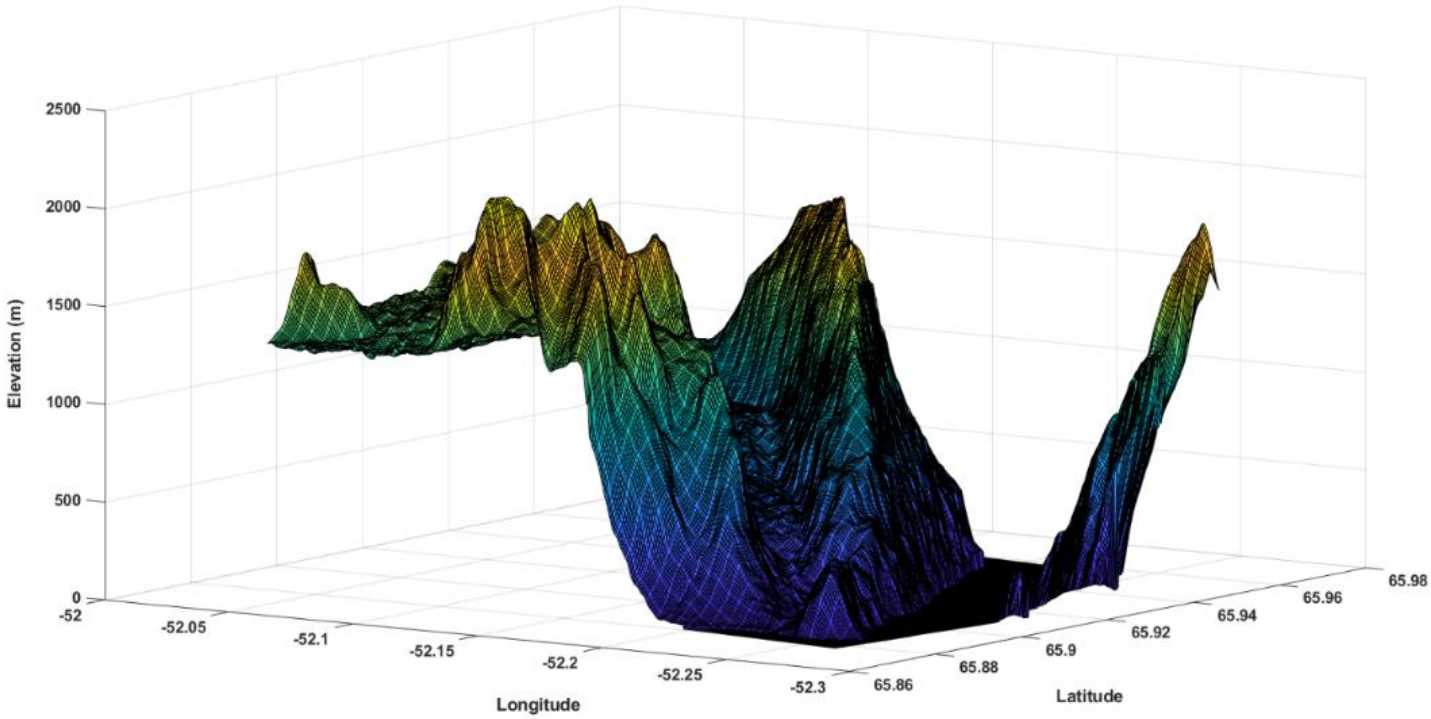

Figure 4: Digital elevation model from GIMP DEM for the L-DWC catchment

3.2 Weather Station Datasets

3.2.1 PROMICE

The Program for Monitoring of the Greenland Ice Sheet (PROMICE) is an ongoing program for monitoring the health of the GrIS. It was installed in 2007 with five pairs of Automatic Weather Stations (AWS), which has since been increased to seven pairs in 2010. They are all currently in operation. One of the weather station pairs is in the accumulation zone of the ice sheet and situated at a higher elevation, whereas, the second one is placed in the ablation zone. Each AWS is configured to take samples every 10 minutes that measure several parameters. The ones required for this study are air temperature (ºC), where the measurement height is positioned approximately 0.1 m or 2.6 m above the bare ice surfaces and air pressure (hPa). The full list of AWS measurements being used for this study can be found in Table 1. Of note, the mean monthly air temperatures are calculated from daily averages (van As et al. 2011). The other variables that are captured by the PROMICE program are: humidity, wind speed, wind direction, sensible heat flux, latent heat flux, shortwave radiation, and long wave radiation.

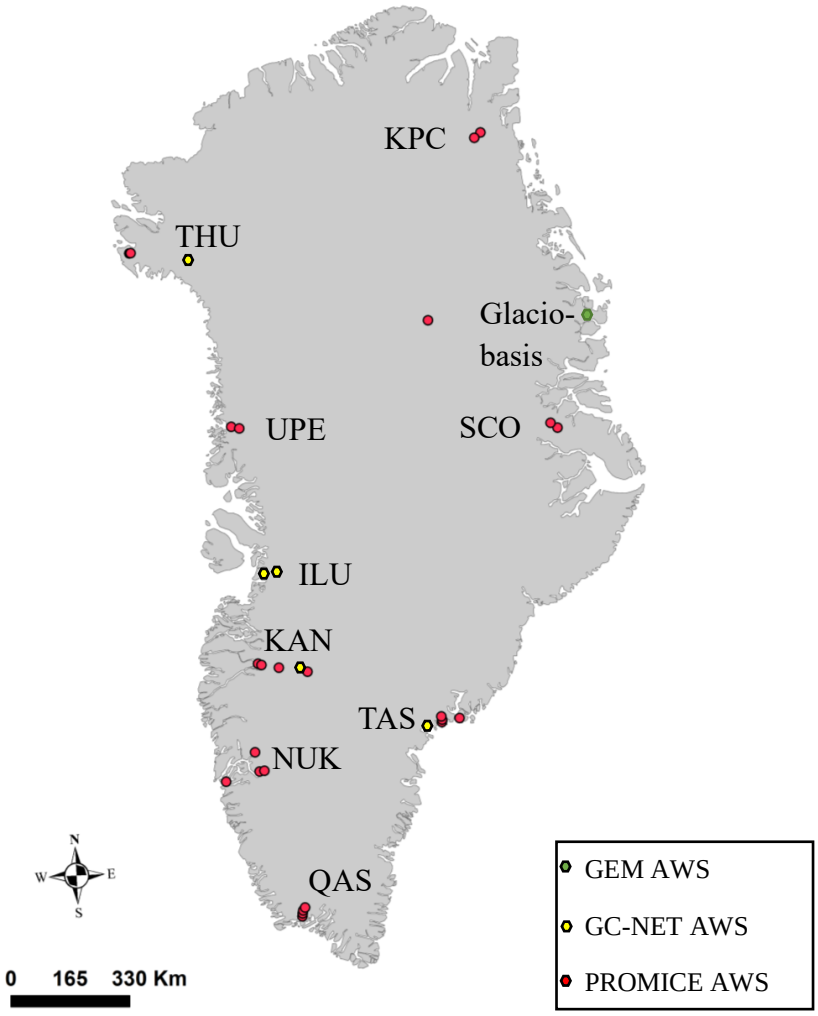

Figure 5: Map of locations of all AWS used in the study for slope lapse rate calculation, and the PROMICE AWS used for the climate model evaluation.

3.2.2 GC-NET

The Greenland Climate Network (GC-NET) was established in 1995 and currently has 18 weather stations distributed across the Greenland ice sheet. These weather stations measure

daily, annual and interannual variability. They are set up to record accumulation rate, surface-climatology, and surface

energy balance to monitor the state of the GrIS. Most of the AWS are located near the 2000 m elevation line in the accumulation zone. The lowest station, JAR2, is located at 568 m above sea level and the highest one is located at Summit station at 3254 m above sea level. Hourly average data is transmitted from the weather stations via a satellite link throughout the year (Steffen et al. 1996). Daily air temperature data for this study was downloaded from the webpage (http://cires1.colorado.edu/steffen/gcnet/) for all stations and this data was then averaged to monthly mean temperatures in MATLAB. GC-NET also captures the following weather variables: wind speed, wind direction, humidity, pressure, surface radiation, sensible and latent heat fluxes, and accumulation rates.

Table 1: List of AWS used and associated periods.

Dataset	AWS	Time Period
PROMICE	KAN_B	2011-2018
	KAN_L	2011-2018
	KAN_M	2011-2018
	KAN_U	2011-2018
	NUK_K	2010-2018
	NUK_L	2015-2018
	NUK_N	2010-2018
	NUK_U	2010-2018
	QAS_A	2016-2018
	QAS_L	2016-2018
	QAS_M	2016-2018
	QAS_U	2016-2018
	UPE_L	2009-2018
	UPE_U	2009-2018
	KPC_L	2009-2018
	KPC_U	2009-2018
	SCO_L	2008-2018
	SCO_U	2008-2018
	TAS_A	2015-2018
	TAS_L	2009-2018
	TAS_U	2009-2015
	MIT	2009-2018
	THU_L	2010-2018
	THU_U	2010-2018
	UPE_L	2009-2018
	UPE_U	2009-2018
GC-NET	01_Swiss_Camp	1996-2018
	04_GITS	2001-2019
	08_DYE2	1996-2018
	09_JAR1	1997-2018
	17_JAR2	1999-2013
	19_JAR3	2000-2004
GEM	GlacioBasis	2008 - 2017

3.2.3 GEM

The Greenland Ecosystem Monitoring (GEM) program is a long-term monitoring program operated by several research institutes in Greenland and Denmark. It consists of five coordinated groups; ClimateBasis, GeoBasis, BioBasis, MarineBasis and GlacioBasis, that are positioned to monitor across three locations in Greenland in the following places: Nuuk; Disko Bay; and Zackenberg. This study uses the data captured by the GlacioBasis program in Zackenberg and it consists of three climate stations that are run by Asiaq – Greenland Survey (Abermann et al. 2019). Hourly air temperature and precipitation data were downloaded and are available for the time between 1995-08-17 to 2017-12-31. This data can be downloaded from the g-e-m.dk webpage.

3.3 Climate models

Climate models can vary from each other with variations from how they are programmed and the different forcings used for each from these for these models. Germane for this paper is the requirement to evaluate how these various models perform in the Greenland environment. Regional climate models are preferred as they produce higher

resolution data, but often the results obtained cause greater uncertainty since these types of models need to be forced at the boundaries by using general circulation models (GCM). The two GCMs, HADGEM and ECHAM, are evaluated in the sections that follow. These two models are used to force the regional climate models (RCM) at the boundaries. This is of importance for this study, as it investigates the periphery glaciers; it is often in these boundary areas where the models tend to lack in performance. When near the boundary regions, these models are more sensitive to inputs than what is typically the case for inland regions.

All outputs from these climate models are downloaded in NetCDF format to obtain the parameters of air temperature and precipitation. The reference to the specific downloadable link is found in each respective section and further detail of the models used are described below.

3.3.1 General Circulation Models (GCMs)

3.3.2 HadGEM

The Hadley Centre Global Environment Model version 2 (HadGEM) general circulation model is a configuration of the Met Office Unified Model stemming from a family of models that address the uncertainty in projections of the climate system. This model includes projections of the atmosphere, ocean and sea-ice models to a well-resolved stratosphere, and Earth System components that include the terrestrial, ocean carbon cycle and atmospheric chemistry. The Met Office Unified Model seeks to address the Earth system feedback in the climate system and the necessity of including such feedback to predict future climate change. (Bellouin et al., 2011). The physical model configuration is derived from the HadGEM1 climate model and has an atmospheric horizontal resolution of 1.25 x 1.875 in latitude and longitude with 38 layers in the vertical, extending to over 39 km in height (Collins et al., 2011). Several experiments were run for the HadGEM model with different projections that predicts future climate. This project uses air temperature and precipitation outputs from representative concentration pathway (RCP) 4.5 which has a monthly time step and ranges from 2005 to 2098. HadGEM was accessed from the World Data Center for Climate (WDC), a webpage by DKRZ (Deutsches Klimarechenzentrum) using the link https://cera-www.dkrz.de/WDCC/.

3.3.3 ECHAM

The European Centre HAMburg (ECHAM) is a fifth generation of the general circulation model and will be evaluated for its performance in Greenland. The model was developed at the Max Planck Institute for Meteorology and built on the European Centre for Medium

Range Weather Forecasts (ECMWF) physics package (Roeckner et al., 2003). The latest version of this model shows improvements for land surface processes and datasets. Surface processes include land surface air temperature, water budget, lake model, sea ice, surface, and albedo. These are coupled to a mixed layer ocean. Monthly air temperature and precipitation were downloaded from https://cera-www.dkrz.de/WDCC as GRIdded Binary (GRIB) files. The temporal coverage of the model is from 800-01-01 to 2100-12-31, noting that only the time from 2005 to 2019 was evaluated in this thesis.

3.3.4 Regional Climate Models (RCMs)

3.3.5 RACMO

The Regional Atmospheric Climate Model (RACMO2.1) is a regional climate model that was developed in the early 1990s at the Royal Netherlands Meteorological Institute (KNMI); it was developed in cooperation with the Danish Meteorological Institute (DMI). This model is based on the High-Resolution Limited Area Model (HIRLAM) numerical weather prediction model. As of 1993, the Institute for Marine and Atmospheric Research Utrecht (IMAU) modified the RACMO model so that it could better model the climate over extreme conditions, such as over glacier surfaces. RACMO2.1 combines HIRLAM with the European Centre for Medium-range Weather Forecasts' (ECMWF) developed integrated forecast system (IFS); this regional climate model has been effectively applied to both the Greenland and Antarctic Ice Sheets. The grid distances are defined in fraction of degrees and they do not have a polar stereographic projection plane. Since RACMO is a regional model, it requires forcing at the boundaries. In this study, two versions of RACMO are used. The first version is RACMO2.1 *GRIS/FUT.* This version is forced by HadGEM2-ES under the RCP 4.5 and spans the time from 1971 to 2100, however, only the period 2005 to 2100 is used in this thesis. It has a spatial resolution of 11 km, 306x312, at 40 levels (van Angelen et al., 2013, Noel et al., 2015). For the remainder of the thesis, this dataset will be referred to as $RACMO_H$. The second version is RACMO2.3p2 *GRIS11/3.* It was used for the observation period to validate the model. It has a spatial resolution of 1km and a temporal resolution of 1958-2019 at daily time steps. The 1 km resolution of RACMO2.3p2 was *statistically* downscaled for all components of the surface mass balance and reflected good agreement with in-situ observations. The model is forced by ECMWF Re-Analysis (ERA- 40) (1958-1978) and ERA-Interim (1979-2019), which are both climate reanalysis models (Noel et al., 2019). This is discussed further in the climate reanalysis section below in 3.3.6 and it will be

referred to as $RACMO_E$ for the remainder of the thesis. The data from IMAU was sent by the author on request.

3.3.6 Climate Reanalysis

ERA-Interim is a climate reanalysis model and is different from the conventional climate models described above, as it gives a numerical description of the recent climate using both model and observational data. Therefore, its use is only available if observational data exists, noting it cannot be used to calculate future projection. Climate reanalysis models are useful for creating continuous climate observations for areas without weather stations and are used as the validation dataset to compare runoff values and to show any improvements within the downscaling process.

3.3.7 MAR

The Modèle Atmosphérique Régional (MAR) model is developed by Xavier Fettweis at the University of Liège in Belgium and is used to simulate climate over the Greenland and Antarctic Ice Sheet. For projections of the future climate in Greenland, MAR is coupled to a 1-D surface vegetation atmosphere transfer scheme Soil Ice Snow Vegetation Atmosphere Transfer (SISVAT). With the snow-ice part of SISVAT, based on the Centre d'Etudes de la Neige (CEN) snow model called CROCUS, it is a one-dimensional multi-layered energy balance model that determines the exchange between the sea ice, the ice sheet surface, the snow-covered tundra and the atmosphere. Several simulations are run with MAR for future projections, but this study uses the outputs at 25km resolution that is forced by HadGEM2-ES RCP 8.5. This corresponds to a high-end scenario with a radiation forcing of $> +8.5$ Wm -2 by 2100 with a greenhouse gas concentration that is projected to occur by the end of this century to a level of > 1370 CO2 equivalent p.p.m. Results of this simulation are assessed as being a considerable overestimation of snowfall and water run-off due to the GCM being too warm at the 700 hPa in summer (Fettweis et al., 2016). The outputs from the MAR model runs were downloaded from http://climato.ulg.ac.be/cms/index.php?climato=en_dr-xavier-fettweis under the heading 'MAR outputs for ISMIP6'.

3.3.8 HIRHAM

HIRLAM ECHAM (HIRHAM) is a state-of-the-art regional climate model developed at the Danish Meteorological Institute (DMI) and is based on a subset of HIRLAM and ECHAM models. The latest version of HIRHAM5 has been updated with the completely new version of ECHAM5. It has been re-written in Fortran 90/95 and its physical parametrizations have

changed within HIRHAM5 (Christensen et al. 2007). HIRHAM has been applied to a wide range of Arctic climate studies (Rinke et al., 2008, Langen, et al. 2017, Vandecrux at el. 2018), the spatial resolution of the model is 0.5^{o} and projected on a rotated-pole grid corresponding roughly to 25 km. The atmosphere has thirty-one vertical layers (Box and Rinke, 2003). The version of HIRHAM used in the thesis is forced by ERA-interim data. Mean monthly temperature data was downloaded over the time period of 1980 to 2014 from http://prudence.dmi.dk.

3.4 Comparing climate model data to observations

All climate model datasets are loaded into MATLAB using the `ncread` function and each variable was extracted from the Network Common Data Form (NetCDF) files (temperature/precipitation, longitude, latitude, and time). The temperature variable was often in a 4-dimensional array with height or pressure making up the 4th dimension. The pressure level was selected to match those of the AWS and the remaining temperature variable was compressed to a 3-dimensional array using `squeeze`. The time dimension from each climate model was in different formats and required it to be converted to a common time unit. For instance, the HadGEM climate model's time unit was reported in days since 1859-12-01 and was converted to MATLABs `datetime` function. The function `datetime` stores points in time as arrays and can account for time zones, daylight savings and leap seconds. All climate model and AWS data are converted to `datetime` for easier interpretation of the time. PROMICE, GEM and GCNET AWS climate data is stored as text files for each station and was imported into MATLAB using `readtable`.

Once MATLAB has processed all the climate data, the graph from it can be evaluated against the observed AWS data. From this, a distance matrix was created to locate the climate model cell centers that are closest to each AWS (Equation. 1). The distance matrix was created by subtracting the AWS coordinates from those of the climate model and taking the square root of the squared differences:

Equation 1: Distance Between AWS Point and Climate Model Grid

$$distance = \sqrt{(lat_{cm} - lat_{aws})^2 + (lon_{cm} - lon_{aws})^2}$$

The index of the minimum distance was found and used to index back into the original coordinate matrix of the climate model. The results of this procedure are then plotted on the

same line graphs for each AWS for further analysis. The details of this will be presented later in the results section.

3.4.1 Statistical Test

To evaluate the models a statistical test was applied on the climate model datasets against the AWS data. The root mean square error (RMSE) is used to measure the difference between values, it is calculated as the standard deviation of the residuals (prediction errors). Where residuals are a measure of the spread from the regression line between the two datasets (Rogerson, 2006). The RMSE is calculated in MATLAB by taking the square root of the mean of the differences between the climate data values and raised to the exponent of 2:

```
RMSE_CM(m,1) = sqrt(nanmean((CM_temperature - AWS_temperature).^2));
```

3.5 Downscaling of Climate Model Data

The following section describes the process of downscaling the outputs from the CM datasets. Both air temperature and precipitation are downscaled using a simple *statistical* downscaling method where the CM data is resampled to higher resolution and corrected for changes in elevation.

3.5.1 Lapse Rate Calculations

The first aspect of the downscaling process is to calculate the slope lapse rate (SLR) from the AWS data. The SLR is the calculation of the change in air temperature with elevation. The calculation of the SLR was based on each set of the AWS in Greenland that were situated closest to the coast and had one or more weather station pairs. In MATLAB, vectors of all the elevations at each of the AWS were created, as well as vectors for all the air temperature data from these AWS for overlapping time periods. The SLR is calculated for all July time periods, as it is the most representative of the melt period in Greenland and has the highest values of SLR throughout the annual cycle (Gardner et al., 2009). The functions `polyfit` and `polyval` are used to fit the data to a polynomial curve, while `polyval` evaluates the polynomial at each point within the AWS data. The slope is then calculated from the relationship between the air temperature from each AWS and elevation. The results of the SLR calculations are presented in Table 3 and discussed later in Section 7.2.2 to show how SLR differs across Greenland. The SLR for precipitation was also calculated, but only in the

area that was downscaled, and it used the same method to calculate the SLR for air temperature.

3.6 Method for Downscaling Climate Model Data

This study uses a *statistical* downscaling method that encompasses the topography variables to adjust climate model outputs. Furthermore, since the study areas are in particularly mountainous terrain, this means that elevation becomes one of the main factors that controls air temperature and precipitation. The goal of downscaling is to have climate model data that is at a higher resolution than its original output. As a result, the climate model data from $RACMO_H$ was downscaled from 11 km to 30 m resolution. The final resolution can be as high as the finest resolution DEM available. The downscaling process was conducted in MATLAB. After several failed attempts in Arc Geographic Information System (ArcGIS), where the workflow was too user intensive, it ended up taking several hours to complete the whole downscaling process. The total time for the script to run in MATLAB was approximately eight seconds. The climate model temperature/precipitation data, climate model topography data and the GIMP DEM are the only inputs required for this downscaling process. The climate model (CM) data is then clipped to the size of the DEM by finding its corner coordinates. The DEM coordinates are then used to find the nearest neighbor of the CM points that would be encompassed by the DEM. The CM data is resampled using nearest neighbor interpolation to create a matrix of climate data with 30 m spacing. The same process is done for the CM topography and it is resampled to the DEM resolution through nearest neighbor interpolation. The resampled CM topography is then subtracted from the DEM and multiplied by the SLR for the area and then added to the resampled CM data. This last step is summarized in the following line in MATLAB:

```
Downscaled = (dem – CM_dem) * SLR + CM_temperature;
```

This process was successfully repeated for all downscaled datasets in the two study areas.

3.7 Method for *Positive Degree Day* (*PDD*) Model

The *positive degree day* model was specifically developed for this study. It was written in MATLAB to simulate the melt from days with above zero temperature. The *PDD* sum was first tested and validated with in-situ data from the Zackenberg area in North Eastern

Greenland, as it is the one location in Greenland with long term climate data that can be used to validate the model. Two methods of calculating the *PDD* sum were also incorporated to test how they compare with observational data. The first of the three methods is the baseline; it is a simple method. This method sums the positive air temperature ($T\,°C$) hourly (h) data for each month and multiplies it by the amount of days in the month (t) and then averages it over the year, as depicted in Equation 2:

Equation 2: *Positive Degree Day* Calculation (Method 1)

$$PDD_{simple} = \left(mean(T_h)\right) t$$

The second method, proposed by Reeh (1991) and later modified by Ahlstrøm (1999), calculates the *PDD* sum from the normal probability distribution around the long term monthly mean temperatures where the annual temperature cycle follows a cosine function, where *TMA* and *TMJ* are the long-term annual mean and mean July air temperatures, respectively, and *A* represents one, for one year. This is shown in Equation 3:

Equation 3: Annual Temperature Cycle

$$TCA = TMA + (TMJ - TMA)\cos\left(\frac{2\pi}{A}\right)$$

Now determined, the *TCA* value is then used in the *PDD* equation to determine the contribution of the annual degree days from the integration of temperature and time over a one-year cycle, as per the following at Equation 4:

Equation 4: *Positive Degree Day* Calculation (Method 2)

$$PDD = \frac{1}{\sigma\sqrt{2\pi}} \int_0^A \int_0^{TCA+2.5\sigma} T \exp\left[\frac{-(T - TCA)^2}{2\sigma^2}\right] dT\, dt$$

Of note, the improvements to the PDD sum equation made by Ahlstrøm (1999) was to adjust the temperature integral, where it goes from 0 to TCA+2.5 standard deviations (σ). His change results in a 99% confidence interval from the normal distribution curve over an annual cycle.

The third and last method uses the semi analytical solution proposed by Calov and Greve (2005). Their method improves the accuracy and processing time when calculating *PDD* sums. Calov and Greve's method removes the need for double integration over temperature

and instead uses a Gaussian distribution for the error function to simulate the probability of temperature around the monthly mean. This is depicted in Equation 5, where T_{ac} is the monthly temperature in °C. The error function, *erfc*, is derived from Equation 6 below and is a built-in function within MATLAB (`erfc`):

Equation 5: *Positive Degree Day* Calculation (Method 3)

$$PDD = \int_0^A \left[\frac{\sigma}{\sqrt{2\pi}}\exp\left(-\frac{T_{ac}^2}{2\sigma^2}\right) + \frac{T_{ac}}{2} erfc\left(-\frac{T_{ac}}{\sqrt{2\sigma}}\right)\right] dt$$

Equation 6: Error Function

$$erfc(x) = 1 - \text{erf}(x) = \frac{2}{\sqrt{\pi}}\int_x^{\infty} \exp(-x^{\sim 2})\, dx$$

The inputs for all *PDD* sum methods are derived from *statistically* downscaled air temperature and a calculated standard deviation; the standard deviation is calculated from observational data. The standard deviation value of 2.5 °C was calculated from observational air temperature data at the KAN AWS site, given its proximity to the location at L-DWC.

3.7.1 Melt Model

The inputs for the melt model are the *PDD* sums, air temperature (°C), precipitation (mm) and an ice and basin mask for the catchment. The melt aspect of the model goes through each month of the year (see Figure 6) and checks to determine if the monthly sum of the *PDD* is above 0. Then it checks to verify if the surface is located over ice or bare ground. Leveraging the work of Janssen and Huybrechts (2000), the melt factors of 2.7 °C mm yr^{-1} for snow and 7.2 °C mm yr^{-1} for ice were used for the catchment area. If there is snow to melt, then the model will begin to melt snow according to the melt factor of 2.7 mm $°C^{-1}$ d^{-1}. Otherwise, if the snowpack is depleted, then there is only ice to melt and a higher melt factor of 7.2 mm $°C^{-1}$ d^{-1} is used. If the melt is over bare ground, meaning that there is no longer any snowpack to melt, then any precipitation that exists is added as rainfall to the total melt. Where the total melt (*M*) in the following equation is a function of snow and ice melt according to the calculated amount of *PDD*:

Equation 7: Total Melt Calculated from the Ice and Snow Factor

$$M = f_{s,i} \sum PDD$$

If the amount of *PDD* is below zero, i.e. no melt, then the precipitation would be added to the snowpack for the next month. See Figure 6 for a schematic of the *positive degree day* model.

3.7.2 Discharge calculation

The discharge was calculated for the basin from the melt results. The basin area was multiplied by the melt values and divided by one billion to achieve gigatons per year of discharge. Where the basin is 35 km² in area and *M* is the runoff values in mm.

Equation 8: Discharge Calculation for the L-DWC Catchment.

$$Q = \frac{[M(0.001)](basin\ area\ m^2)}{1000000000}$$

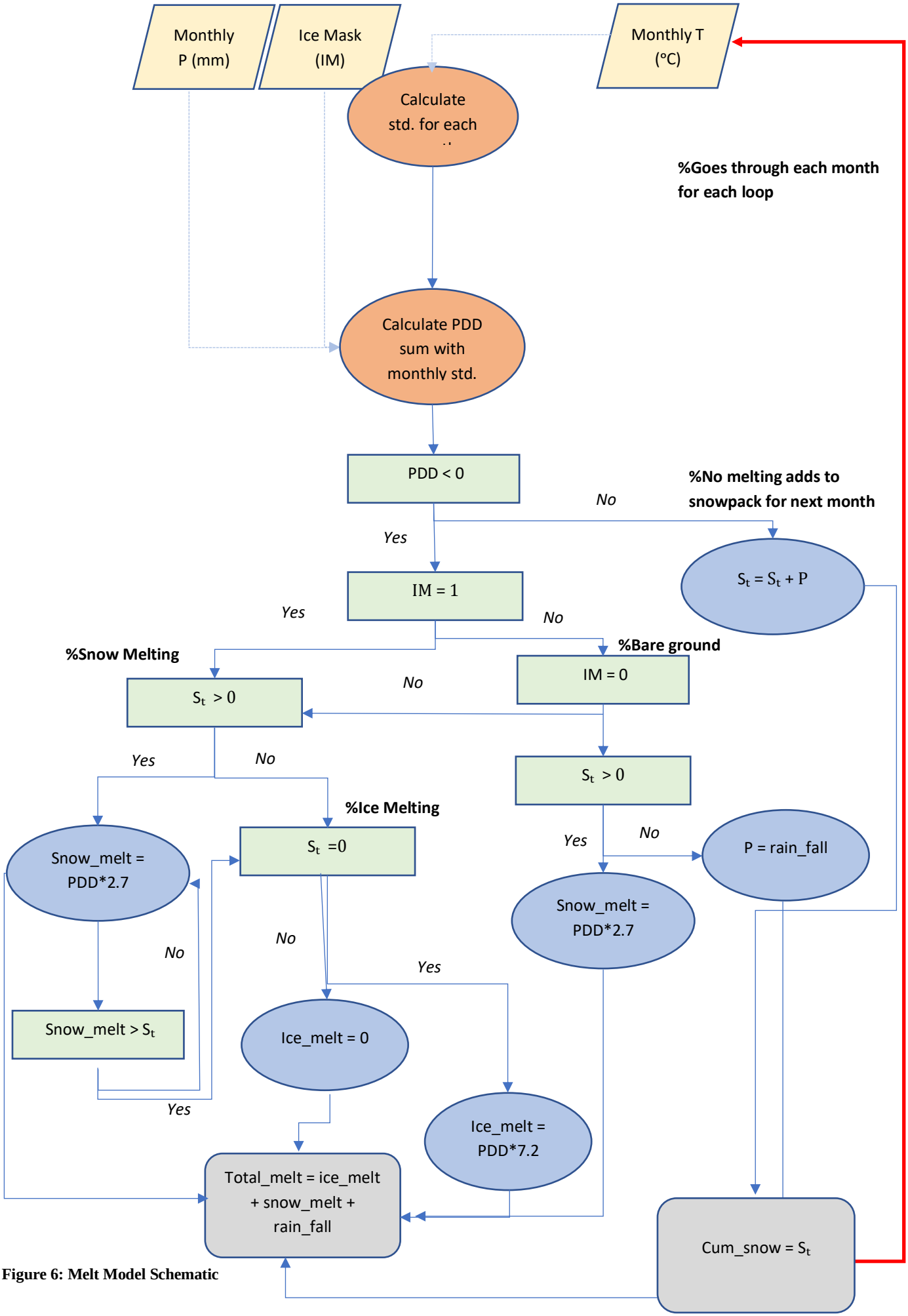

Figure 6: Melt Model Schematic

4 Results of Model Intercomparison

4.1 Comparison of Climate Models to Observational Data

Due to the remoteness and lack of data in the catchment areas, climate models are the best method for providing continuous climate data coverage of these locations. In this section six climate models will be compared and then evaluated against the available observation data for specific locations across Greenland from the Program for Monitoring of the Greenland Ice Sheet (PROMICE) weather stations**.** Of note, given the lack of observational data for precipitation, it was not possible to evaluate this performance aspect across Greenland, ergo constituting a limitation. In this section, the data series generated through the PROMICE weather stations are compared against each climate model to illustrate how air temperature can be simulated over the interannual cycle. It will only be the graphs for the first two AWS at Kangerlussuaq and Nuuk (Figure 7 and 8, respectively) that are presented in this part, the remainder of the graphs for the stations at Upernavik, Qassimuit, Scoresby Sund, Tasiilaq, Thule and Kronprins Kristian Land can be found in the Appendix. The results of the RMSE statistical test can be found in Table 2 for all the weather stations.

4.1.1 Kangerlussuaq Weather Stations

In the Kangerlussuaq region there are four weather stations situated at different elevations along a transect: KAN_L (350 m), KAN_B (670 m), KAN_M (1270 m) and KAN_U (1840 m). The weather stations have a monthly mean air temperature range between -31.85 ^{o}C to 8.91 ^{o}C. The results are plotted in Figure 7. At the lowest elevation station, the data from HadGEM has the lowest RMSE (5.04 ^{o}C). There was good agreement when comparing HadGEM's temporal series against the observational data than from ECHAM. As the weather stations increased in elevation ECHAM was found to outperform HadGEM, this is supported by a lower RMSE values and an interannual cycle that resembles closer to the temporal curve of the PROMICE data. The highest RMSE values for HadGEM occurred at the upper station, noting that there was a lack of time series data for HadGEM across its upper station. Throughout all, the time series data from each weather station at KAN, it is HadGEM that produces the coldest extremes. To that end, it can be deduced that HadGEM performs better where air temperatures are above zero and conversely overestimates the air temperature during the months that are below zero degrees.

In comparing the regional climate models, HIRHAM performed very well on the interannual cycle for all the KAN weather stations, with the exception of that at KAN_B, where overprediction of the temperature occurred by 2 ^{o}C to 5 ^{o}C for air temperatures that were above zero: nevertheless, this model was better at replicating air temperatures below zero. Despite this, HIRHAM is assessed as being the RCM that agrees the closest to the observational data. At the two lower stations, both RACMO$_{H}$ and MAR produced larger cold biases for the winter months and both predicted temperatures of up to 20 ^{o}C colder than that recorded. These two RCMs were better at replicating air temperatures that were above zero degrees, noting that RACMO$_{H}$ performed slightly better than MAR over the summer periods.

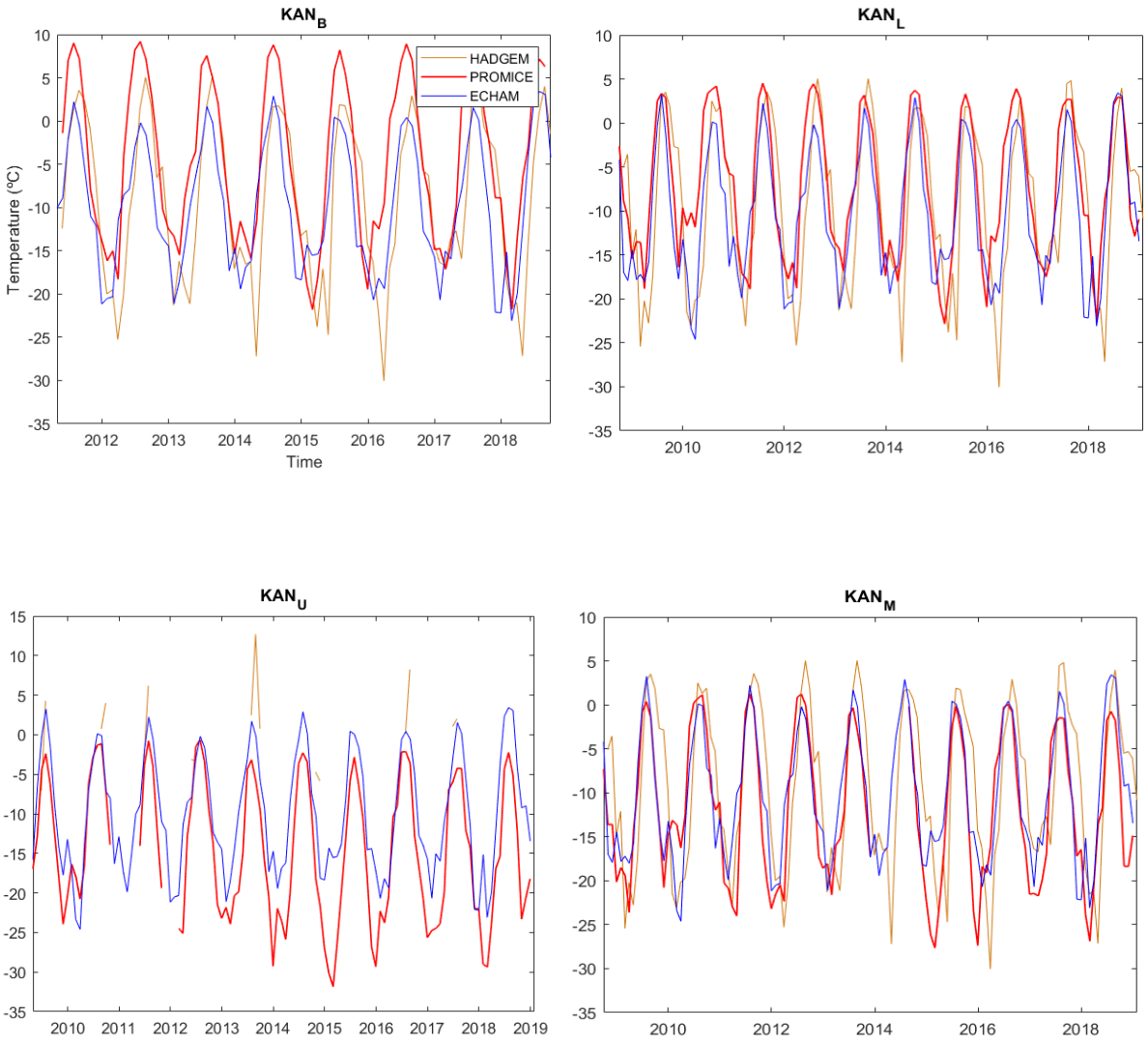
KAN_B
KAN_L
KAN_U
KAN_M
HADGEM
PROMICE
ECHAM
Temperature (°C)
Time

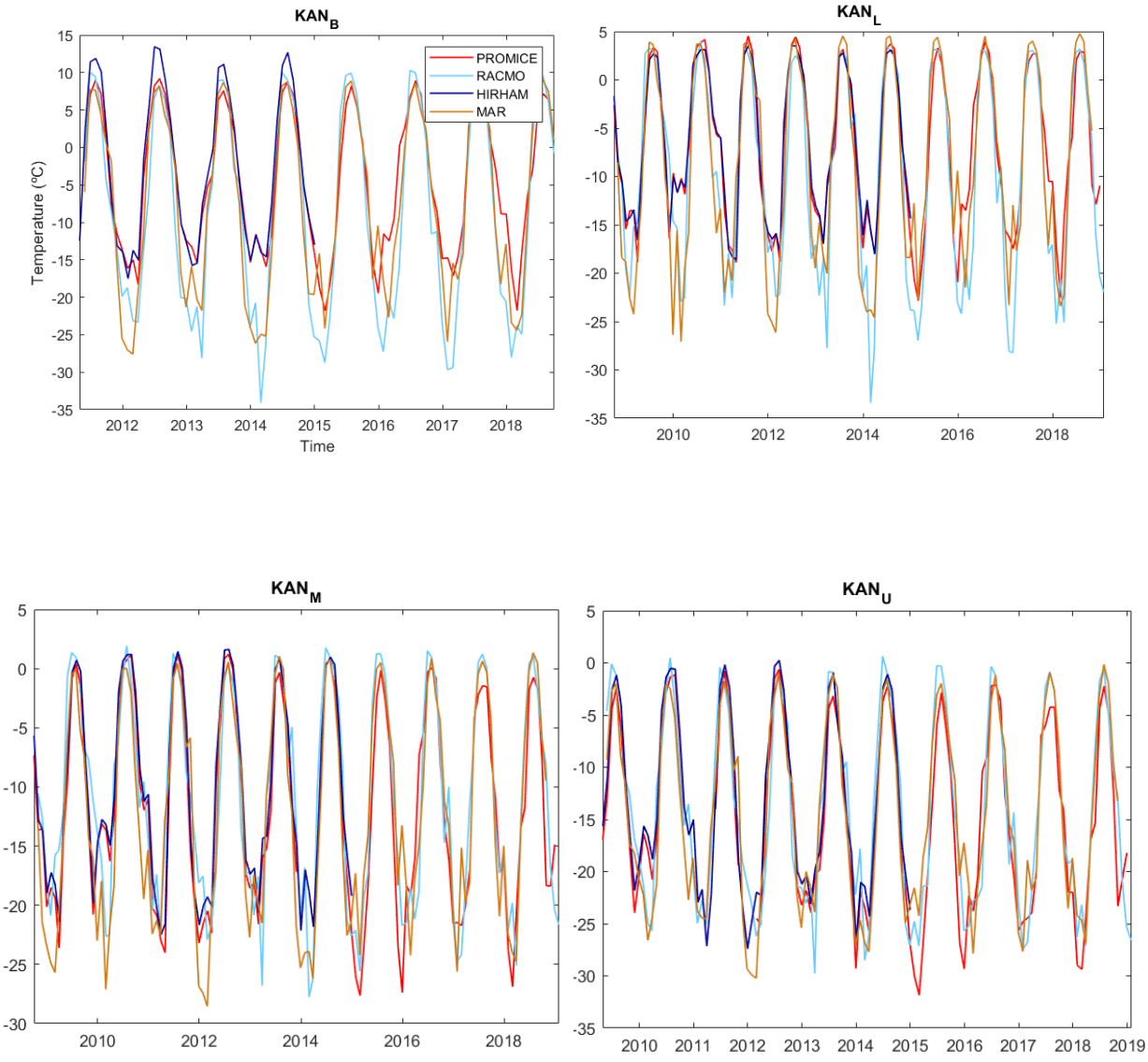

Figure 7: Top four graphs (previous page) are GCM plotted with PROMICE KAN AWS air temperature. Bottom four graphs are RCMs plotted with PROMICE KAN AWS air temperature, description of the graphs in Section 4.1.1.

4.1.2 Nuuk Weather Stations

The Nuuk AWS consists of four weather stations at the following elevations: NUK_L (530 m), NUK_K (710 m), NUK_N (920 m) and NUK_U (1120 m). The monthly mean air temperature range for these stations range between -22.96 °C to 6.57 °C. The results are plotted in Figure 8. Beginning with the two GCMs, HadGEM and ECHAM, both have very similar RMSE values observed across all four stations. Like that observed at the KAN AWS, HadGEM overpredicts for negative temperatures, reflecting extremes of 15 °C colder than that observed. For NUK_L, HadGEM was shown to be the best choice in replicating the positive air temperatures, as ECHAM was underpredicting the positive air temperatures by as much as 5 °C. For the other three stations, ECHAM produced better results that more closely simulated the air temperature to the observational data than did HadGEM.

At the lowest station in Nuuk, $RACMO_H$ was assessed as performing the best for positive degree temperatures. When comparing it with MAR, MAR consistently overestimates how warm it was by 3 °C to 7 °C, whereas $RACMO_H$ predicted air temperatures within an accuracy of 1 °C to 2 °C.

Throughout, $RACMO_H$ continued to predict very extreme cold temperatures during the winter months, of note were those recorded in December 2014 where it showed an air temperature drop down to -33 °C and the station at NUK_L recorded a monthly mean of only -8 °C. HIRHAM was able to simulate the annual cycle the best, but it still consistently reflected air temperatures that were several degrees colder than that measured at NUK_L.

At Nuuk's highest station there were more periods of missing data in the PROMICE record, but in the years that temperature was being recorded the two climate models are closely comparable in their performance in predicting positive air temperatures. In the later years, between 2016 to 2018 MAR overestimated the positive air temperatures, whereas $RACMO_H$ more closely replicated the observed air temperatures.

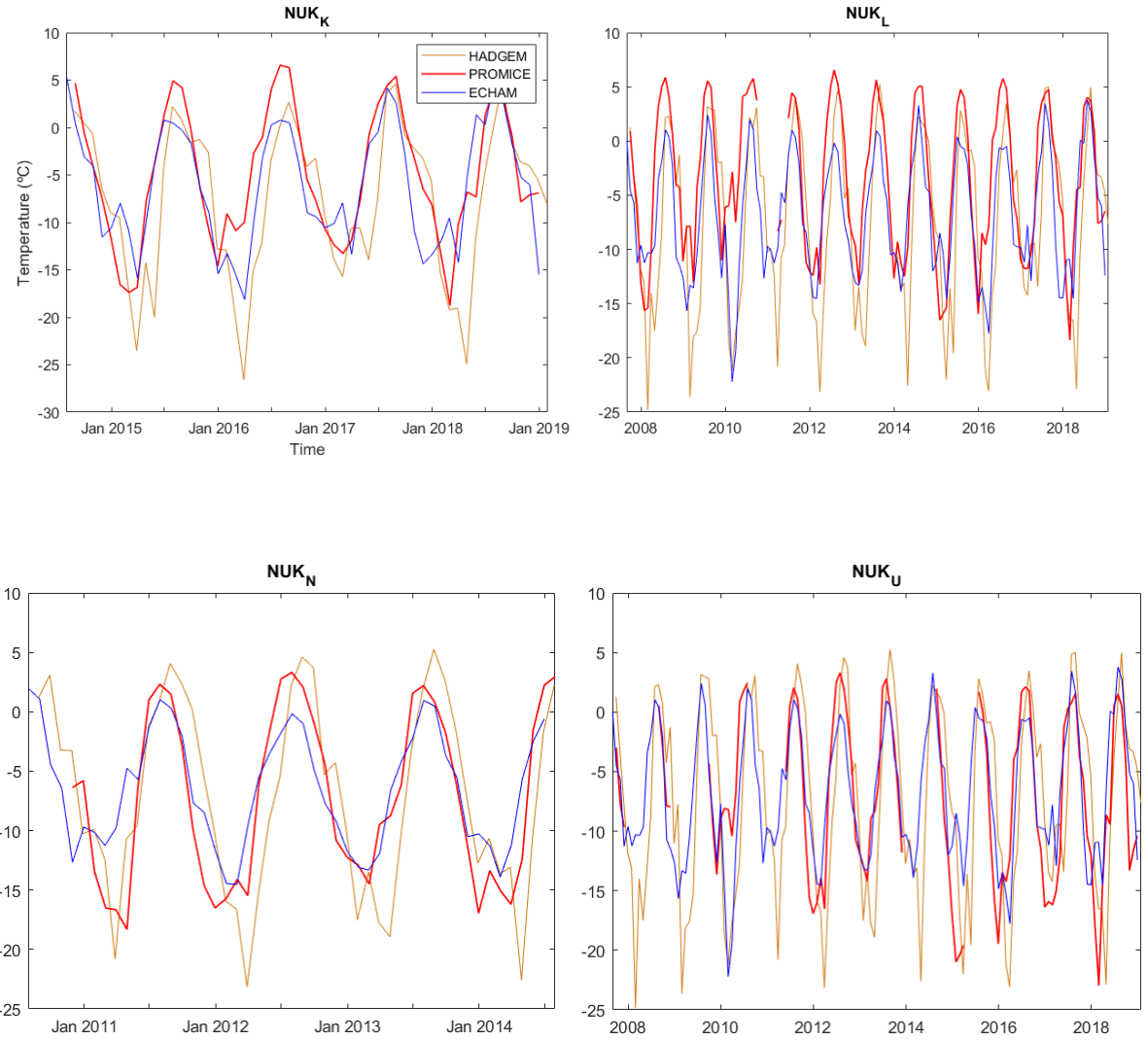
NUK_K
HADGEM
PROMICE
ECHAM
Temperature (°C)
Time
Jan 2015
Jan 2016
Jan 2017
Jan 2018
Jan 2019
NUK_L
2008
2010
2012
2014
2016
2018
NUK_N
Jan 2011
Jan 2012
Jan 2013
Jan 2014
NUK_U

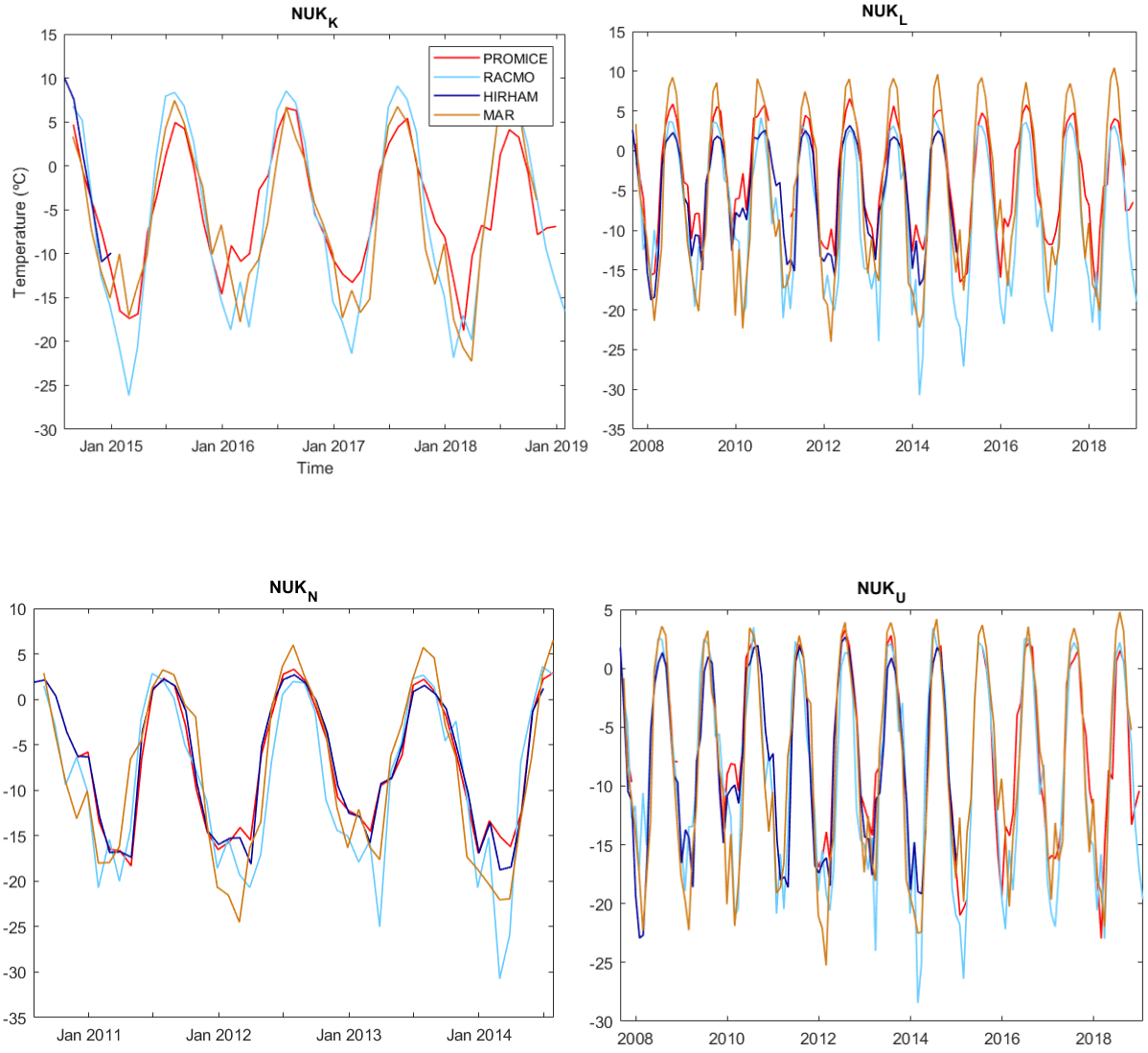

Figure 8: Top four graphs (previous page) are GCM plotted with PROMICE NUK AWS air temperature. Bottom four graphs are RCMs plotted with PROMICE NUK AWS air temperature, description of the graphs in Section 4.1.2.

Table 2: Root mean square error (RMSE) values for all the climate models and PROMICE data. N/A values occur where the climate model does not have coverage to compare with the observational data.

PROMICE Stn	HadGEM	ECHAM	$RACMO_H$ (11 km)	MAR	HIRHAM	$RACMO_E$ (1 km)
KPC_L	4.45	6.84	8.70	3.17	4.50	1.46
KPC_U	6.25	7.74	7.35	3.35	2.72	1.98
EGP	N/A	15.15	8.46	4.33	N/A	N/A
SCO_L	3.26	7.61	11.41	3.67	2.81	8.20
SCO_U	3.87	6.37	10.07	2.90	2.55	2.59
MIT	4.35	4.28	3.93	3.13	3.49	1.13
TAS_L	4.80	4.15	4.24	2.72	2.51	1.27
TAS_U	3.40	3.42	3.96	2.48	1.59	1.48
TAS_A	2.89	3.27	4.08	2.35	1.51	0.76
QAS_L	5.42	4.68	4.75	3.52	2.87	1.20
QAS_M	2.70	4.33	4.57	2.84	N/A	N/A
QAS_U	3.78	4.13	3.94	3.21	0.98	1.35
QAS_A	4.62	5.51	4.93	3.37	1.44	0.62
NUK_L	5.86	5.83	7.16	5.34	2.54	1.68
NUK_U	4.59	4.89	5.04	4.20	1.28	0.94
NUK_K	5.20	5.45	6.22	4.18	2.30	2.21
NUK_N	3.72	4.98	6.71	4.37	N/A	0.98
KAN_B	6.15	7.98	9.24	5.48	2.41	1.07
KAN_L	5.04	6.57	7.21	4.99	0.98	0.67
KAN_M	5.41	6.02	5.71	4.32	1.35	0.82
KAN_U	10.97	7.76	6.13	3.86	1.66	1.11
UPE_L	5.46	8.45	9.41	5.39	2.58	1.04
UPE_U	4.16	6.09	7.25	4.39	0.94	0.53
THU_L	4.19	6.67	8.88	5.44	1.72	0.77
THU_U	3.85	6.72	8.26	5.51	1.69	0.61

4.1.3 Qassimuit Weather Stations

The Qassimuit weather stations are the southernmost stations in the PROMICE, and the third of three weather station series with four stations set up at varying elevations in proximity to one another. The weather stations are situated at heights of; QAS_L at 280 m, QAS_M at 630 m, QAS_U at 900 m and QAS_A at 1000 m. The weather stations have a monthly mean temperature range of -20.16 ^{o}C to 5.93 ^{o}C. At the lower station, the GCM ECHAM is the one that most closely replicated the observational data for those temperatures above zero degrees. For the air temperatures below zero, both GCMs overestimated the cold amplitudes, but it is HadGEM that created the greater extreme dips in temperature. At the QAS_U station, both climate models had similar RMSE scores, 3.78 ^{o}C or HadGEM and 4.13 ^{o}C for ECHAM.

Meaning that the performance of both models was similar in being able to predict air temperature, but with more investigative work in the interannual cycle, it was shown that they were outperforming one another. For air temperatures above zero, ECHAM more frequently replicated the positive amplitudes as per that seen in the observational data, but conversely it struggled to simulate the air temperature lows during the winter months, where it was underpredicting colder air temperatures at QAS_U. HadGEM, however, produced more extreme negative temperature amplitudes than that which was observed, with 2015, 2017 and 2018 being the exception where the observed data was several degrees colder than either of the models predicted.

In terms of the performance of the three RCMs at QAS_L, each were able to simulate the interannual cycle, however, misalignment with the amplitude's peaks and troughs were observed. $RACMO_H$ is assessed as being the one that most closely resembles the observed temperature at the QAS_L station, with 2013 being the exception when the MAR's amplitude was a closer fit with that of the observed data. At the upper station (QAS_U), $RACMO_H$ underperformed when compared against the observed data, whereas HIRHAM and MAR simulated the observed data the closest. HIRHAM had better result in producing the troughs of the annual cycle, whereas MAR would over predict how cold it was during the winter months.

4.1.4 Tasiilaq Weather Stations

On the Eastern side of Greenland, the Tasiilaq weather stations are the most southerly, located near the settlement of Tasiilaq. The monthly mean temperature profile for this area has a smaller temperature range, averaging between 3.96 ^{o}C in the summer months to a low of -16.96 ^{o}C in the winter months. There are three weather stations at this location: TAS_L (250 m), TAS_U (570 m) and TAS_A (890 m). TAS_U was discontinued in August 2015. At the TAS_L location there are periods of missing data for 2011 and 2017. When further examining this site HadGEM was found to overpredict the temperature of the mean monthly coldest trough, while ECHAM was assessed as being able to better simulate the negative temperatures during the interannual cycle. For those temperatures above zero, both ECHAM and HadGEM appear to simulate the temperatures at the lower station with mixed results. In certain years HadGEM better simulated the climate, particularly in 2012, 2013, 2015, 2016, and 2018, whereas for the remaining years ECHAM is better at simulating the positive air temperatures at TAS_L. At the two upper stations, HadGEM simulated the observed

temperatures slightly better than ECHAM for the positive temperatures. HadGEM continued to overpredict the coldest monthly means.

The regional climate models were assessed as performing better than the GCMs at TAS_L, with $RACMO_H$ simulating the temperature better than the other two RCMs for positive temperatures. At the lower station MAR was overpredicting the temperature profile between a range of 2 ^oC to 5 ^oC. HIRHAM replicated the air temperatures annual cycle better as it did not overestimate the monthly mean of the coldest temperature, but it had a greater challenge in simulating the maximum positive temperatures during the months where the temperature was above zero degrees. For the upper stations (TAS_A and TAS_U) the performance of the climate models was like that of the lower stations.

4.1.5 Scoresby Sund Weather Stations

Near Scoresby Sund there are two weather stations located inland at the following elevations: SCO_L at 460 m and SCO_U at 970 m. The monthly mean temperature range for the weather stations were -22.84 ^oC to 4.6 ^oC. At the lower and upper station, ECHAM underperformed as compared to HadGEM. ECHAM reported negative values when the AWS was recording air temperatures well above zero. Furthermore, HadGEM did not over predict the coldest mean month, rather it was able to simulate the observed temperature with good agreement at the lower station. At the upper station HadGEM temperatures were warmer than the monthly cold mean by up to a difference of 5 ^oC.

At the regional level HIRHAM performed well in simulating the coldest monthly mean, while overpredicting the positive monthly mean by 4 ^oC for each annual cycle. Compared to $RACMO_H$ which over predicts the cold monthly mean temperature, again by reporting values that were up to 15 ^oC colder than the observed data. Whereas, MAR's overall performance was better at the lower station, it ably simulated the temperature throughout the whole interannual cycle. At SCO_U HIRHAM performed better than the other two RCMs in simulating positive temperatures, but it was outperformed by MAR when simulating negative temperatures. While $RACMO_H$ overpredicts the positive temperatures by 2 ^oC to 3 ^oC, it continued to overpredict negative temperatures by up to 13 ^oC of difference for the coldest monthly mean.

4.1.6 Konprins Kristians Land Weather Stations

The Konprins Kristian Land weather stations are the most northerly weather stations situated in North East Greenland within the National Park. The air temperature range measured for the period was between and -32.26 °C to 1.66 °C. It contains two weather stations located at: KPC_L at 370 m and KPC_U at 870 m. There is a gap in data at KPC_L during the years 2011 and 2012. Throughout the annual cycle at KPC_L both HadGEM and ECHAM were comparable in performance with only slight deviations from each other. Although more often HadGEM simulated the observed air temperatures better as compared to ECHAM, which was reinforced through the RMSE values, where HadGEM had a lower RMSE than ECHAM (4.45 °C and 6.84 °C, respectively). At KPC_U the GCMs also performed in a similar manner, each following the other quite closely in the interannual cycle with RMSE scores of 6.25 °C for HadGEM and 7.75 °C for ECHAM. The weak points of both GCMs were the ability to simulate the coldest mean monthly temperatures, as they underpredicted the temperatures by up to 10 °C warmer than the observed data. Both had strengths in being able to simulate the temperature at positive temperature months.

For the regional climate models at KPC_L HIRHAM and $RACMO_H$ both overpredicted the maximum temperatures for positive monthly means by 4 °C to 6 °C prior to 2014. $RACMO_H$ overpredicted the monthly mean for the positive temperature by 2 °C to 7 °C for the remainder of the period. MAR was able to best simulate the air temperature at KPC_L, but it still reflected differences of up to 4 °C for some of the monthly means within the interannual cycle. This was reinforced by the RMSE scores for all three RCMs of 8.7 °C for RACMO, 4.50 °C for HIRHAM and 3.17 °C for MAR. At the KPC_U site, the results were the same as at the lower station, where MAR performed more closely to the interannual cycle of the observed temperatures at KPC_U. The best match for MAR with that of the AWS data occurred during the positive temperature monthly means. During the negative temperature monthly means it was $RACMO_H$ that was able to simulate the climate more accurately.

4.1.7 Thule Weather Stations

The Thule weather stations are the northern most stations on the West Coast of Greenland. There are two weather stations located at Thule: THU_L at 570 m and THU_U at 760 m. Of note, there is a gap in data during the winter months of 2016. The temperature in this region ranges from to -30.17 °C to 4.63 °C. ECHAM consistently replicated the interannual air temperature cycle at THU_L more accurately than HadGEM. However, when comparing the results of the RMSE it was HadGEM with a lower RMSE of 4.2 °C, whereas ECHAM had a

RMSE of 6.68 °C. In way of assessment these results could be reflecting how HadGEM was better at simulating the most extreme of the coldest monthly means compared to ECHAM. These results were similarly reflected at the upper station at Thule.

At THU_L all the RCMs were in good agreement with the AWS during the period 2011 to 2014, as they can replicate the positive monthly mean temperatures within 1 °C to 2 °C. HIRHAM more closely simulated the negative monthly mean within a range of 2 °C to 5 °C, while $RACMO_H$ and MAR overpredict by up to 11 °C for the whole period. These results were similarly reflected at the upper station at Thule.

4.1.8 Upernavik Weather Stations

Upernavik weather stations are located at a similar latitude to the Scoresby Sund stations, but they are located on the West Coast of Greenland. There are two weather stations located in this area: UPE_L at 220 m and UPE_U at 940 m, with data gaps at UPE_L during the winter of 2013. The temperature range at the weather stations range between -28.78 °C to 7.09 °C. At both the upper and lower stations HadGEM can better simulate the temperature profiles of the AWS. Although HadGEM overpredicted the coldest months up to a 14 °C of difference during the winter of 2017. When comparing the RMSE, HadGEM had a lower result of 5.46 °C and 4.16 °C respectively at the lower and upper stations, while ECHAM's RMSE results were 8.48 °C and 6.09 °C.

At the upper station, HIRHAM simulated the interannual cycle better than $RACMO_H$ or MAR since it did not produce overpredicted air temperature values for the coldest monthly means. For the positive temperature values the three climate models agreed well with each other as compared to the AWS. At UPE_L it was MAR that outperformed the other two for air temperatures that were above zero degrees. During the colder monthly means that were below zero, MAR and $RACMO_H$ continued to overpredict the extreme temperatures.

4.1.9 Climate Reanalysis Versus AWS

Climate reanalysis data was used for validation of the downscaled methods and was first evaluated to show the agreement between the climate reanalysis data and observational data. The RACMO2.3p2 ($RACMO_E$) downscaled dataset is presented in its own section since it is reanalysis data and was shown to outperform the rest of the climate models. This was expected since it is forced using observational data. The results (Figure 9) produced in this paper are in good agreement with the study done by Noel et al. (2019). In it, it compared the same dataset to PROMICE and GC-NET. They concluded that the $RACMO_E$ dataset

accurately replicated the climate of Greenland. Their results reflected small air temperature biases of 0.14 ^{o}C that likely reflect uncertainty in the sensor measurements. The results from this study are presented in the graphs, providing an example of how RACMO$_{E}$ accurately simulates the PROMICE AWS data (Figure 9). Of note is the exception at the Scoresby Sund station (not shown) where a large root mean square error of 8.2 ^{o}C was observed. The remainder of the AWS comparisons to RACMO$_{E}$ had smaller root mean square errors of 0.7 ^{o}C to 2.2 ^{o}C. However, at the Zackenberg station, RACMO$_{E}$ was not able to replicate the climate to the same degree as that of the PROMICE stations. The RMSE was higher than the PROMICE stations at a root mean square error of 4.8 ^{o}C. During the negative degree air temperatures, the RACMO$_{E}$ was unable to replicate the extremes as well as during the positive degree months. However, overall, it was able to simulate the interannual cycle with good agreement. It was this RACMO$_{E}$ dataset that was used during the reference period for the validation of the downscaled methods and runoff modeling for this paper.

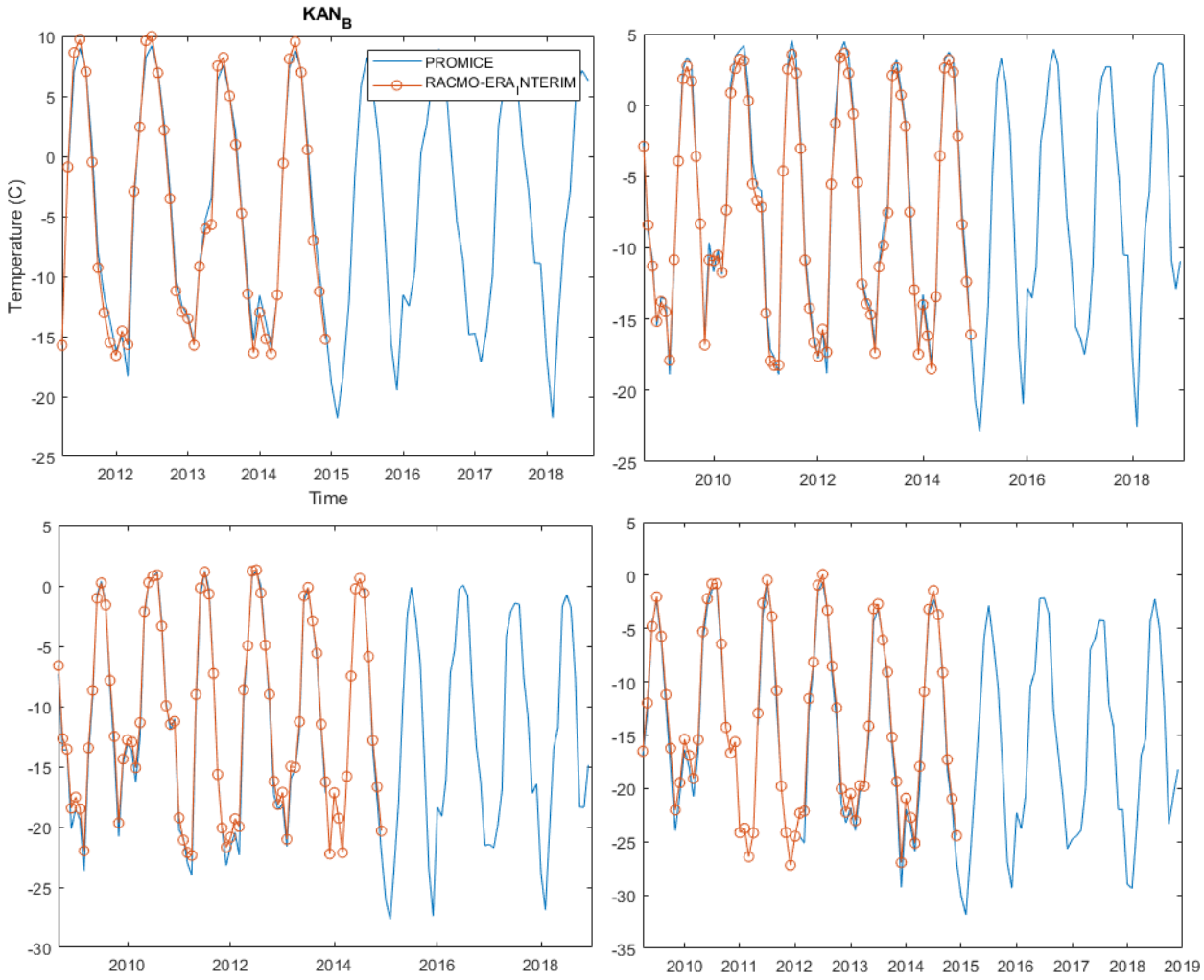

Figure 9: RACMO forced by ERA INTRIM plotted with PROMICE AWS air temperature data from KAN_B, KAN_L, KAN_M and KAN_U

5 Results of Downscaling

Downscaling climate model data is the next and necessary step to acquire high resolution temperature and precipitation data for the small-scale drinking water catchments. This section will show the results of the downscaling process. This process involves calculating lapse rates, creating downscaled air temperature matrices and from these the downscaled climate data will be compared using downscaled $RACMO_H$ that has been forced by reanalysis data for Greenland.

5.1.1 Slope Lapse Rates Over Greenland

The slope lapse rates (SLR) for July were calculated across Greenland from nine different sets of weather stations (Table 3) and ranged from -2.2 ºC/km (±0.95) at Tasiilaq to -6.3 ºC/km (±0.42) at Kangerlussuaq. The Eastern and Southern regions of Greenland represent the areas with the lowest SLRs, with Scoresby Sund and Qassimuit having the same mean monthly July SLRs of -2.3 ºC/km (±0.85 and ±0.47, respectively). In the North of Greenland, the SLRs are more comparable to the ones in the West. This is exampled by the locations at Nuuk, where the SLR is -5.1 ºC/km (±0.72) and in Thule and Konprins Kristian Land, where the values are -4.9 ºC/km (±1.48) and -5.6 ºC/km (±0.59) respectively. Higher SLRs are generally a sign of colder climates and less melt activity over the glacier surfaces, which generates less area at the surface at a fixed surface temperature of 0 ºC (Gardner et al., 2009). At the Northern stations, the mean monthly July air temperature ranges between 1.66 ºC and 4.63 ºC, while the higher SLRs in Western Greenland have higher July air temperatures of 2.69 ºC to 6.52 ºC, in which the difference between the Northern and Western difference in the respective magnitude of range could be explained by the location of the weather stations. Specifically, the lower stations at KAN and NUK are located on bare ground, while the upper stations are located over glacier ice and are therefore exposed to the cooling effect from the glacier. As a result, this can produce artificially high SLRs since the lower stations are not as affected by the cooling effect. The correlation coefficients between the air temperature and elevation were also calculated for each July SLR over an eight-year period using the observed air temperatures with the resulting range of r = -0.98 to -0.91.

Table 3: Slope lapse rates (SLR) for temperature and standard deviations for nine regions in Greenland.

Location	Region (Short name)	Slope Lapse Rate (°C/km)	Std Dev. (°C/km)
West	Kangerlussuaq (KAN)	-6.3	0.42
	Nuuk (NUK)	-5.1	0.72
	Ilulissat (ILU)	-4.4	0.48
	Upernavik (UPE)	-4.8	1.1
South	Qassimiut (QAS)	-2.3	0.47
East	Scoresby Sund (SCO)	-2.3	0.85
	Tasiilaq (TAS)	-2.2	0.95
North	Thule (THU)	-4.9	1.48
	Konsprins Land (KPC)	-5.6	0.59

5.1.2 Catchment Scale Results

To show if there had been any improvements from the downscaling procedure, the downscaled outputs were compared to the $RACMO_E$ dataset. $RACMO_E$ was downscaled to the same resolution as that of the $RACMO_H$ dataset, using the same downscaling method. These two datasets were compared to determine where the biases occurred and to see how well $RACMO_H$ was able to replicate the temperature as a downscaled output. The period from 2005 to 2014 was used as the reference time frame to compare the two.

5.1.3 Drinking Water Catchment

In comparing the results from the downscaled data, it is obvious that from the procedure used, it can create high resolution data that covers the entire area on a continuous basis (Figure 10). Upon further investigation, there are still large discrepancies between the two datasets. In general, the $RACMO_H$ downscaled is less accurate in replicating air temperature at higher elevation, as it creates biases of 3 °C + at elevations above 1000 m.a.s.l. during the summer months. Within the valley systems, at lower elevations below 1000 m.a.s.l., the biases

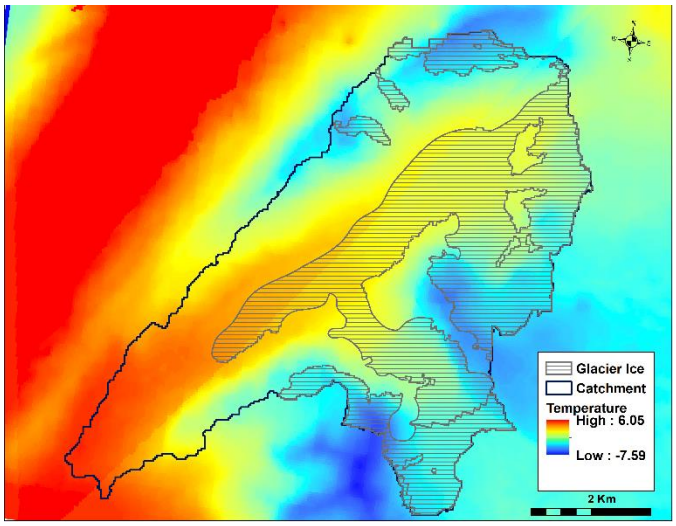

Figure 10: Example of downscaled temperature: July 2006 for catchment L-DWC.

are smaller. During the winter months, larger differences are observed up to 28 ºC at the higher elevation points. The summer months consistently produce lower biases between 2 ºC to 10 ºC, whereas the larger biases are observed at the higher elevations. $RACMO_H$ is predicting colder air temperatures at higher elevations and predicting warmer ones at lower elevations than that observed from $RACMO_E$. Figure 11 plots downscaled $RACMO_H$ monthly air temperatures against $RACMO_E$. The results show that $RACMO_H$ has a cold bias at extreme winter temperature values but was able to replicate the interannual cycle with better agreement.

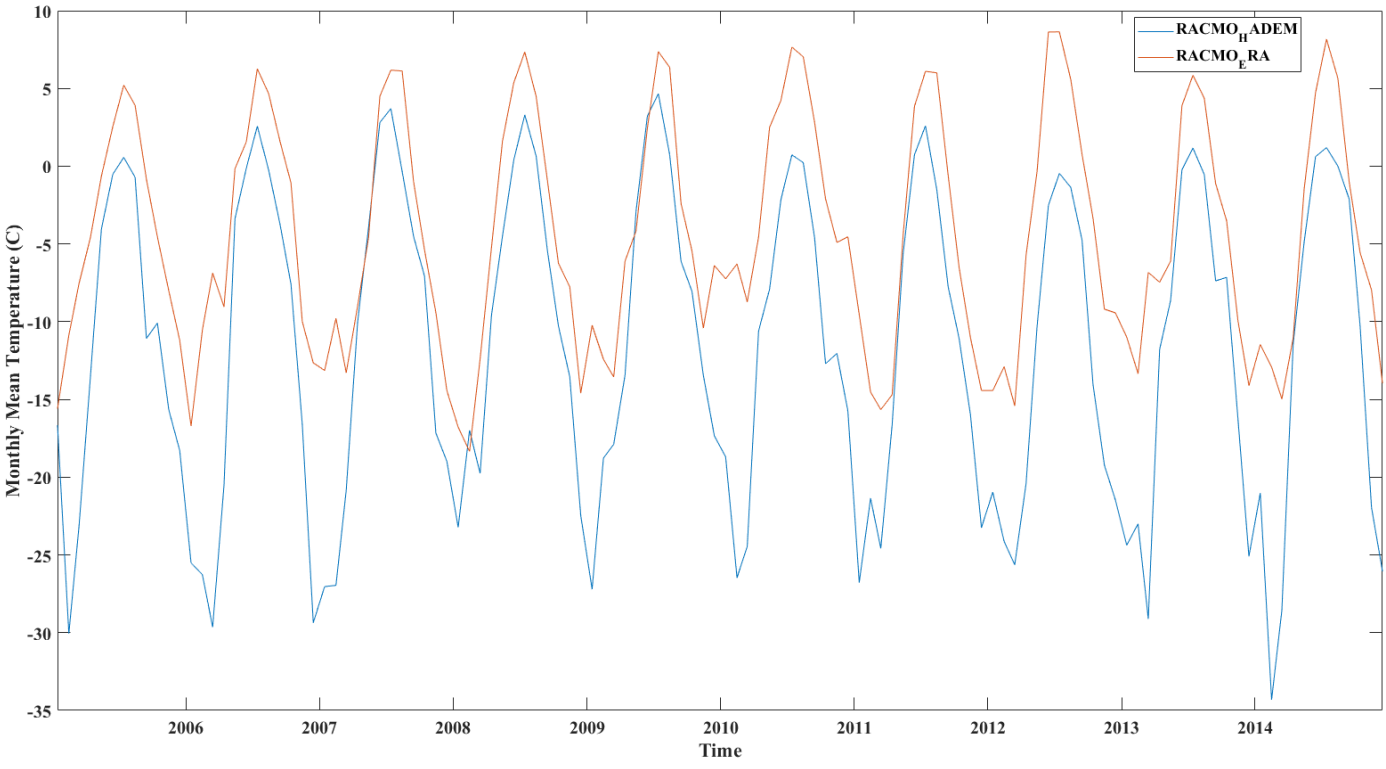

Figure 11: Downscaled $RACMO_H$ air temperature plotted with $RACMO_E$ for the reference period of 2005 to 2014

5.1.4 Zackenberg Catchment

$RACMO_E$ was similarly downscaled in the catchment of Zackenberg and compared with the downscaled $RACMO_H$. The summer months show the best agreement between the datasets, with smaller biases of up to 10 °C and as low as 0.16 °C across the catchment. While in the winter months larger biases are produced between the two datasets, for instance in February 2010 a bias of up to 20 °C was produced in higher elevation parts of the catchments. Furthermore, during the summer months there is also larger biases at higher elevations where A.P. Olsen Ice Cap is located, while within the valleys and the lower elevations (below 1000 m) produce smaller biases and better agreement to $RACMO_E$ dataset is achieved.

Due to the availability of observational data the downscaled $RACMO_H$ dataset was also compared with observational data to show if any improvements from $RACMO_H$ at 11 km resolution. The plot below in Figure 12 shows how the downscaled datasets resolves the winter temperatures with better agreement but is not able to accurately predict the observed data. During the summer months overall, the downscaled dataset has better agreement except, during the years 2012 and 2013. The downscaled $RACMO_H$ has a smaller average bias of 6.32 °C than 11 km $RACMO_H$ with a bias of 9.92 °C.

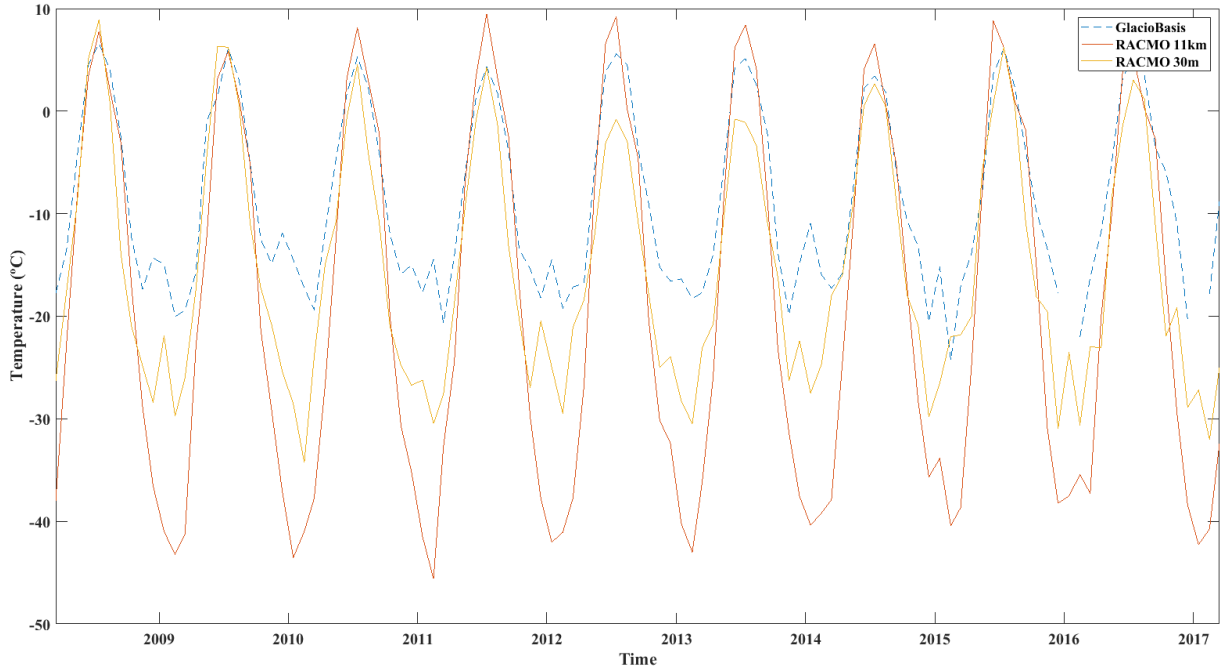

Figure 12: $RACMO_H$ 11km and *statistically* downscaled $RACMO_H$ at 30m compared with observation data at Zackenberg

6 Results from *Positive Degree Day* Modeling

The final step of this thesis is to determine the amount of future meltwater runoff from the catchment areas in Greenland in being able to predict drinking water availability and its viability for commercial means. This will be done using downscaled climate model data that will be run through the *positive degree day* (*PDD*) model that has been written specifically for this purpose. Described in this section will be the validation and the steps used in calculating the *PDD* sum against the observational data at the A.P. Olsen Ice Cap located in Zackenberg, as well as the results of the runoff modeling for the amount of drinking water produced at the respective catchment area. Recalling that the Zackenberg and L-DWC locations were selected as the sites respectively for the observational data and the area catchment runoff.

6.1.1 *PDD* Sum at Zackenberg

Earlier in this paper it described the various methods to calculate *positive degree day* sums. Three methods used are: (1) Simple, (2) Reeh (1991), and (3) Calov and Greve (2005). The observational data obtained for each of these methods is the hourly air temperature from the A.P. Olsen Ice Cap. The aim in doing this was to validate the performance of the statistical methods for (2) Reeh, and (3) Calov and Greve and compare them to the data observed (1) simple. As can be observed in Figure 13, where the three methods are plotted and the relative comparisons made, it demonstrates that both methods 2 and 3 reflect an accurate simulation to the observed *PDD* sum of method 1, showing good agreement across all three. The largest discrepancy between the methods is noted in 2014 where the 3rd method has a 10 ^{o}C days difference than that observed with the 1st method. Of note, during this same year there was less discrepancy between methods 2 and 1. As a result, the 3rd method by Calov and Greve was selected for the meltwater modeling primarily due to

its computational simplicity of a single integration over time instead of the method used by Reeh, in which a double integration over time and temperature is used.

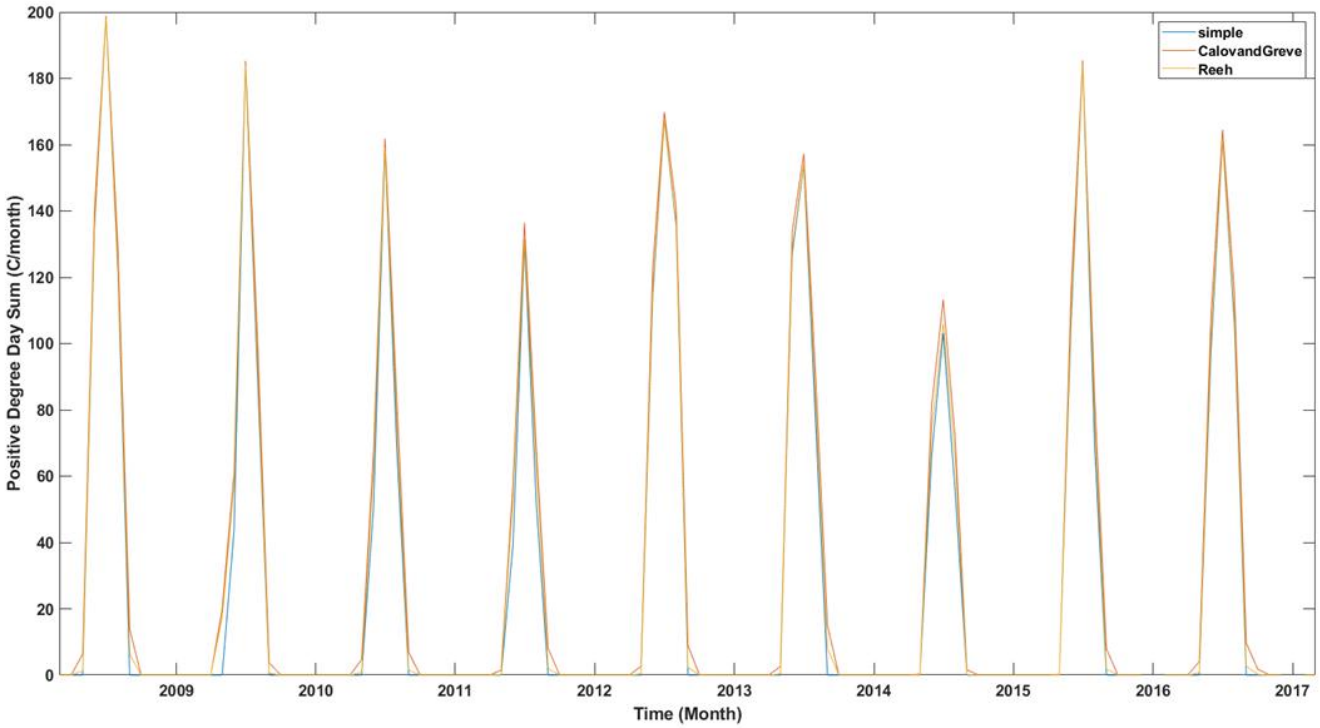

Figure 13: Calculated *PDD* sum at A.P Olsen Ice Cap for 2008 to 2017 using three different methods: simple (blue), Calov and Greve (orange) and Reeh (yellow).

6.1.2 Total Runoff

Confident that the *PDD* sums are accurately simulated using the Calov and Greve method, this melt model was subsequently applied at drinking water catchment area L-DWC. The mean total meltwater runoff over time in the three different periods is reflected in Figure 14 for the following timeframes: 2005-2019, 2020-2040 and 2041-2060. Based on the result, the runoff is predicted to increase in the future. During 2005-2019 the mean monthly value during the melt season is 123.51 mm w.e, whereas 2020-2040 the mean monthly runoff value is 131.50 mm w.e and 140.35 mm w.e in 2041-2060. The largest values of runoff are observed at the tongue of the glacier and the lowest values are seen at the higher elevation areas.

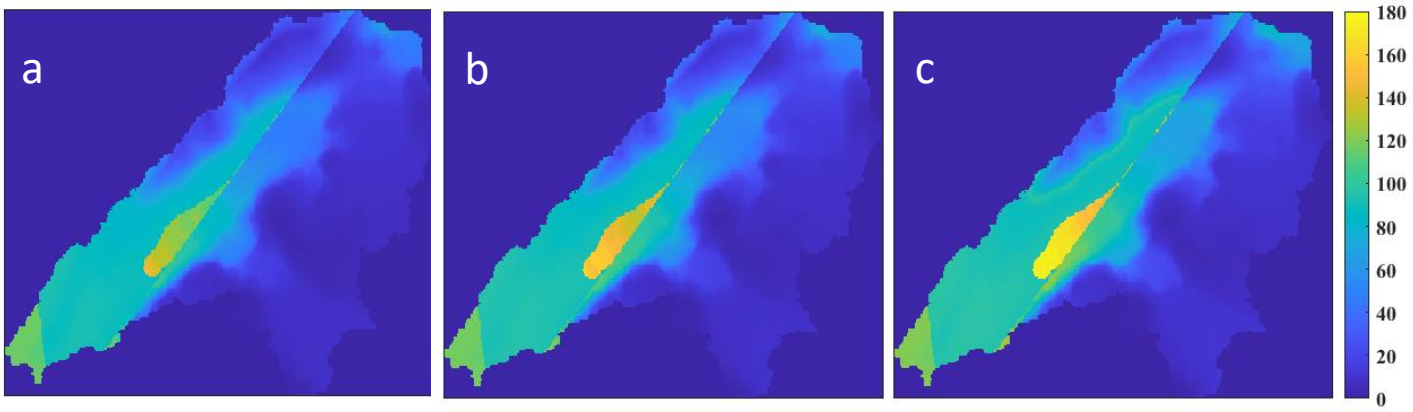

Figure 14: Total mean runoff (mm) for the three time periods: (a) 2005-2019 (b) 2020-2040 (c) 2041-2060 in the drinking water catchment.

6.1.3 Spatial Distribution of Runoff

Three points (A, B, C) in the catchment area, shown in Figure 15, were selected, and evaluated to show the spatial distribution of the total runoff between each point. Where point A is located at the outlet of the basin, B is in the ablation area of the glacier and C is located further up in the glacier's accumulation zone. For the period 2005 to 2019, point B consistently has the highest runoff values, the exception being where the meltwater runoff at point A surpassed that of point B in 2012. Whereas point C had the least amount of meltwater runoff of all three points. It was also observed that point B had the sharpest peaks of meltwater runoff, while the other two points had more gradual transitions into and out of the peak runoff values. From the results, shown in Figure 16, it is assessed that over the next five years (2020-2025) the amount of runoff from the three points is predicted to be similar to that experienced in the previous period, the amount being between a monthly mean of 500 to 1000 mm w.e. of runoff at one 30 m data point. In the follow-on period from 2026 to 2033 the runoff from point B is predicted to be between 1200 mm w.e to 2200 mm w.e. After 2033 the total runoff of the three points will be like the first observational period, at which in 2039 it starts to increase again for three more years. Looking beyond 2039, for the next 20 years the runoff values fluctuate, but continue to have greater runoff values than the first period. Overall, the largest runoff value occurs at point B in 2060, where its runoff amount approaches 2500 mm w.e.

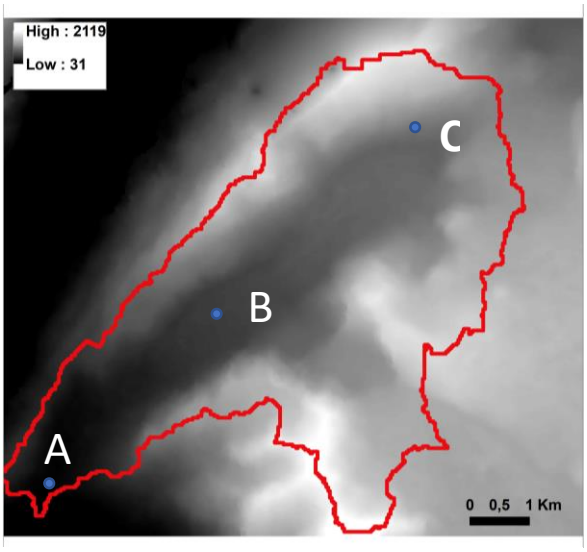

Figure 15: Locations of A, B, C, within the L-DWC plotted in Figure 16. GIMP DEM (in meters) as the background image.

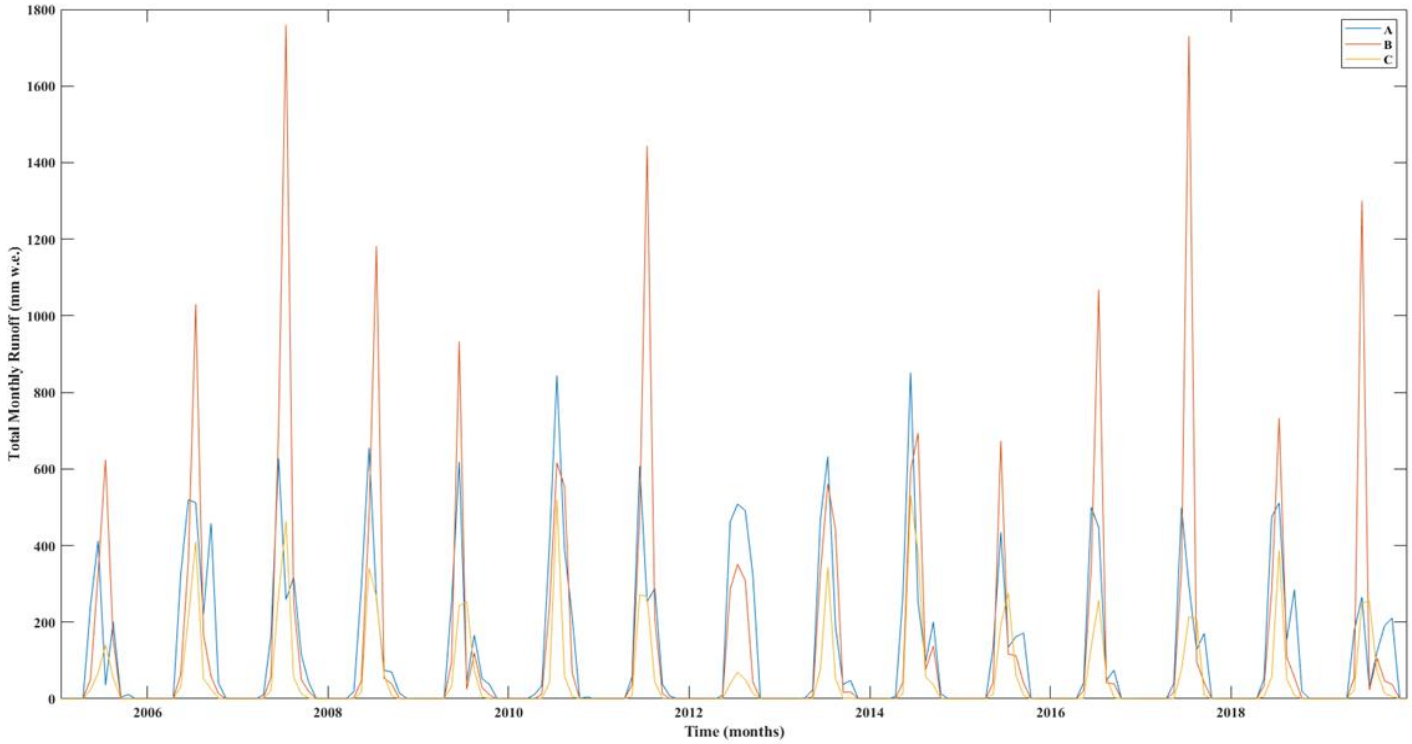
Total Monthly Runoff (mm w.e.)
Time (months)
A
B
C

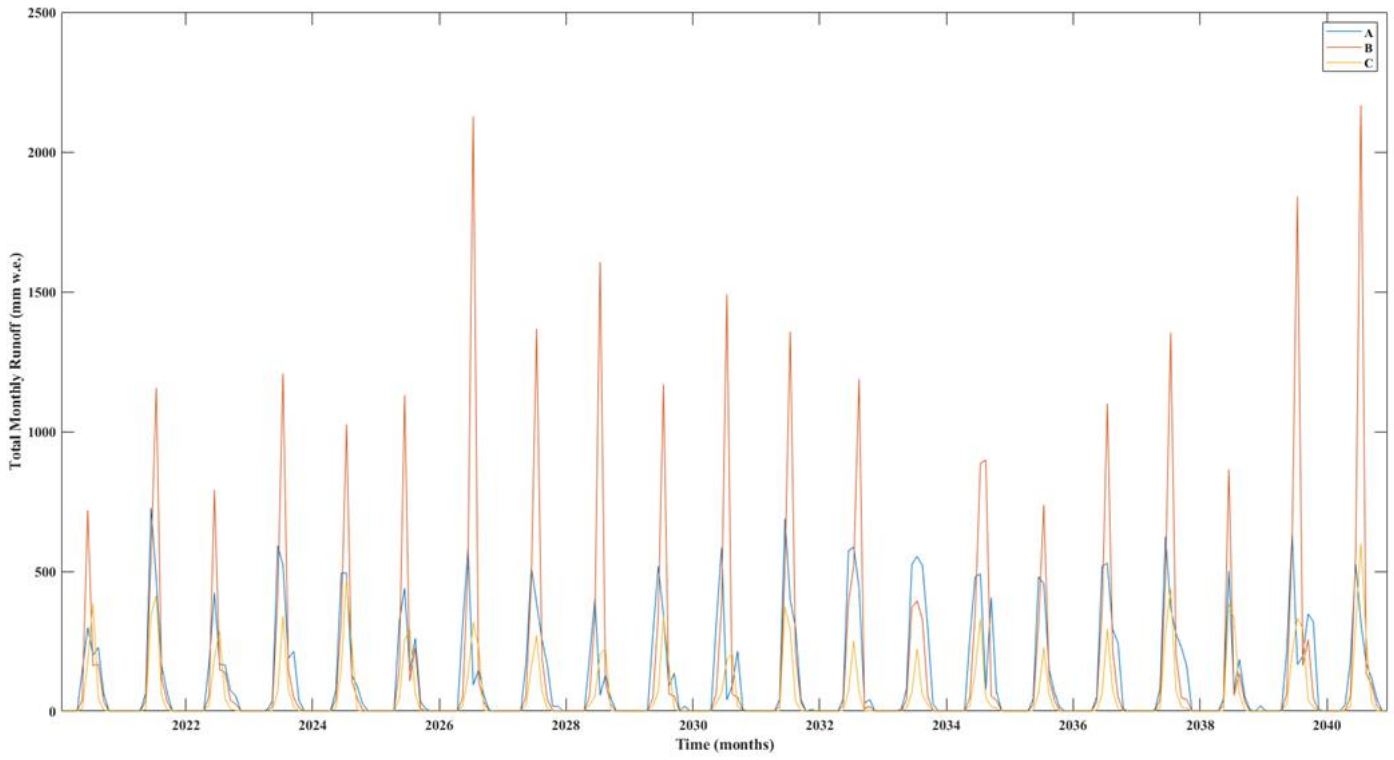
Total Monthly Runoff (mm w.e.)
Time (months)
A
B
C

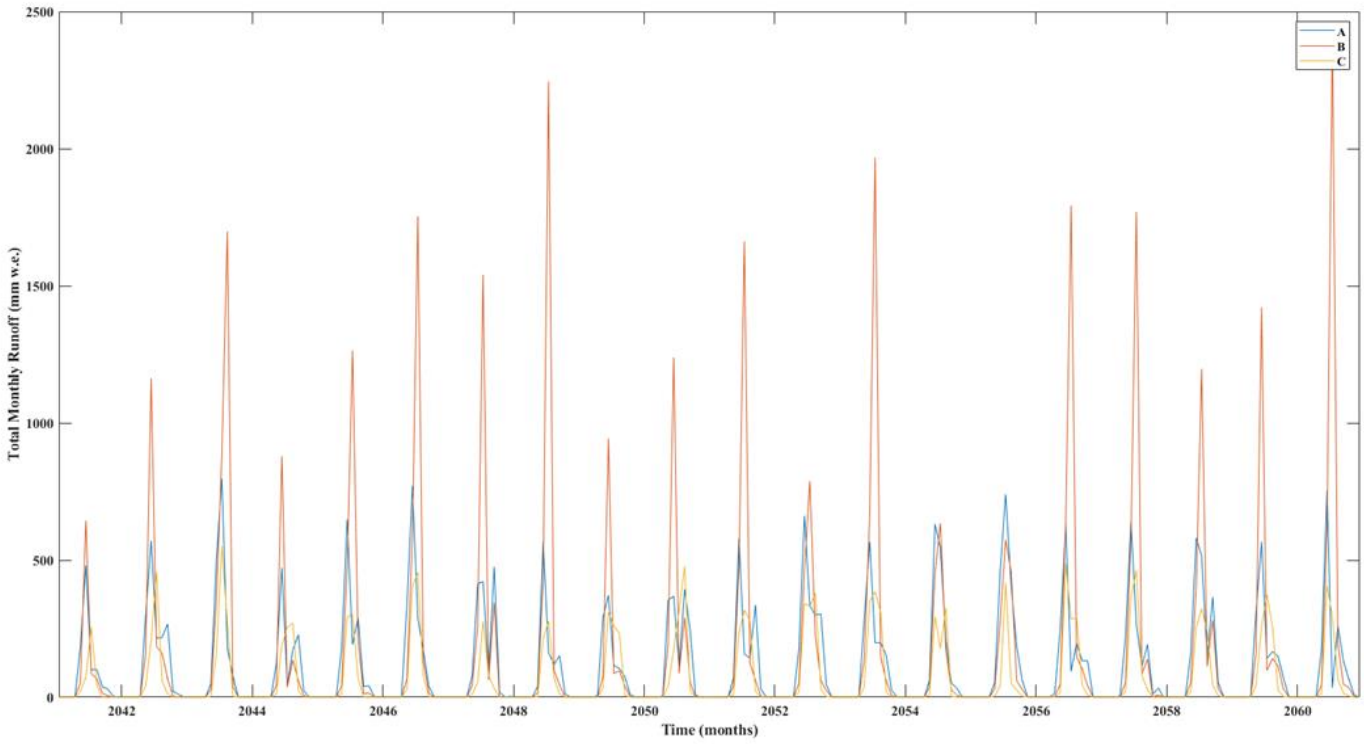

Figure 16: Total Monthly Runoff (mm w.e) at three different points in the catchment from 2005 to 2060 as depicted in Figure 15. The graphs from 2005 to 2019 and 2020 to 2041 are located on the previous page. Note the varying scales between the graphs.

6.1.4 Total Discharge

To estimate the volume of the runoff for the drinking water industry, the discharge from the catchment was also calculated and evaluated over time. The discharge from each cell of the basin was then summed for each year of the period and plotted in Figure 17. The discharge over the period 2005 to 2019 has a peak discharge in 2007 with 0.0121 Gt and a minimum in 2005 at 0.0051 Gt. In the period between 2020 and 2040 the values are similiar to that of the previous period with a slighltly greater peak discharge in 2040 of 0.0136 Gt, this is also the maximum for the whole period. The year directly after 2040 is a minimum peak discharge of 0.0065 Gt for the final period of 2041 to 2060 and a maximum of 0.0114 Gt in 2043. Through out all the years the peak discharge occured in the month of July. The discharge was similiarily calculated using the $RACMO_E$ dataset presented in Figure 18. The results of the discharge from $RACMO_E$ was in total greater than from the downscaled $RACMO_H$. The peak discharge year is in 2010 at a rate of 0.033 Gt per year.

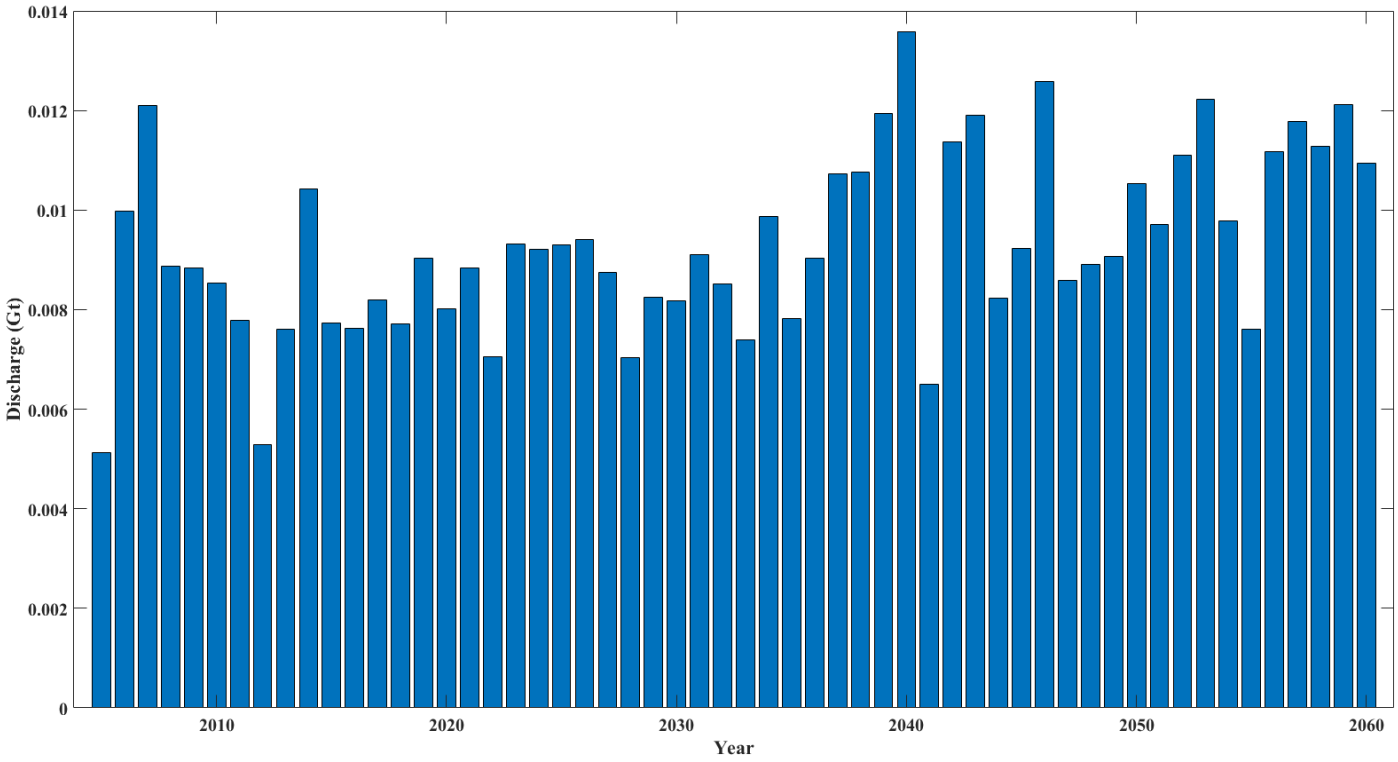

Figure 17: Yearly discharge (Gt) for the period 2005 to 2060 at the L-DWC catchment.

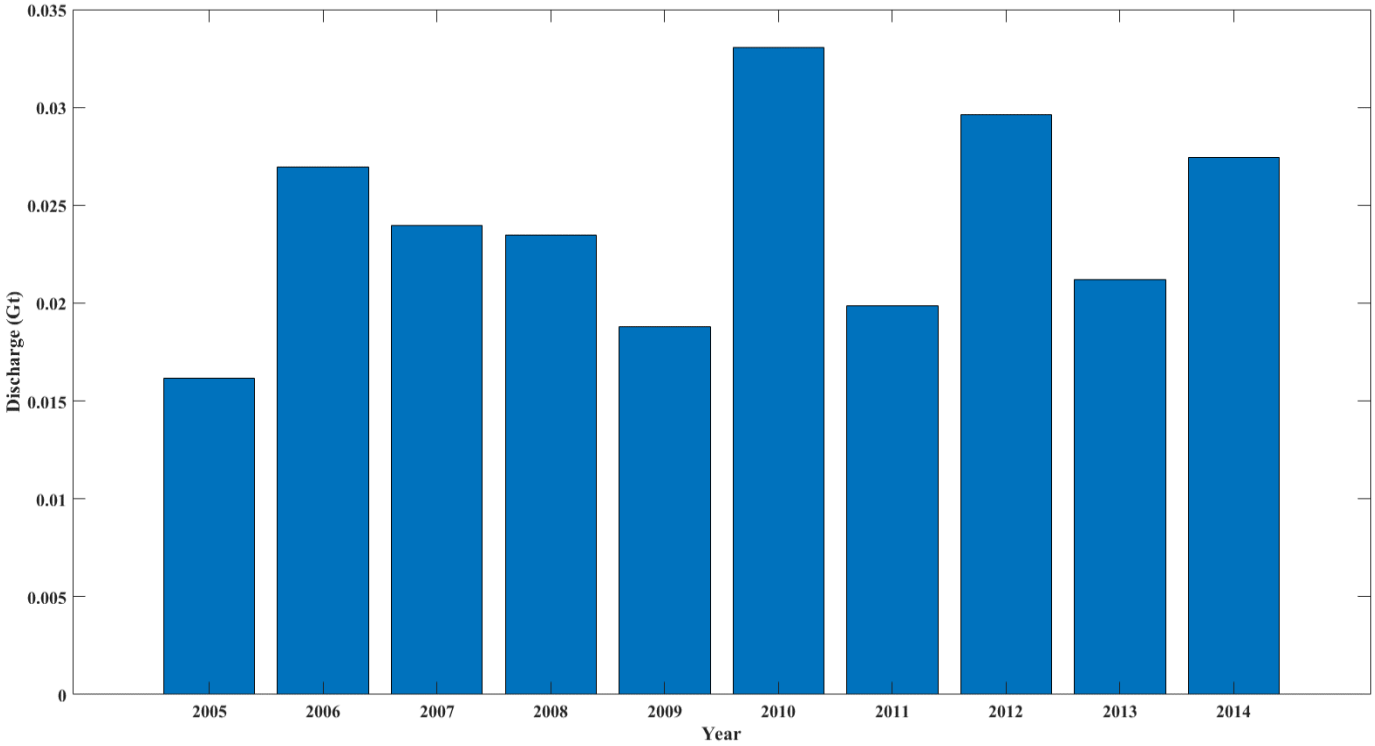

Figure 18: RACMOE discharge in Gt for 2005 to 2014.

7 Discussion

Recalling the underlying aim of this thesis, the meltwater runoff for the period of 2005-2060 was calculated using climate model data and a *positive degree day* (PDD) model. The *PDD* model developed for this project had to be validated against observed data. The challenge being that no observed data exists at location L-DWC, the catchment area of interest for this study, ergo *PDD* model validation had to be done using a suitable automatic weather station (AWS). The AWS at Zackenberg was selected, as it had extensive observational data and like L-DWC, it too, is a partially glaciated catchment. Once the *PDD* model was validated, it was then used to calculate the amount of future meltwater runoff.

The process to quantify the amount of runoff commenced with selecting the climate model that best replicates the observational data. Using a *statistical* downscaling method, air temperature and precipitation from $RACMO_H$ was downscaled from 11 kms down to a favorable resolution of 30 m. This downscaled data was subsequently run through the *PDD* model to calculate future meltwater discharge.

In the Discussion section that follows, climate model performance will be assessed based on the questions presented in the Thesis Objective outlined in the Introduction section. Each aspect will be addressed based on the findings of this paper and compared with other relevant studies. The limitations will also be presented in each section.

7.1 Climate Model Performance for Greenland

Many climate models exist for varying regions across the globe, whereas for Greenland only three RCMs are currently used (Fettweis et al., 2012). The results from these three and the two GCMs that force them at the boundaries were presented earlier in Chapter 4. A byproduct from the results has been the process used to choose a climate model deemed most feasible, to select the most appropriate one, based on the specifics of a study area in Greenland. Observational data is necessary to validate climate models and to determine their ability to predict future projections of climate more accurately. These projections, from validated climate models, have played and will continue to play an important part in being able to better predict and inform adaptation plans for future shifts in climate, where the potential effects resulting from them, such as: sea level rise, water shortages, increased severity of weather patterns and other global phenomena.

Therefore, an important aspect for this study was the need to evaluate existing climate models for Greenland. As the catchments are located near the boundaries and at small scales, it will be an RCM that is most realistically able to simulate conditions to the applicable scale of the catchment. In selecting the best one, it is also necessary to determine any uncertainties affecting runoff results stemming from the input data of the chosen climate model. However, the fact that these glacier catchments are placed near the boundaries of the RCM reconstructions, necessitates a thorough evaluation of the low-resolution GCMs used to force the RCMs, with respect to possible leakage of GCM biases into the RCM model domain.

The observational data obtained through PROMICE was used to evaluate the climate models. Although the PROMICE database captures the full breadth of weather variables, air temperature is the only one evaluated for this study, because it is the one weather variable that most affects the amount of meltwater runoff produced and the only input used for the *PDD* model (Braithwaite, 1995). The following subsections describe the analysis done to select the most suitable climate model and it then provides an explanation for discrepancies that still exist between the different models studied.

7.1.1 Temporal Comparison

Assessing the accuracy of climate models over the interannual cycle, for the purposes of calculating runoff from glacier catchments fringing the GrIS, is an important aspect when selecting the most appropriate one, particularly when determining runoff during the summer months. Of the five climate models selected for comparison, the three RCMs were assessed as being better when simulating Greenland's summer months as compared to the two GCMs. During the winter months, all five climate models would generally overpredict air temperature amplitudes, accentuating cold climate conditions.

When comparing the relative performance of each climate model, HadGEM would often overpredict extremely cold temperatures during the winter months and this was similarly reflected in the RCMs that were forced by it. In doing a similar comparison between the two RCMs receiving boundary conditions from HadGEM, $RACMO_H$ also overpredicts air temperature amplitudes during the cold months when comparing it to the outputs of MAR. In contrast, ECHAM had a more conservative simulation of the air temperature throughout Greenland, which was the same for HIRHAM. Of note, both ECHAM and HIRHAM best reflected Greenland's interannual cycles, but were often less able to recreate the extreme high and low temperatures within that cycle. To that end, given the significance of accurately

determining summer air temperatures for this study, both ECHAM and HIRHAM were assessed as not being as ideal when compared to the RCMs forced by HadGEM. Among the two remaining RCMs, $RACMO_H$ showed better agreement with the observational values in the summer months and a higher level of disagreement in winter. Overall, this reflected the general limitations of these climate models to reliably simulate the climate dynamics in Greenland, in which each exacerbated the air temperatures during the winter months.

Since the focus for this study is to select the best climate model that aligns with the ablation period, $RACMO_H$ was selected when compared with the other models.

7.1.2 Spatial comparison

Temperature patterns across Greenland's various regions are not uniform. In this section, a comparison between each will be made to better understand the dynamics that contribute to these heterogeneities. A map of all eight regions evaluated across Greenland is presented in Figure 19, with four examples used from KAN, QAS, KPC and SCO to help guide the discussion. From the results obtained in East Greenland, where the temperature range is less over the interannual cycle, climate model figures reflect the observed air temperature data more realistically. Moreover, due to the proximity of the GrIS and lower proportion of bare ground in the east, this combination contributes to a more stable temperature pattern (Stendel et al., 2008). At Tasiilaq, where the temperature ranges from -16.25 ^{o}C to 3.96 ^{o}C, climate models performed with a high level of accuracy, whereas, in the other regions, where larger air temperature range exist, climate model predictions are conversely less accurate. For example, the South West coast of Greenland experiences an air temperature range from -31.85 ^{o}C to 8.91 ^{o}C and is exposed to a larger influence of the sea surface temperatures, where circulation of warmer water along the coast prevents the formation of sea ice at the lower latitudes and hence drives a higher variability in winter temperatures. While on the East Coast of the island, the formation of sea ice during the winter months, creates a more stable temperature with a lower air temperature gradient between land and sea (Li et al., 2005). In the South of Greenland, at Qassimuit, $RACMO_H$ was assessed as the best performer out of all the regions in terms of replicating the interannual cycle when comparing it to the observational data. At this location, the air temperature ranges from -20.16 ^{o}C to 5.93 ^{o}C and represents a smaller span when comparing it with the temperatures at the South West stations in Greenland.

In general, my assessment of the five climate models across the various regions of Greenland revealed better performance at lower elevations when compared to the observational data obtained at higher ones. On reflection, this result was somewhat unexpected, as I intuitively figured that the RCMs would perform better at higher elevations due to the *dynamical downscaling* that is forced over finer resolution topography. The glacial runoff being modelled is located within the valley at lower elevations, which is typically below 1000m. This reinforces the selection of $RACMO_H$ as the most suitable CM for use in this study.

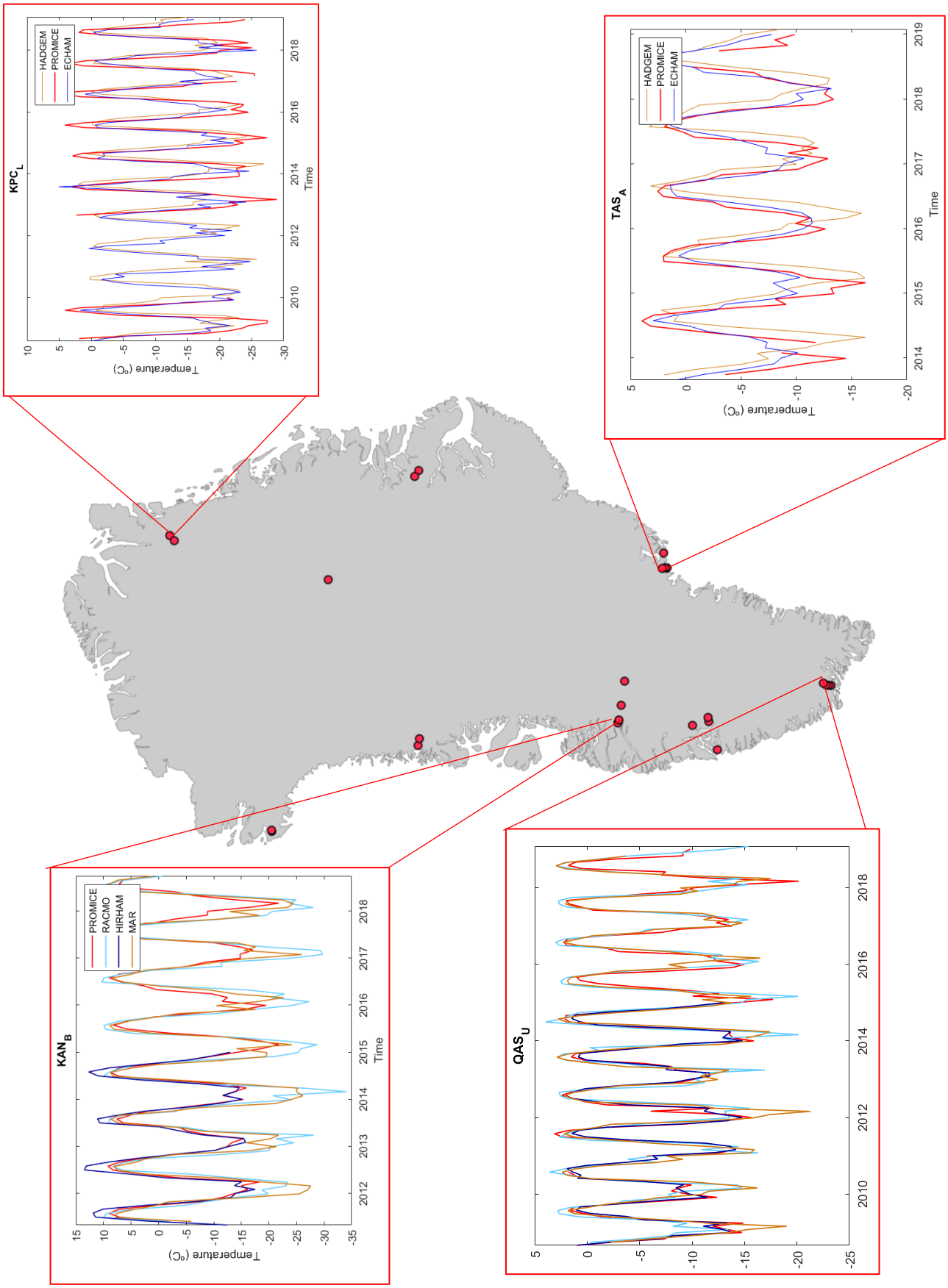

Figure 19: Eight regions in Greenland (red dots) discussed in Section 7.1.2. With examples from KAN, QAS, KPC and SCO, of the climate model air temperature data plotted with PROMICE data.

7.1.3 Possible Drivers of Difference Between Two RCMs

With $RACMO_H$ as the selected CM for this study, for completeness, this section takes a more in depth look between the regional models $RACMO_H$ and MAR as forced by HadGEM. Doing this will help provide a better understanding of the drivers of the differences between them.

The discrepancies between these two models can partially be explained in how they are set up and initialized. One differentiating factor is ice mask selection when simulating the climate over Greenland; MAR uses the ice mask from Bamber et al. (2013), whereas the ice masks produced from GIMP are adapted by $RACMO_H$. The ice mask product developed by Bamber et al. (2013) is part of a bed elevation dataset that includes a land surface mask created from aerial photography of the GrIS. This product differentiates between permanent ice and the tundra through the percentage of cells that were covered by ice. From Bamber et al.'s work, the combined errors of the land surface ice mask product are dependent on the distance from where the airplane photographed the landscape. The locations that were closer to the aircraft's flight path showed better results, whereas those areas photographed in the periphery, that were not on the direct flight path, had greater errors when extrapolating from the different flight path angles (Bamber et al., 2013). Furthermore, depending on how the ice mask coverage is depicted in the cell, it can have a large effect when comparing it to the climate simulation results (Vernon et al., 2013). The land and ice mask from GIMP used by $RACMO_H$ is derived from three geospatial products of existing DEMs: SPIRIT DEM, GDEM2 and Photo-Enhanced Bamber. Each of these geospatial datasets is described in Howat et al. (2014). The combined data products from the work done by Howat et al., have been validated with the ICEsat dataset and from their work the RMSE values were calculated to be 8.5 m over ice and 18.3 m over bare ground (Howat et al., 2014). The higher RMSE value for bare ground illustrates the complexities of interpreting the margins of Greenland, where steeper terrain presents a challenge when differentiating bare ground from ice.

In addition to factoring in the effect of ice masks on the two models, the differences produced by the various elevation models must also be taken into consideration. MAR uses the same ice mask dataset to produce elevation data from the work championed by Bamber et al., (2013). Their work was based on multiple airborne ice thickness surveys from 1970 to 2012, where they state error estimates that range from ±10 m to about ±300 m. In comparison,

RACMO used the 90 m GIMP DEM, where the overall RMSE value for Greenland was calculated to be 9.1 m when compared with the validation dataset of ICEsat (Howat et al., 2014). From this, it confirms the $RACMO_H$ produced dataset as being a better reflection of that observed.

Understanding that RCMs are forced by GCMs, when MAR and $RACMO_H$ are forced by HadGEM there are different biases in air temperatures when compared against each other. A study by Fettweis et al. found HadGEM to be the best GCM in producing the atmospheric circulation over Greenland, however a drawback is that it simulates an atmosphere that was too warm in the summer months. As a result, it overestimates the ice melt by a factor of two (Fettweis et al., 2012). However, this overestimation is not reflected in the RCMs when forced by HadGEM. When comparing $RACMO_H$ to HadGEM, $RACMO_H$ was assessed as being able to better simulate the interannual climate cycle. This difference in their respective outputs is due to the surface processes that are better accounted for in $RACMO_H$. The work done by van Angelen et al., showed that $RACMO_H$ produces a more realistic representation of snow albedo and reacts more sensitively to snow metamorphism at higher temperatures (van Angelen et al., 2013). This result is due to a *positive feedback* between higher temperatures and changes in the snow grain size that better captures the air temperature during the ice melt season. Furthermore, $RACMO_H$'s tendency to overestimate in the winter months was due to insufficient downward longwave radiation (Ettema et al., 2010). This observation in winter months has been equated to the difficulty in predicting cloud cover; the ability to do this is based on accurately predicting downward longwave radiation. Generally, what has been described when forcing $RACMO_H$ to HadGEM is similar when doing the MAR to HadGEM comparison (Fettweis et al., 2012)

Another important comparison when assessing MAR against $RACMO_H$ output is the grid cell resolution data. The resolution for the MAR grid cells are 25 km, whereas for $RACMO_H$ they are 11 km. Based on this, the spatial simulation of the climate is better resolved when using $RACMO_H$ and it more accurately captures the intricacies of both the landscape and the atmosphere at higher resolutions.

It can therefore be deduced from the analysis of the three drivers presented, that their differences as compared between MAR and $RACMO_H$ vary. What is important, is understanding the degree of difference between them to determine which performs better. $RACMO_H$ was assessed as having lower errors for both ice mask data and data derived

from digital elevation models, as well as a higher grid cell resolution output. In comparing these differences, $RACMO_H$ performs better than MAR.

7.1.4 Climate Model Intercomparison Conclusions

The right climate model selected is critical when studying specific areas within a vast territory such as Greenland. Factored into this selection, is dealing with the complexity to integrate other types of inputs that form part of the CM whole, such as: ice mask data, digital elevation models and grid cell resolution. In analyzing the various climate models, I agree with the other experts in this field, confirming that there is no overall one 'best-fit' RCM. For example, as stated by Stendel et al, each climate model has its degree of uncertainty when downscaling the RCMs, and from that, the notable variations in output from each, in their respective performance (Stendel et al. 2008). Internal differences exist in the representation of relevant physical processes and boundary conditions that may capture regional climate more realistically in one area or during one season, while causing less realistic results in other regions and during other time periods. Therefore, when conducting smaller scale modeling, it is important to consider the specific areas and temporal intervals of interest and from that verify which model performs best when comparing it to observational data. Alternatively, another approach is to use an ensemble of climate models to produce a wider range of the outputs.

For this study, in assessing the modeling requirements for reliable simulation over the winter month, neither models forced by HadGEM produced sufficiently reliable winter air temperatures. As a result, $RACMO_H$ was selected due to its better performance in summer months and at lower elevations, as well as the resulting lower errors in the ice mask data, lower errors in the digital elevation model and a higher resolution in the climate output grid cells when using this RCM.

7.2 Downscaling within catchments

The previous chapter presented the arguments that resulted in the selection of $RACMO_H$ as the most suitable RCM to be used for this study. However, even RCMs currently provide climate variables at the resolution, which is too low for resolving melt water runoff at the glacier catchment scale (11 km resolution for RACMOH and 25 km for MAR versus meter resolution required). Hence, the data from RACMOH needed to be downscaled to a high resolution of glacier catchments prior to it being fed into the PDD model. This subsection discusses the outcomes of *statistical* downscaling of air temperature for the catchment area

that can be upscaled to the island wide applications. Furthermore, I here analyze spatial variations in the major parameter of the *statistical* downscaling method, the slope lapse rates (SLR) across nine regions in Greenland to determine the values that are most representative of the areas under investigation.

7.2.1 Discussion of Downscaled Outputs

Inherently, there is a tremendous level of complexity whenever attempting to model the climate dynamics. As described (see Section 2.1.5), there are various methodologies that help illustrate the challenges in dealing with the complexities of nature and how each method deals with climate downscaling. Using the *statistical* method for this paper, the air temperature was downscaled to a fine of 30m, which is currently beyond the resolution enabled by dynamical downscaling methods. As shown earlier, the downscaled $RACMO_H$ was compared to that of the downscaled $RACMO_E$ to emphasize the improvements of the resolution enhanced temperature field as compared to the coarser resolution climate model output. As a result, the downscaling method enabled a significantly improved spatial representation of air temperature variations over the complex terrain with landforms, which are not adequately captured by the topographic boundary conditions of $RACMO_H$, such as fjords, mountains, and ice caps. These have become more distinguishable in the respective air temperature profiles and are assessed as being better resolved both spatially and temporally at low elevations. Furthermore, at the catchment in Zackenberg, when comparing downscaled $RACMO_H$ and 11 km $RACMO_H$ to observational data on the glacier, it was shown that large improvements were noted during the winter months. During the summer months it was also shown that downscaled $RACMO_H$ can replicate observations more accurately for all years except 2012 and 2013, both of which were rather exceptional in terms of heat waves and surface melt extents across Greenland.

Accounting for the differences between $RACMO_E$ and $RACMO_H$ could be due to an inaccurate SLR that was used to downscale the RCM data to the finer resolution. Again, as expected, better performance of the resolution enhanced dataset was also observed during summer months in both catchment areas over those in winter, due to the bias that has been inherited from the original $RACMO_H$ dataset. This analysis has therefore shown that *statistical* downscaling enables improvement in the RCM derived air temperature data when considering elevation at the catchment scale, although the results of downscaling can be further improved through the selection of more representative terrain-sensitive regional values for the SLR parameters.

7.2.2 Slope Lapse Rates in Greenland

To add more physical and dynamic variation to the *statistical* downscaling methods on regional scales, I have analyzed the spatial variability in its major parameter, SLR, based on the observational data for the warmest summer months, July, which is most relevant for the scope of the present study.

When calculating SLR there is a large uncertainty due to the presence of inversions during the period being calculated. This occurs when the normal profile of decreasing air temperature with elevation is inverted. Inversions occur when a warmer air layer sits over top a cooler one. To account for this process concerning daily time steps, the values with warmer air temperatures at higher elevations could be eliminated from the SLR calculation (Zhang et al. 2011). Since this study is working with monthly datasets, vice daily, it was not necessary to eliminate the warmer air temperatures at higher elevations. The study done by Gardner et al., (2009) supports the use of a SLR in summer, as they demonstrate a linear relationship between air temperatures in summer and less so in winter, when inversions can be more persistent. Gardner et al., provides an example of this when they calculated the slope lapse rates in the Canadian Arctic and found that the monthly mean air temperature correlated better with elevation in the summer than in winter. As a result, this observation is consistent with the relationship of a linear SLR during the summer months in Greenland. During the winter months in the Arctic, a persistent lower-tropospheric temperature inversion is observed creating lower SLRs than that recorded in the summer. Lapse rates can fluctuate on a diurnal scale, as well as a seasonal scale, and as a result it would be most appropriate to use a SLR that fluctuates over time. This is particularly true when dealing with the uncertainty of future climate change, as historically SLRs have changed over longer time periods between interglacials. A study from Erokhina et al. (2017) compared the SLR over the GrIS from the Holocene and the Last Glacial Maximum (LGM), which represent two extreme states of climate during the last glacial cycle and showed that their SLRs vary significantly when compared to each other. For instance, during the LGM the SLR was 0.85 - 1.71 ^{o}C/km above interglacial values and had great variations in lapse rates during the late winter. Conversely, in the early Holocene, pre-industrial, and the observational period, they found larger differences between the autumn and spring months for the SLRs (Erokhina et al., 2017). Concluding that the relationship between SLR and elevation would remain the same, would be an oversimplification and becomes a limitation to be factored into this thesis (Praskievicz, 2018).

Using a SLR that varies spatially acknowledges that it is a variable that typically has large fluctuations from region to region and over time. In doing this, the process of calculating the SLR in the nine regions selected across Greenland produced noteworthy results.

The SLR results from the two stations, SCO (-2.3 °C/km) and TAS (-2.2 °C/km), located along the East Coast of Greenland and the most Southern stations, QAS, (-2.3 °C/km) produced the lowest July SLR, while higher SLRs were observed along the Western Coast of Greenland. The high July SLR from several of the more coastal stations, such as NUK (-5.1 °C/km) and UPE (-4.8 °C/km), were more prone to inversions during the summer months due to effects from being in proximity to the sea. As a result, contributing to the likelihood that artificially high SLRs were being produced in these areas. Whereas, for the stations that were more inland, such as KAN (-6.3 °C/km), KPC (-5.6 °C/km), SCO (-2.3 °C/km), they were less affected by inversions and were assessed as likely being truer predictions of the SLRs. Furthermore, colder air temperatures were creating high SLRs, this was reflected at the KAN stations where large temperature ranges were observed.

The automatic weather station (AWS) setup for the PROMICE and GC-NET programs are used to monitor the GrIS and are in proximity to or on the ice sheet. This creates a limitation for the calculation of the SLRs, as there is a lack of AWSs within valley systems in Greenland (Abermann et al., 2019). Although the AWS setup through PROMICE differs in elevation over space, the AWSs are mainly located over the GrIS and there are subsequent implications for the dynamics of the weather when air masses are travelling over ice as opposed to bare ground. Not being able to obtain more accurate SLR within mountain valley systems in Greenland is therefore assessed as a limitation. However, in this study I use air temperature data to capture the air temperature variability above the ice surface more accurately since air temperature over an ice surface is always fixed at zero during ablation months (Gardner et al. 2009).

Another key aspect underpinning the selection of SLR values for downscaling is the effect of continentality as presented by Taurisano et al. (2004), where they studied the differences in air temperature and precipitation between the AWS in Nuuk fjord situated on the coast to that of an AWS located 115 km in-land and 700 m higher in elevation. The results of this work reflect large spatial temperature gradients between stations located on the coast versus those that are inland. Their study also emphasized that lapse rates can change over time.

Given the above considerations and the proximity of the KAN stations to the area of where the downscaling and runoff modeling are tested, I have adapted the SLR estimates from the KAN region within the catchment at L-DWC.

7.2.3 Downscaling Conclusions

In sum, this section presented the discussion of the results of *statistical* downscaling of air temperature. Of the three methods mentioned earlier (*dynamical*, *hybrid* and *statistical*) the *statistical* downscaling one was selected as being feasible for resolving air temperature at fine resolution required by this study, with an outlook for the future possibilities to extend its applications to the glacier systems across the entire island. The ability to equitably compare between the three downscaling methods was not fully pursued due to the complexity and limitations articulated earlier. Nevertheless, the outcome of the *statistical* downscaling method used, did show significant improvements for coarse resolution outputs obtained from climate models. For the purposes of this study, the *statistical* downscaling method was deemed sufficient in advancing the follow-on work for this project. To add a dynamic region-specific component to the downscaling, the major parameter of the downscaling method, SLR, was calculated based on observations from the nine regions across Greenland. Although more needs to be done to improve these preliminary SLR estimates given the scarcity of observation data along Greenland's coast and the potential impacts of inversions.

7.3 Meltwater Runoff

The last section in this chapter addresses whether future meltwater runoff is assessed as being a viable resource to be extracted in the long-term. Here I discuss the *PDD* model, including its major parameters, and the results of the runoff modeling demonstrated for an exemplary case of the catchment area located at L-DWC.

7.3.1 PDD Validation

The melt model (using *PDD*), developed as part in this thesis, was used to quantify the meltwater runoff from the drinking water catchments. *PDD* models, as discussed in the introduction, are commonly used for calculating meltwater runoff from glaciers, regardless of their simplicity and limitations. Such models are based on a simple statistical method that uses air temperature as an input to determine the amount of runoff based on the sum of days and degrees above zero in a certain month. The *PDD* sum is multiplied by the snow and ice melt factors to determine meltwater in mm. The melt factors are known to vary across regions and are often used as tuning factors for calibrating the model (Wake and Marshall,

2015). Given that there is no observational data in the catchment areas, the melt factors were taken from literature to apply to these catchments. Measured ice and snow factors vary significantly through time and space, ranging from 2.7 mm $^{o}C^{-1}$ d^{-1} to 11.6 mm $^{o}C^{-1}$ d^{-1} for ice and 5.5 mm $^{o}C^{-1}$ d^{-1} to 20 mm $^{o}C^{-1}$ d^{-1} for snow. While 8.8 mm $^{o}C^{-1}$ d^{-1} for ice and 2.8 mm $^{o}C^{-1}$ d^{-1} for snow has observational support for the GrIS (Wake and Marshall, 2015). The standard deviation used in the calculation of the *PDD* sum is also known to change over space and time and is observed as being lower in the ablation areas of the GrIS, and similarly during the summer months for local glaciers and ice caps. Therefore, a growing number of studies have incorporated a temporally and spatially varying standard deviation (Wake and Marshall, 2015, Rogozhina and Rau, 2014). With the lack of observational data in the catchment, the closest AWS was selected for this thesis to calculate the standard deviations of air temperature throughout the summer months. Based on my calculations from observational data, an average value of 2.5 ^{o}C standard deviation was calculated for the summer months which is lower than the commonly used fixed values of standard deviation of 4.5- 5 ^{o}C that have been applied in previous studies (Fausto et al., 2009, Calov and Greve, 2005, and Janssens and Huybrechts et al., 2000), but is similar to the values inferred from climate reanalysis by Rogozhina and Rau (2014) along the GrIS margins.

As explained earlier (Section 3.7), the calculation of the *PDD* sum was validated through observational data from the Zackenberg area using a *statistical* method to determine *PDD* sums from hourly air temperature data in the catchment. This then yielded good agreement between the three methods (see Section 3.7). Among these, the largest deviation of 10 ^{o}C days is observed in the model by Calov and Greve (2005) during the year 2014. The above validation approach is based on the work done by Braithwaite (1995), who calculated *PDDs* from both Switzerland and Western Greenland and used a simple method with the observed values that were compared against the calculated *PDD* sums using a *statistical* method. His findings at Qamanarssup Sermia showed quite good agreement between the calculated and observed values (Braithwaite, 1995). Therefore, it can be concluded that the *PDD* sums as calculated in this study are deemed to be sufficiently accurate in determining meltwater runoff from the $RACMO_H$ air temperature dataset.

7.3.2 Runoff in the Near Future

Determining the runoff in the foreseeable future is a key aspect for the scope of this thesis. In Chapter 6, I presented the runoff results over the next 40 years and determined that the calculated amount available for drinking water export will continue increase over the highlighted timeframe. Over this period, the summer air temperatures are predicted to stay within a similar range as during the historical period since 2005. In addition, the winter air temperatures are predicted to increase and ablation season to extend, representing an important reason for a subsequent increase of future meltwater runoff. As observed during the reference period (2005 to 2014), when calculating the *PDD* runoff results of $RACMO_{H}$ can be shown that its values are underestimated when compared to that of $RACMO_{E}$. Specifically, downscaled $RACMO_{H}$ is underpredicting this discharge by a factor 2.5 to 5, depending on the year. This was expected as when comparing the downscaled air temperatures, $RACMO_{E}$ was often a few degrees warmer than $RACMO_{H}$ during the ablation period meaning that the projected discharge represents a conservative estimate for future runoff and could likely be two to five times greater than that calculated. This result reflects by the insufficient quality of RCMS when forced by GCMs and supports the need to further validate RCMs across other regions in Greenland.

Furthermore, other factors that have not been accounted for in this study will need to be considered when more accurately calculating future meltwater runoff. The two principal ones being: glacial retreat and the snowpack. With warming temperatures contributing to glacial retreat, the quantity of ice that will melt will be somewhat lessened in the future as ice-covered areas shrink. Bjørk et al. (2018) calculated that Periphery Glaciers and Ice Caps (PGIC) have been retreating at 16.6 m per year in the West of Greenland. This means that the glaciers in the catchment area of interest, L-DWC (which has a length of 4 km), will continue to produce meltwater runoff at an increasing rate over the next four decades, but potentially over a smaller area. Of note and adding to this, with warmer winter months, runoff will increase further due to precipitation occurring in the form of rain as opposed to it being stored as firn (Vandecrux et al., 2018) and the associated decrease in the surface albedo will further accelerate surface melting during the early stage of the ablation seasons. Furthermore, warming temperatures will also cause melting of the snowpack, and coupled with an increase in precipitation, will result in these both contributing to an increase in the amount of runoff being produced.

7.3.3 Broader Implications of Increasing Meltwater Runoff

As was outlined earlier, the runoff produced from glacial melt is an important source that contributes to the global rise in sea level. Another known phenomenon of concern from this runoff is the effect that it has on ocean currents, freshening of the seawater and the subsequent impact it has on the marine ecosystems. Studies have shown that the Arctic Ocean has significantly increased its freshwater content, within the past decade due to accelerating climate change from melting sea ice, glaciers, ice sheet, and ice caps (Sejr, 2017, Dukhovskoy, 2019). Specifically, a study from Northeast Greenland has shown that the accelerated melting of glaciers could influence deep water convection, due to the reduced density of water in the Sub-Arctic Ocean (Sejr, 2017). The salinity of the oceans has varied over the Earth's geological history. As recently as 8200 years ago, a freshening of the Atlantic Ocean occurred during the terminal stage of the Laurentide Ice Sheet disintegration in North America. The effect from this was a rapid cooling between 1 ^{o}C to 3 ^{o}C in the Northern Hemisphere resulting from the freshening of the Labrador Sea and a subsequent a slowdown in the Atlantic Meridional Overturning Circulation (AMOC) (Lochte et al., 2019), the thermohaline circulation system that transports warm seawater from the southern oceans, northward.

An additional benefit from the methodology used in this study in determining the amount of meltwater runoff and providing local validation of climate model projections could be further exploited across all similar small-scale catchments in Greenland. The figures obtained from this work could then be used to inform the studies used to determine the rate of freshening that affects the slowdown of the AMOC. Industries that are reliant on the marine ecosystems would benefit from the insight it could provide.

7.3.4 Uncertainties in the *PDD* model

The simplicity of the *PDD* model, which only accounts for air temperature impacts on surface melting and does so through a statistical relation utilizing largely unconstrained parameters, implies certain limitations to this method and the results derived from it. These include variations in local conditions that are not adequately reflected in the static melt factors. The melt factors can change depending on the slope, aspect, surface roughness and local weather conditions (wind, cloud cover and humidity), which are important contributors to the total sum of melt (Wake and Marshall, 2015). Other physical characteristics, such as the presence of firn, have different properties of albedo and meltwater retention (Shea et al., 2009), which are not accounted for within the *PDD* model developed in this thesis. Finally, the ice masks within the catchments are assumed to be constant in time, which is not the case, as the

geometry of the glacier changes over time as it melts. To account for these complex processes, one would need to use a dynamic glacier model coupled to surface energy and snowpack models, which is unfeasible given the temporal limitations and format of a master study and is therefore outside its scope.

7.3.5 Meltwater Runoff Conclusion

This final section of the thesis demonstrates the runoff from the selected drinking water catchment to be a long-term resource for drinking water for export purposes. The monthly *PDDs* were validated against observations and used to calculate the melt across the catchment, using varying melt factors for snow and ice. Although the absolute values of projected melt rates should be treated with caution due to several limitations that could cause errors in the quantification of the melt rates, the approach proposed here has allowed for a significant insight into the inadequate quality of the RCM projections currently available for Greenland and enormous impacts of climate model inaccuracies on local projections of the surface melt. Such inaccuracies should therefore be treated with priority, before an adaptation of more complex, computational demanding workflows for local downscaling of climate variables and calculation of meltwater trends within catchments is justified.

8 Conclusion

As the temperature of the planet continues to rise, it will have both debilitating consequences as well as some beneficial outcomes and regardless of outcomes adaptation to these changing conditions will be necessary. The fact that humanity must deal with rising sea levels and degrading marine ecosystems has grown in importance over the last few decades, with an accelerating importance of it not only capturing much of the media headlines, but it has been an increasing area of focus for science and scientific research. As a result, from the growing body of knowledge and research work that has emerged from it, the world has developed a better understanding of climate change around the globe in determining what has occurred well before to help us better understand what is likely to occur in future. The significance of better understanding the future is that it will better inform decision making, so humankind is able to minimize any devastating impact, while taking advantage of opportunities in preparing for what may lie ahead.

Throughout the progression of climate change, Greenland has been prominent in the conversation. This is understandable given the important role Greenland's ice masses play in contributing to the planet's climate due to their location, size, and the impacts from the meltwater produced. Greenland has attracted a significant amount of scientific research over the last half century and continues to do so. This research has predominantly been focused on the Greenland Ice Sheet (GrIS), whereas less scientific attention has been devoted to the study of Periphery Glaciers and Ice Caps (PGIC).

In contributing to this growing body of scientific knowledge, this thesis adds to better understanding of the anticipated responses of PGIC to climate change, by developing a workflow for a validation of regional climate model (RCM) projections on local scales and obtaining the meltwater runoff from the small catchment areas. Different stages of the workflow are tested and validated across disparate spatial scales, zooming into a catchment in Southwest Greenland, where all workflow stages are sequentially applied to estimate the future viability of the amount of drinking water. While contributing to the overarching objective of the thesis, the methods and results of this study address the three initial research questions:

(1) How well do climate models simulate climate in Greenland on local scales?

(2) Do regional climate models and their downscaled products replicate observations from weather stations more accurately than coarse resolution global climate model outputs?

(3) Is the selected drinking water site viable for a consistent long-term extraction of this resource?

By answering these research questions, the present study enables a better understanding of the climate model skills to simulate the present-day and future climate conditions along the periphery of Greenland, as well as the future effects of climate change on partially glaciated catchment areas and local meltwater production.

From this study, the regional climate model, RACMO, was selected as best suited when compared amongst the three RCMs used in Greenland and the two global climate models that forced these RCMs at the lateral boundaries of model domains. Of note, climate model intercomparison showed that all climate models overpredicted air temperature during the winter months, but were shown to perform better in summer, which coincides more favorably with the period of interest for this study. Regardless of the above climate model inaccuracies leaking into the generated outputs of *statistical* downscaling, the new resolution-enhanced products have been found to capture air temperature variations on local scales more accurately than the non-downscaled ones. Stemming from the *positive degree day* model that was particularized for this study, the meltwater discharge rate calculated for one of the potential drinking water sites selected by GEUS, indicates that over the next forty years it will be a commercially viable resource with a peak discharge rate of 0.0136 Gt occurring in the year 2040. An important conclusion that emerges from this is the viability in harnessing the vast amount of drinking water that is being and will continue to be produced. If applied over larger scales along the periphery of Greenland, an exploitation of meltwater runoff for industrial purposes will simultaneously contribute to the UN sustainable goal on water security and reduce impacts of freshwater discharge on the ocean circulation and marine ecosystems.

Given the limitations of the methods used within the study, its results should be used as a first order estimate in determining the future runoff potential from PGIC catchments in Greenland. Nevertheless, the presented workflow has clearly demonstrated the worth of this relatively simple approach, namely the use of the *positive degree day* model and *statistical* downscaling, for the validation of climate model projections on local catchment scales and the need to

prioritize improvements of such projections to justify the use of more complex, computationally demanding methods for downscaling and modeling. When comparing air temperatures from the best performing RCM ($RACMO_H$) to the dynamically downscaled reanalysis dataset ($RACMO_E$), it had an underestimation of meltwater runoff by a factor of 2.5 to 5 during the observational period. Results from this thesis provide an in depth look at one catchment in Greenland, but the inferred trend of increasing runoff in the future aligns with other studies that have also shown similar trends regarding the changing state of glaciers and ice caps around the world. This means that as the Earth's climate continues to warm, the ability to quantify meltwater runoff from the world's glaciers and ice caps is of utmost importance in adaptation strategies for its future impacts on freshwater availability, sea level rise and seawater freshening, including its effects on ocean currents and the marine ecosystems.

From a climate change perspective, it is understood that what is happening in Greenland will be a significant driver of global change that will greatly affect the future of the planet. The work emanating from this study is contributing to the existing body of knowledge that has amassed and as it pertains to the less observed phenomena around PGIC.

References

Abermann, J., Van As, D., Wacker, S., Langley, K., Machguth, H., & Fausto, R. S. (2019). Strong contrast in mass and energy balance between a coastal mountain glacier and the Greenland ice sheet. *Journal of Glaciology*, *65*(250), 263-269.

Ahlstrøm, A. P., Albers, C. N., Andersen, S. B., Andresen, C. S., van As, D., Citterio, M., Fausto, R. S., Hansen, K., Hasholt, B., Johnsen, A, R., Kjeldsen, K, K., Solgaard., A, M. (2018). Greenlandic Ice Cap Water: Technical Report on five potential locations for meltwater export. *Danmarks og Grønlands Geologiske Undersøgelse Rapport 2018/29.*

Ahlsrøm, A.P., Albers, C.N., Kjeldsen, K.K., Johnsen, A.R., Larsen, S.H., Lisager, P., Nauta, M., Mankoff, K.D., Bech, T.B., Hasholt, B., Hallé, D., Hansen, K., Andersen, S.B., Andresen, C.S., Citterio, M., Fausto, R.S., & Solgaard, A.M. (2019). Greenlandic Ice Cap Water: Technical Report on five potential locations for meltwater export for the 2nd licensing round. *Danmarks og Grønlands Geologiske Undersøgelse Rapport 2019/39.*

Ahlstrøm, A.P. (1999). *Coupled Ice Sheet-Geodynamics Model Applied to West Greenland.* MSc Thesis. University of Copenhagen, Copenhagen.

Andersson, M., & Erikson, E. (2018). The Ability of Regional Climate Models to Simulate Weather Conditions on Nordenskiöldbreen, Svalbard. Independent Project at the Department of Earth Sciences. Uppsala Universitet.

Arnold, N. S., Willis, I. C., Sharp, M. J., Richards, K. S., & Lawson, W. J. (1996). A distributed surface energy-balance model for a small valley glacier. I. Development and testing for Haut Glacier d'Arolla, Valais, Switzerland. *Journal of Glaciology*, *42*(140), 77-89.

Bamber, J. L. , Griggs, J. A. , Hurkmans, R. T. W. L. , Dowdeswell, J. A. , Gogineni, S. P. , Howat, I. , Mouginot, J. , Paden, J. , Palmer, S. , Rignot, E. and Steinhage, D. (2013): A new bed elevation dataset for Greenland , The Cryosphere, 7 (2), pp. 499-510

Bellouin, N., Collins, W. J., Culverwell, I. D., Halloran, P. R., Hardiman, S. C., Hinton, T. J., McDonald, R.E., McLaren, A.J., O'Connor, F.M., Roberts, M. J., Rodriquez, J.M., Woodward, S., Best, M.J, Brooks, M.E., Brown, A.R., Butchart, N., Dearden, C., Derbyshire, S.H., Dharssi, I., Dountriaux-Boucher, M., Edwards, J.M., Falloon, P.D, Gedney, N., Gray, L.J., Hewitt, H.T., Hobson, M., Huddleston, M.R., Hughes, J., Ineson, S., Ingram, W.J., James, P.M, Johns, T.C., Johnson, C.E., Jones.A., Jones, C.P., Joshi, M.M., Keen, A.B., Liddicoat, S., Lock, A.P., Maidens, A.V., Manners, J.C., Milton, S.F., Rae, J.G.L., Ridley, J.K., Sellar, A., Senior, C.A., Totterdell, I.J., Verhoef, A., Vidale, P.L. & Wiltshire, A.

(2011). The HadGEM2 family of met office unified model climate configurations. *Geoscientific Model Development*, *4*(3), 723.

Bjørk, A. A., Aagaard, S., Lütt, A., Khan, S. A., Box, J. E., Kjeldsen, K. K., Larsen, N.K., Korsgaard, N.J., Cappelen, J., Colgan, W.T., Machguth, H., Andresen, C.S., Peings, Y. & Kjær, K.H. (2018). Changes in Greenland's peripheral glaciers linked to the North Atlantic Oscillation. *Nature Climate Change*, *8*(1), 48-52.

Bolch, T., Sandberg Sørensen, L., Simonsen, S. B., Mölg, N., Machguth, H., Rastner, P., & Paul, F. (2013). Mass loss of Greenland's glaciers and ice caps 2003–2008 revealed from ICESat laser altimetry data. *Geophysical Research Letters*, *40*(5), 875-881.

Box, J. E., & Rinke, A. (2003). Evaluation of Greenland ice sheet surface climate in the HIRHAM regional climate model using automatic weather station data. *Journal of climate*, *16*(9), 1302-1319.

Braithwaite, R. J. (1995). Positive degree-day factors for ablation on the Greenland ice sheet studied by energy-balance modelling. *Journal of Glaciology*, *41*(137), 153-160.

Calov, R., & Greve, R. (2005). A semi-analytical solution for the positive degree-day model with stochastic temperature variations. *Journal of Glaciology*, *51*(172), 173-175.

Cappelen, J. (2019). Greenland-DMI Historical Climate Data Collection 1784-2018. *DNI Report 19-04*.

Christensen, O. B., Drews, M., Christensen, J. H., Dethloff, K., Ketelsen, K., Hebestadt, I., & Rinke, A. (2007). The HIRHAM regional climate model. Version 5 (beta).

Collins, W. J., Bellouin, N., Doutriaux-Boucher, M., Gedney, N., Halloran, P., Hinton, T., Hughes, J., Jones, C.D., Joshi, M., Liddicoat, S., Martin, G., O'Connor, F., Rae, J., Senior, C., Sitch, S., Totterdell, I., Wiltshire, A. & Woodward, S. (2011). Development and evaluation of an Earth-System model–HadGEM2. *Geosci. Model Dev. Discuss*, *4*(2), 997-1062.

Dimri, A. P. (2009). Impact of subgrid scale scheme on topography and landuse for better regional scale simulation of meteorological variables over the western Himalayas. *Climate dynamics*, *32*(4), 565-574.

Dukhovskoy, D. S., Yashayaev, I., Proshutinsky, A., Bamber, J. L., Bashmachnikov, I. L., Chassignet, E. P., et al. (2019). Role of Greenland freshwater anomaly in the recent freshening of the subpolar North Atlantic. Journal of Geophysical Research: Oceans, 124, 3333–3360.

Durand Y, Brun E, Merindol L, Guyomarch G, Lesaffre B, Martin E (1993) A meteorological estimation of relevant parameters for snow models. Ann Glaciol 18:65–71

Edward, H., Pattyn, F., Navarro, F., Favier, V., Goelzer, H., van den Broeke, M. R., Vizcanio, M., Whitehorse, P.L., Ritz, C., Bulthuis, K., & Smith, B. (2019). Mass balance of the ice sheets and glaciers–progress since AR5 and challenges. *Earth-science reviews.*

Erokhina, O., Rogozhina, I., Prange, M., Bakker, P., Bernales, J., Paul, A., & Schulz, M. (2017). Dependence of slope lapse rate over the Greenland ice sheet on background climate. *Journal of Glaciology*, *63*(239), 568-572.

Ettema, J., Van den Broeke, M. R., Van Meijgaard, E., Van de Berg, W. J., Box, J. E., & Steffen, K. (2010). Climate of the Greenland ice sheet using a high-resolution climate model-Part 1: Evaluation. *The Cryosphere*, *4*(4), 511-527.

Fausto, R. S., Ahlstrøm, A. P., Van As, D., Bøggild, C. E., & Johnsen, S. J. (2009). A new present-day temperature parameterization for Greenland. *Journal of Glaciology*, *55*(189), 95-105.

Fettweis, X., Box, J. E., Agosta, C., Amory, C., Kittel, C., and Gallée, H.: Reconstructions of the 1900–2015 Greenland ice sheet surface mass balance using the regional climate MAR model, The Cryosphere Discuss., doi:10.5194/tc-2016-268, in review, 2016.

Fettweis, X., Franco, B., Tedesco, M., Van Angelen, J. H., Lenaerts, J. T., van den Broeke, M. R., & Gallée, H. (2012). Estimating Greenland ice sheet surface mass balance contribution to future sea level rise using the regional atmospheric climate model MAR. *Cryosphere discussions*, *6*, 3101-3147.

Fiddes, J., & Gruber, S. (2014). TopoSCALE v. 1.0: downscaling gridded climate data in complex terrain. *Geoscientific Model Development*, *7*(1), 387-405.

Finsterwalder, S. and H. Schunk. (1887). Der Suldenferner Zeitschrift des Deutschen und Osterreichischen Alpenvereins 18, 72-89.

Gardner, A. S., Sharp, M. J., Koerner, R. M., Labine, C., Boon, S., Marshall, S. J., Burgess, D.O., & Lewis, D. (2009). Near-surface temperature lapse rates over Arctic glaciers and their implications for temperature downscaling. *Journal of Climate*, *22*(16), 4281-4298.

Giorgi, F., Francisco, R., & Pal, J. (2003). Effects of a subgrid-scale topography and land use scheme on the simulation of surface climate and hydrology. Part I: Effects of temperature and water vapor disaggregation. *Journal of Hydrometeorology*, *4*(2), 317-333.

Hanna, E., Huybrechts, P., Cappelen, J., Steffen, K., Bales, R. C., Burgess, E., McConnell, J.R., Steffensen, J. P., Broeke, M.V, Wake, Leanne, W., Bigg, G., Griffiths, M., & Savas, D. (2011). Greenland Ice Sheet surface mass balance 1870 to 2010 based on Twentieth Century Reanalysis, and links with global climate forcing. *Journal of Geophysical Research: Atmospheres*, *116*(D24).

Hewitson, B. C., & Crane, R. G. (1996). Climate downscaling: techniques and application. *Climate Research*, *7*(2), 85-95.

Howat, I.M., A. Negrete, and B.E. Smith, 2014, The Greenland Ice Mapping Project (GIMP) land classification and surface elevation datasets, *The Cryosphere*, 8, 1509-1518, doi:10.5194/tc-8-1509-2014.

Hostetler, S. W., Alder, J. R., & Allan, A. M. (2011). Dynamically downscaled climate simulations over North America: Methods, evaluation, and supporting documentation for users (No. 2011-1238). US Geological Survey.

Jacob, T., Wahr, J., Pfeffer, W. T., & Swenson, S. (2012). Recent contributions of glaciers and ice caps to sea level rise. *Nature*, *482*(7386), 514-518.

Janssens, I., & Huybrechts, P. (2000). The treatment of meltwater retention in mass-balance parameterizations of the Greenland ice sheet. *Annals of Glaciology*, *31*, 133-140.

Jarosch, A. H., Anslow, F. S., & Clarke, G. K. (2012). High-resolution precipitation and temperature downscaling for glacier models. *Climate Dynamics*, *38*(1-2), 391-409.

Krebs-Kanzow, U., Gierz, P., & Lohmann, G. (2018). Estimating Greenland surface melt is hampered by melt induced dampening of temperature variability. *Journal of Glaciology*, *64*(244), 227-235.

Langen, P. L., Fausto, R. S., Vandecrux, B., Mottram, R. H., & Box, J. E. (2017). Liquid water flow and retention on the Greenland ice sheet in the regional climate model HIRHAM5: Local and large-scale impacts. *Frontiers in Earth Science*, *4*, 110.

Li, C., Battisti, D. S., Schrag, D. P., & Tziperman, E. (2005). Abrupt climate shifts in Greenland due to displacements of the sea ice edge. *Geophysical Research Letters*, *32*(19).

Lochte, A. A., Repschläger, J., Kienast, M., Garbe-Schönberg, D., Andersen, N., Hamann, C., & Schneider, R. (2019). Labrador Sea freshening at 8.5 ka BP caused by Hudson Bay Ice Saddle collapse. *Nature communications*, *10*(1), 1-9.

Machguth, H., Rastner, P., Bolch, T., Mölg, N., Sørensen, L. S., Aðalgeirsdottir, G., van Angelen., J.H., van den Broeke, M.R., & Fettweis, X. (2013). The future sea-level rise contribution of Greenland's glaciers and ice caps. *Environmental Research Letters*, *8*(2), 025005.

Noël, B. et al., 2015. Evaluation of the updated regional climate model RACMO2.3: summer snowfall impact on the Greenland Ice Sheet. *The Cryosphere*, **9**, 1831-1844, doi:10.5194/tc-9-1831-2015.

Noël, B., van de Berg, W. J., Van Wessem, J. M., van Meijgaard, E., Van As, D., Lenaerts, J., Lhemitte, S., Munneke, P.K, Smeets, P.C.J.P., van Ulft, L., Van De Wal, R. S., VanDen Broeke, M.R. (2018). Modelling the climate and surface mass balance of polar ice sheets using RACMO2-Part 1: Greenland (1958-2016). *Cryosphere*, *12*(3), 811-831.

Noël, B., van de Berg, W. J., Lhermitte, S., & van den Broeke, M. R. (2019). Rapid ablation zone expansion amplifies north Greenland mass loss. *Science advances*, *5*(9), eaaw0123.

Oerlemans, J. (2010). *The microclimate of valley glaciers* (pp. 1-138). Igitur, Utrecht Publishing & Archiving Services.

Pfeffer, W. T., Arendt, A. A., Bliss, A., Bolch, T., Cogley, J. G., Gardner, A. S., Hagen, J.O., Hock, R., Kaser, G., Kienholz, C., Miles, E. S., Moholdt, G., Molg, N., Paul, F., Radic, V., Rastner, P., Raup, B. H., Rich, J., Sharp., M. J., & The Randolph Consortium (2014). The Randolph Glacier Inventory: a globally complete inventory of glaciers. *Journal of Glaciology*, *60*(221), 537-552.

Praskievicz, S., (2018) Downscaling climate-model output in mountainous terrain using local topographic lapse rates for hydrologic modeling of climate-change impacts, Physical Geography, 39:2, 99-117, DOI: 10.1080/02723646.2017.1378555

Raju, K. S., & Kumar, D. N. (2018). Downscaling techniques in climate modeling. In *Impact of Climate Change on Water Resources* (pp. 77-105). Springer, Singapore.

Rasmussen LA and Conway H (2001) Estimating South Cascade Glacier (Washington, U.S.A.) mass balance from a distant radiosonde and comparison with Blue Glacier. J Glaciol 47:579–588

Reeh, N. (1991). Parameterization of melt rate and surface temperature in the Greenland ice sheet. *Polarforschung*, *59*(3), 113-128.

Rinke, A., Kuhry, P., & Dethloff, K. (2008). Importance of a soil organic layer for Arctic climate: A sensitivity study with an Arctic RCM. *Geophysical Research Letters*, *35*(13).

Roeckner, E., Bäuml, G., Bonaventura, L., Brokopf, R., Esch, M., Giorgetta, M., Hagemann, S., Kirchner, I., Kornblueh, L., Manzini, E., Rhodin, A., Schlese, U., Schulzweida, U., & Tompkins, A. (2003). The atmospheric general circulation model ECHAM 5. PART I: Model description. Max-Planck-Institut fur Meteorologie, Hamburg, Germany.

Rogerson, P.A. (2006). *Statistical Methods for Geography: A Student's Guide. Second Edition.* Sage Publications, London.

Rogozhina, I., Rau, D. (2014): Vital role of daily temperature variability in surface mass bala nce parameterizations of the Greenland Ice Sheet. - The Cryosphere, 8, 2, 575-585

Sejr, M. K., Stedmon, C. A., Bendtsen, J., Abermann, J., Juul-Pedersen, T., Mortensen, J., & Rysgaard, S. (2017). Evidence of local and regional freshening of Northeast Greenland coastal waters. *Scientific reports*, *7*(1), 1-6.

Shea JM, Moore RD and Stahl K (2009) Derivation of melt factors from glacier mass-balance records in western Canada. J. Glaciol., 55(189), 123–130.

Steffen, K., J. E. Box, and W. Abdalati, 1996 "Greenland Climate Network: GC-Net", in Colbeck, S. C. Ed. CRREL 96-27 Special Report on Glaciers, Ice Sheets and Volcanoes, trib. to M. Meier, pp. 98-103.

Steffen, K., & Box, J. (2001). Surface climatology of the Greenland ice sheet: Greenland Climate Network 1995–1999. *Journal of Geophysical Research: Atmospheres*, *106*(D24), 33951-33964.

Stendel, M., Christensen, J. H., & Petersen, D. (2008). Arctic climate and climate change with a focus on Greenland. *Advances in Ecological Research*, *40*, 13-43.

Søndergaard, J., Tamstorf, M., Elberling, B., Larsen, M. M., Mylius, M. R., Lund, M., Abermann, J., & Rigét, F. (2015). Mercury exports from a High-Arctic river basin in Northeast Greenland (74 N) largely controlled by glacial lake outburst floods. *Science of the Total Environment*, *514*, 83-91.

Taurisano A, Bøggild CE, Karlsen HG and Boggild CE (2004) A century of climate variability and climate gradients from coast to Ice sheet in West Greenland. Geogr. Ann. Ser. A Phys. Geogr., 86(2), 217–224

van Angelen et al., 2013. Rapid loss of firn pore space accelerates 21st century Greenland mass loss. *Geophys. Res. Lett.*, **40**,

van Angelen, J. H., Van den Broeke, M. R., Wouters, B., & Lenaerts, J. T. M. (2014). Contemporary (1960–2012) evolution of the climate and surface mass balance of the Greenland ice sheet. *Surveys in geophysics*, *35*(5), 1155-1174.

van As, D., Fausto, R. S., Ahlstrøm, A. P., Andersen, S. B., Andersen, M. L., Citterio, M., Edelvang, K., Gravesen, P., Machguth, H., Faezeh, M., Nielsen, S., & Weidick, A. (2011). Programme for Monitoring of the Greenland Ice Sheet (PROMICE): first temperature and ablation records. *Geological Survey of Denmark and Greenland Bulletin*, *23*, 73-76.

Vandecrux, B., Fausto, R. S., Langen, P. L., Van As, D., MacFerrin, M., Colgan, W. T., Ingeman-Nielsen, T., Steffen, K., Jensen, N.S., Møller, M.T., & Box, J. E. (2018). Drivers of firn density on the Greenland ice sheet revealed by weather station observations and modeling. *Journal of Geophysical Research: Earth Surface*, *123*(10), 2563-2576.

Vernon, C. L., Bamber, J. L., Box, J. E., Van den Broeke, M. R., Fettweis, X., Hanna, E., & Huybrechts, P. (2013). Surface mass balance model intercomparison for the Greenland ice sheet. *The Cryosphere*, *7*, 599-614.

Wake, L. M., & Marshall, S. J. (2015). Assessment of current methods of positive degree-day calculation using in situ observations from glaciated regions. *Journal of Glaciology*, *61*(226), 329-344.

Zhang, Y., Seidel, D. J., Golaz, J. C., Deser, C., & Tomas, R. A. (2011). Climatological characteristics of Arctic and Antarctic surface-based inversions. *Journal of Climate*, *24*(19), 5167-5186.

Appendices

Appendix 1: Remainder of the Model Intercomparison Graphs with the Station Names Indicated in the Title.

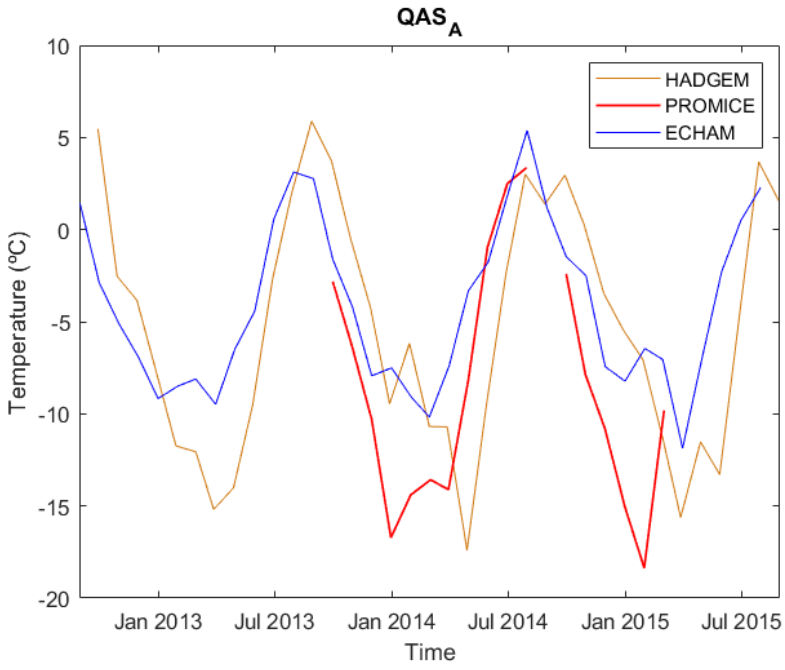

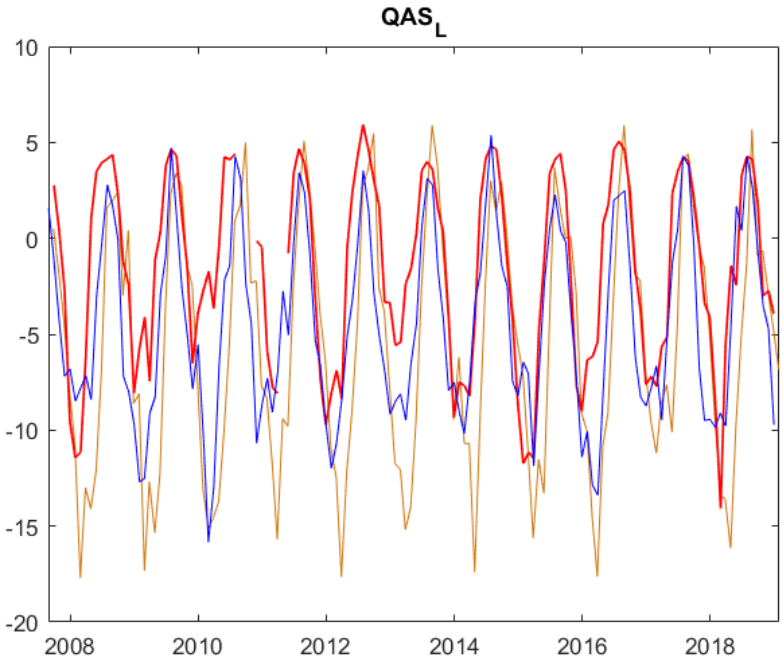

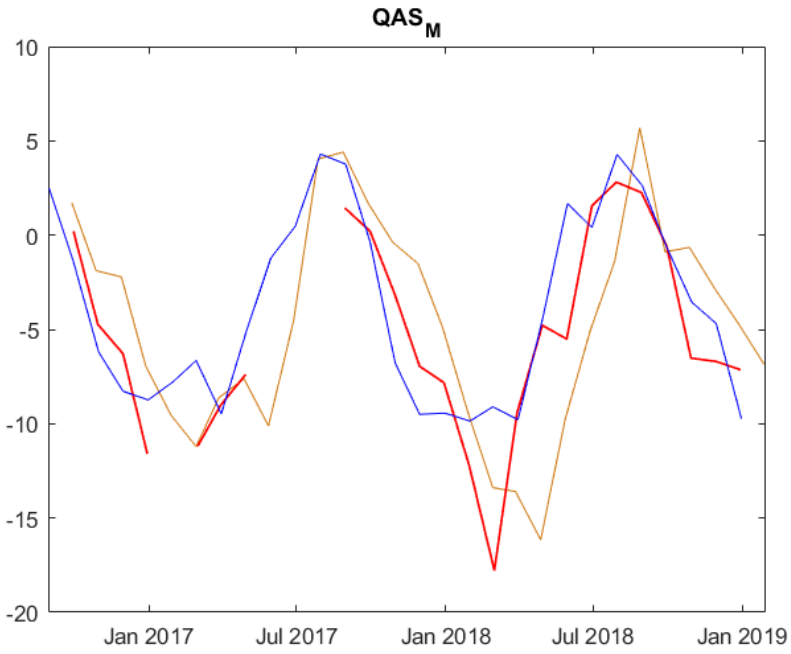
QAS_M
10
5
0
-5
-10
-15
-20
Jan 2017
Jul 2017
Jan 2018
Jul 2018
Jan 2019

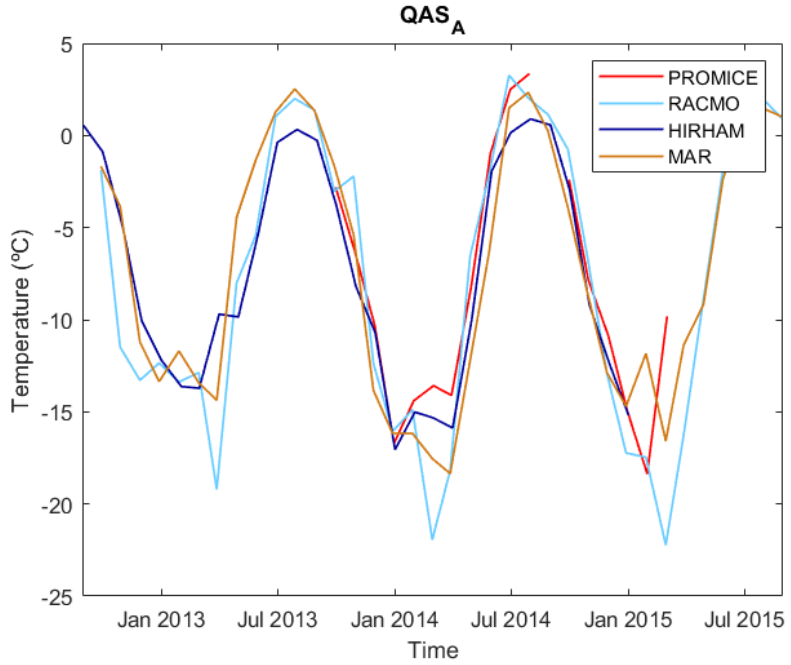
QAS_A
PROMICE
RACMO
HIRHAM
MAR
Temperature (°C)
5
0
-5
-10
-15
-20
-25
Jan 2013
Jul 2013
Jan 2014
Jul 2014
Jan 2015
Jul 2015
Time

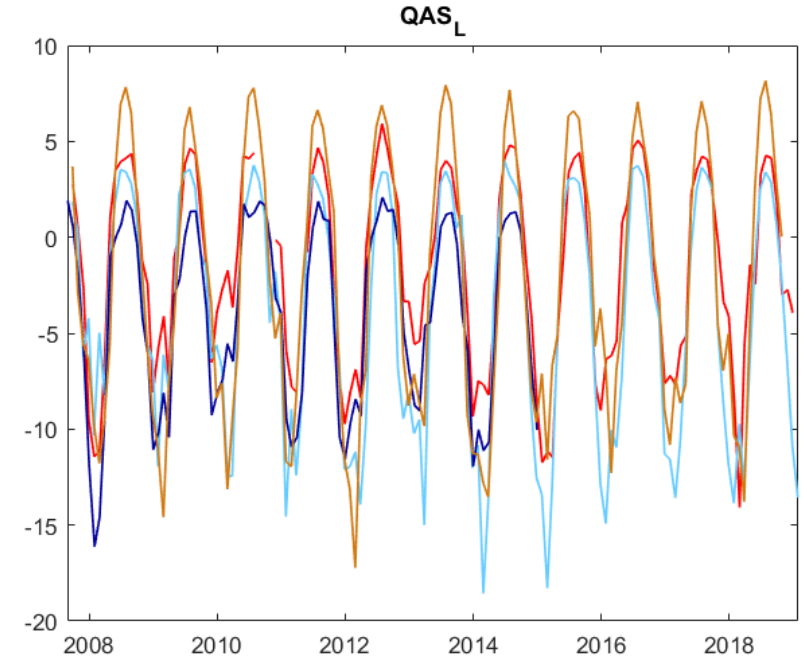
QAS L
10
5
0
-5
-10
-15
-20
2008
2010
2012
2014
2016
2018

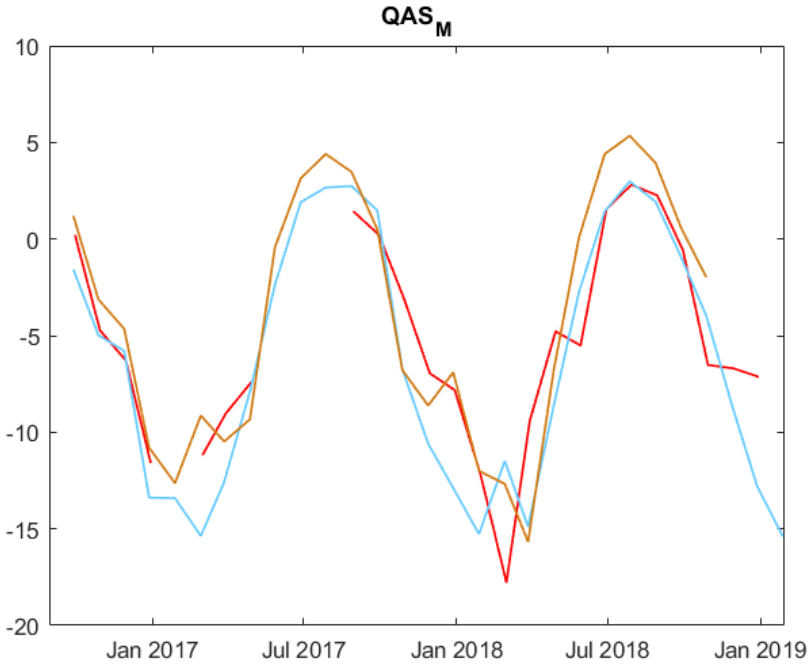
QAS M
10
5
0
-5
-10
-15
-20
Jan 2017
Jul 2017
Jan 2018
Jul 2018
Jan 2019

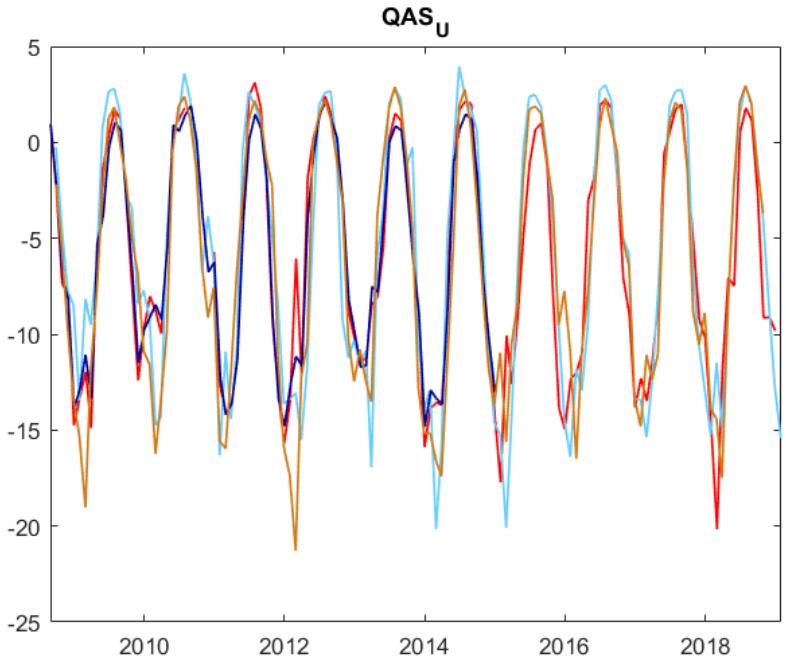
QAS_U
5
0
-5
-10
-15
-20
-25
2010
2012
2014
2016
2018

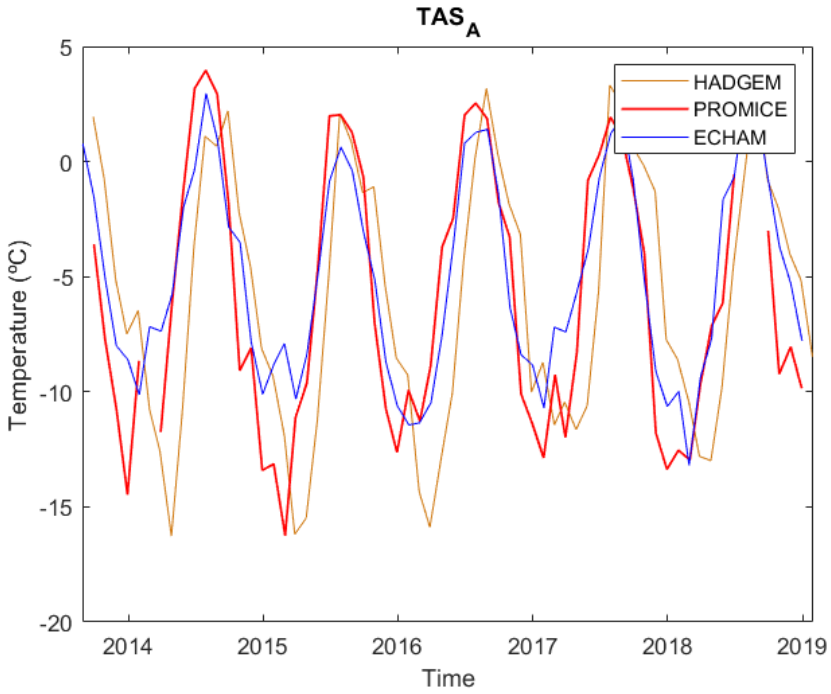
TAS A
HADGEM
PROMICE
ECHAM
Temperature (°C)
5
0
-5
-10
-15
-20
2014
2015
2016
2017
2018
2019
Time

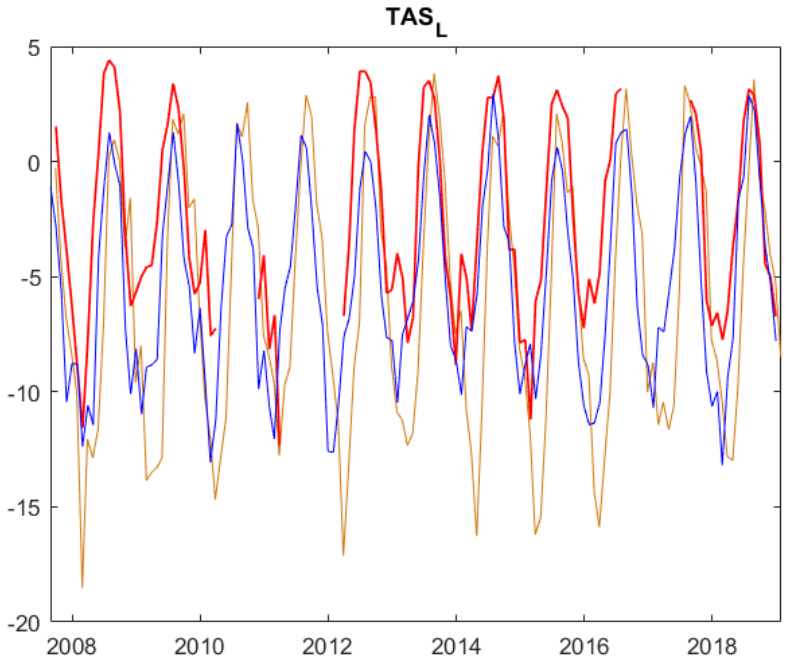
TAS L
5
0
-5
-10
-15
-20
2008
2010
2012
2014
2016
2018

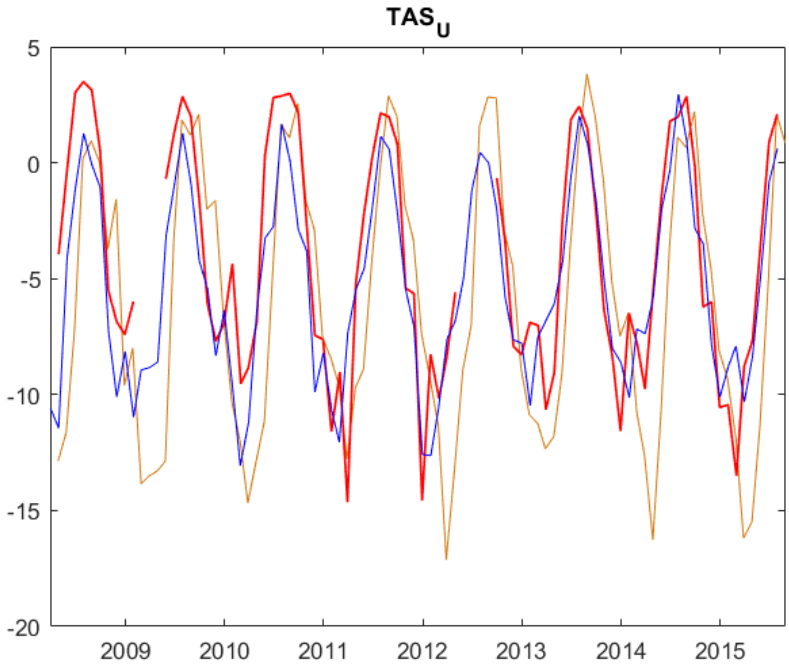
TAS_U
5
0
-5
-10
-15
-20
2009
2010
2011
2012
2013
2014
2015

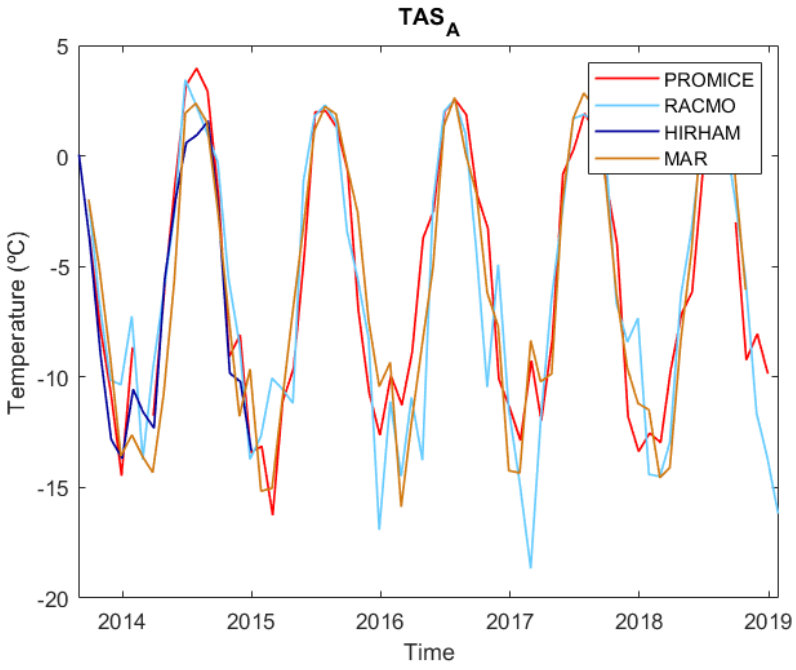
TAS_A
PROMICE
RACMO
HIRHAM
MAR
Temperature (°C)
5
0
-5
-10
-15
-20
2014
2015
2016
2017
2018
2019
Time

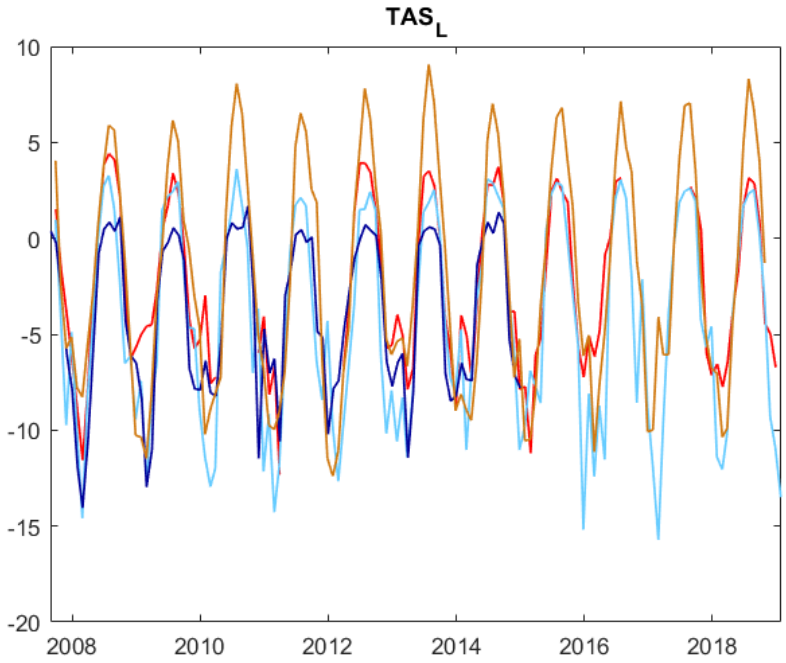
TAS_L
10
5
0
-5
-10
-15
-20
2008
2010
2012
2014
2016
2018

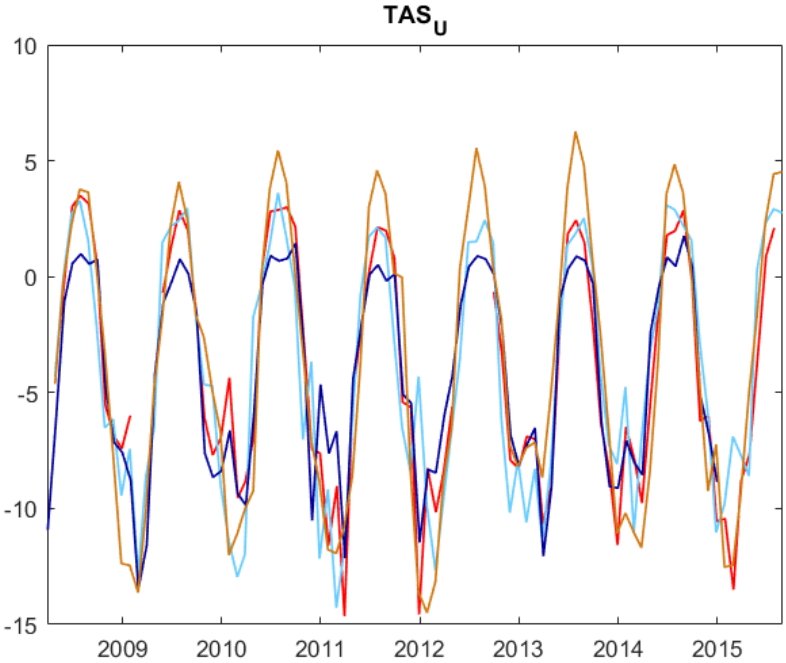
TAS_U
10
5
0
-5
-10
-15
2009
2010
2011
2012
2013
2014
2015

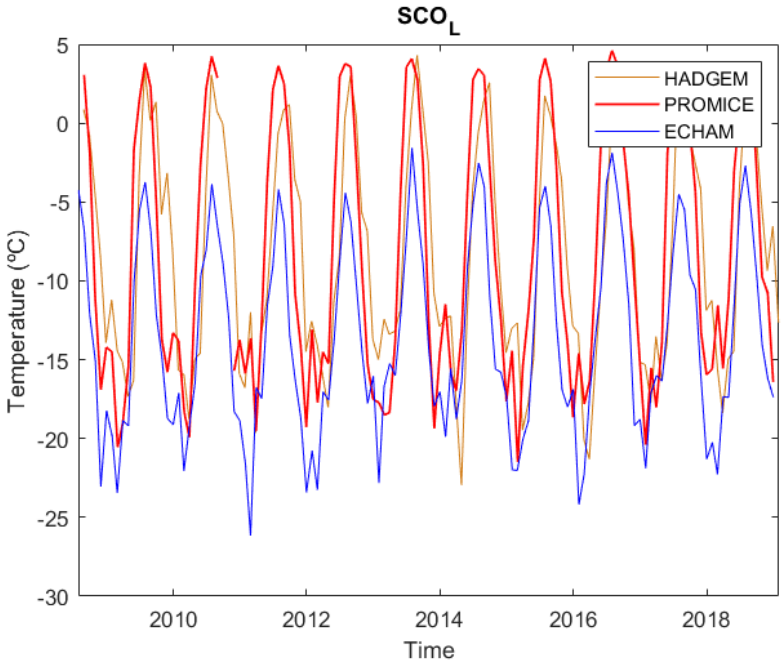
SCO_L
HADGEM
PROMICE
ECHAM
Temperature (ºC)
5
0
-5
-10
-15
-20
-25
-30
2010
2012
2014
2016
2018
Time

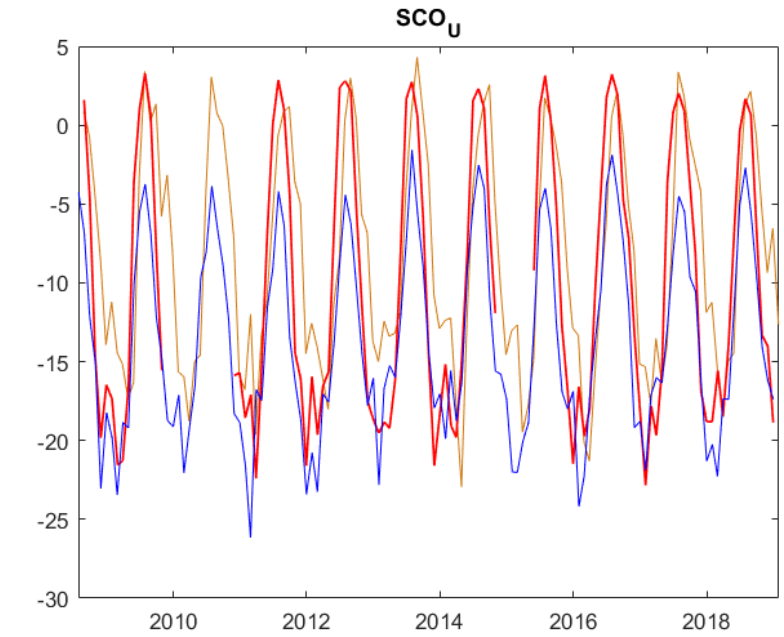
SCO_U
5
0
-5
-10
-15
-20
-25
-30
2010
2012
2014
2016
2018

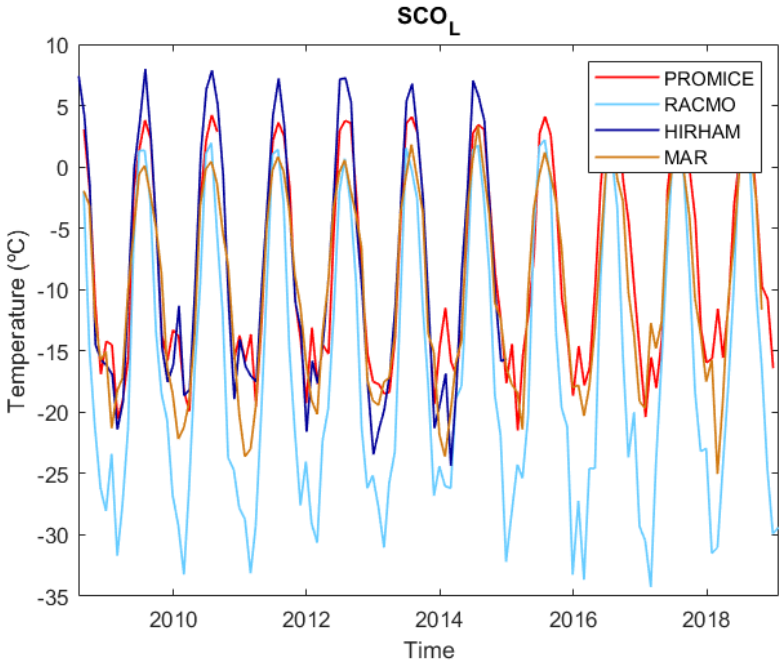
SCO_L
PROMICE
RACMO
HIRHAM
MAR
Temperature (ºC)
Time
10
5
0
-5
-10
-15
-20
-25
-30
-35
2010
2012
2014
2016
2018

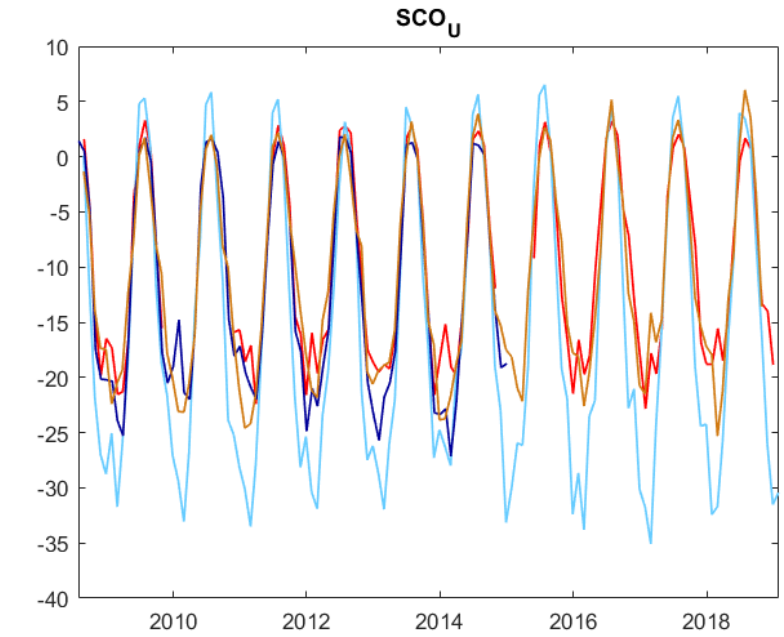
SCO_U
10
5
0
-5
-10
-15
-20
-25
-30
-35
-40
2010
2012
2014
2016
2018

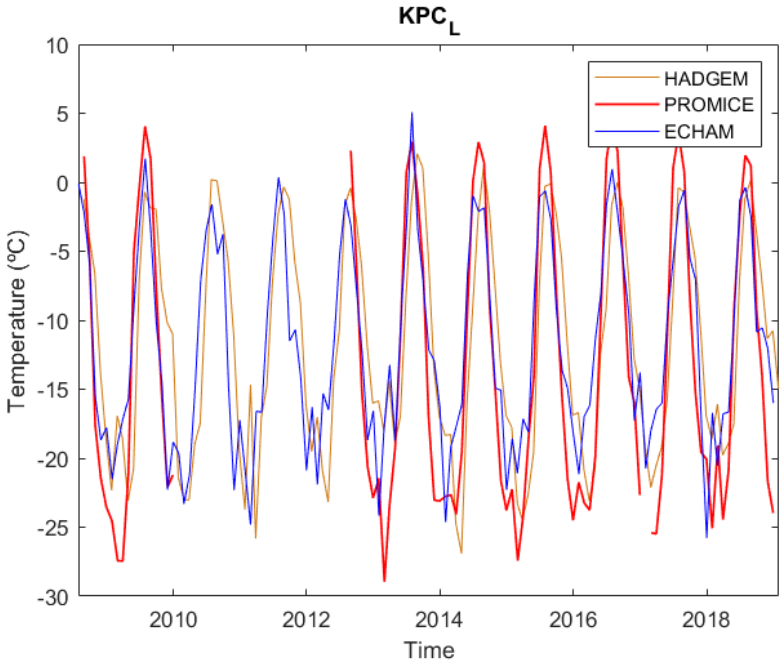
KPC_L
HADGEM
PROMICE
ECHAM
Temperature (ºC)
Time
10
5
0
-5
-10
-15
-20
-25
-30
2010
2012
2014
2016
2018

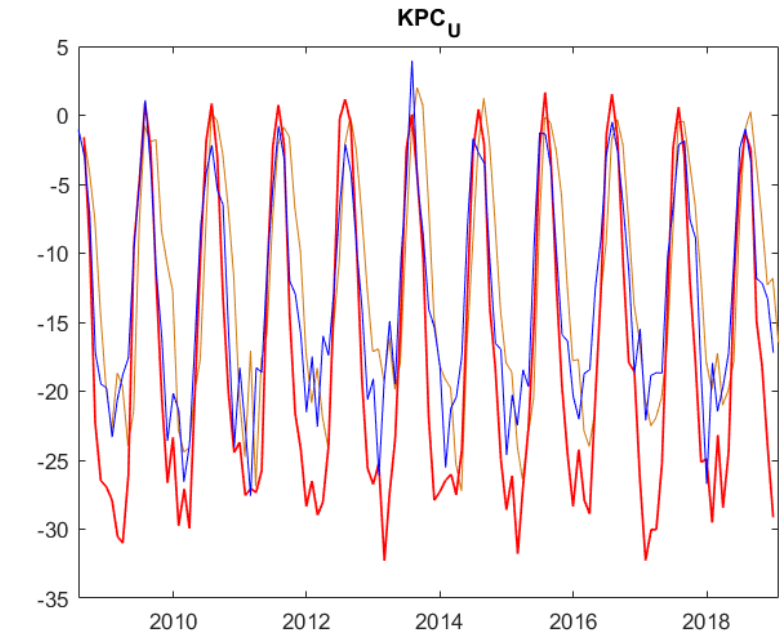
KPC_U
5
0
-5
-10
-15
-20
-25
-30
-35
2010
2012
2014
2016
2018

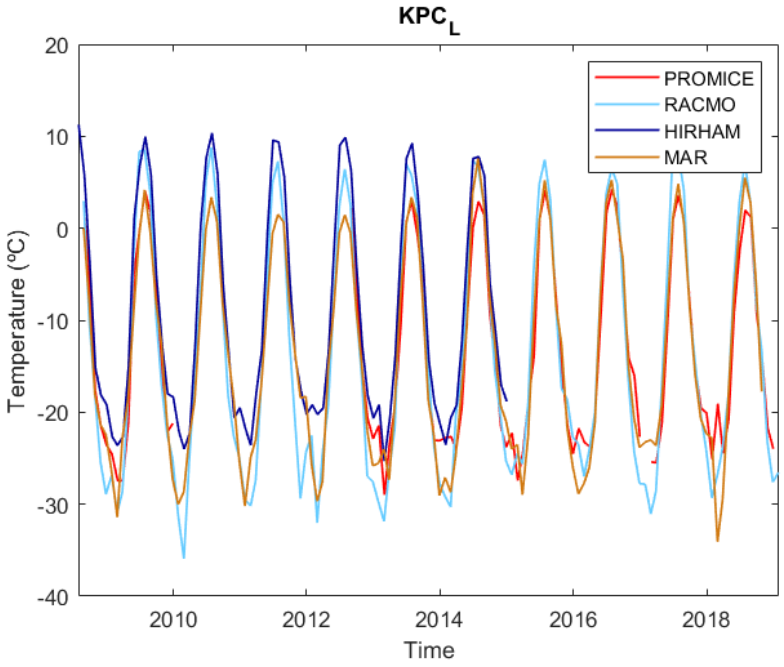
KPC_L
PROMICE
RACMO
HIRHAM
MAR
Temperature (°C)
Time
20
10
0
-10
-20
-30
-40
2010
2012
2014
2016
2018

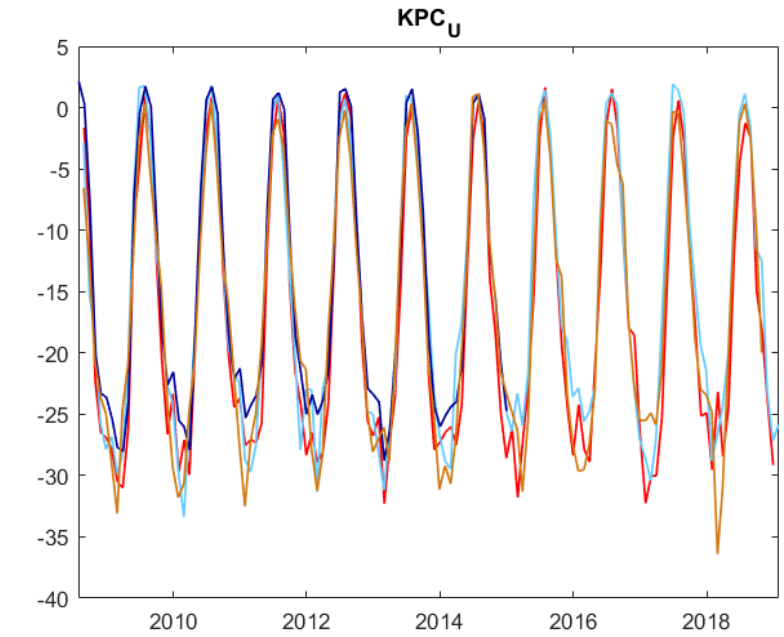
KPC_U
5
0
-5
-10
-15
-20
-25
-30
-35
-40
2010
2012
2014
2016
2018

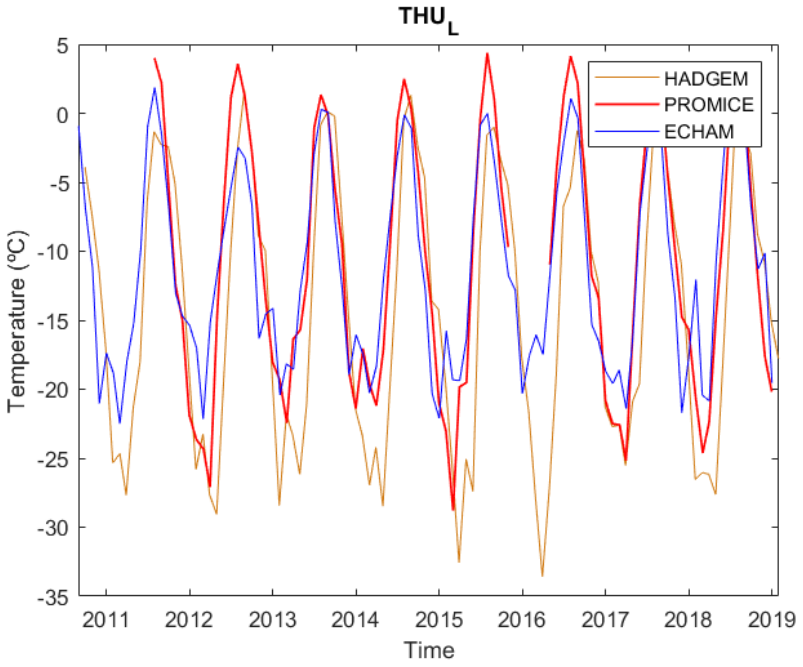
THU L
HADGEM
PROMICE
ECHAM
Temperature (ºC)
5
0
-5
-10
-15
-20
-25
-30
-35
2011
2012
2013
2014
2015
2016
2017
2018
2019
Time

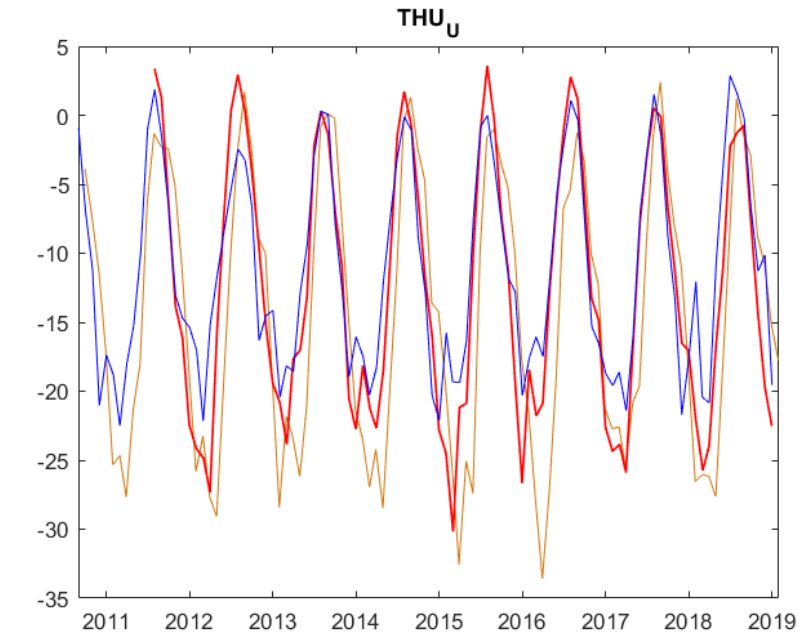
THU U
5
0
-5
-10
-15
-20
-25
-30
-35
2011
2012
2013
2014
2015
2016
2017
2018
2019

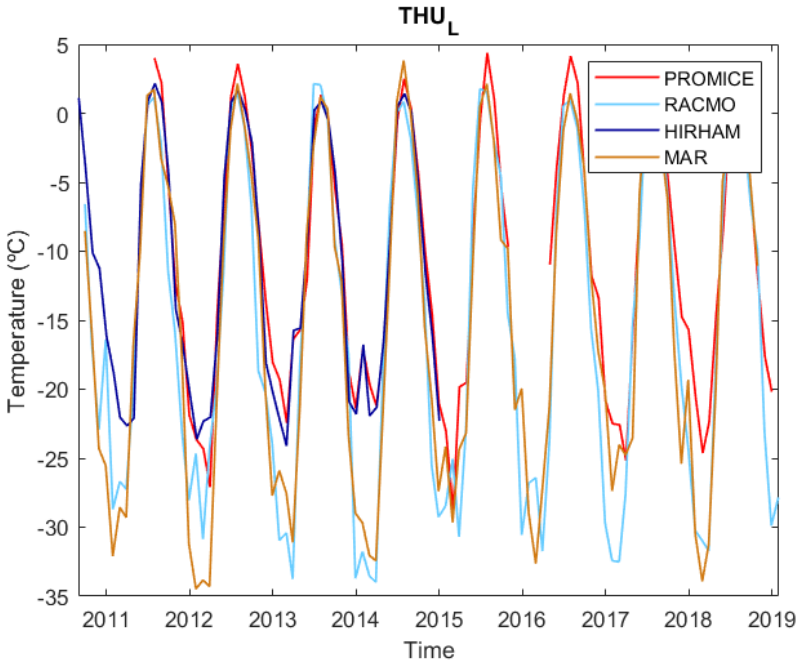
THU L
PROMICE
RACMO
HIRHAM
MAR
Temperature (°C)
5
0
-5
-10
-15
-20
-25
-30
-35
2011
2012
2013
2014
2015
2016
2017
2018
2019
Time

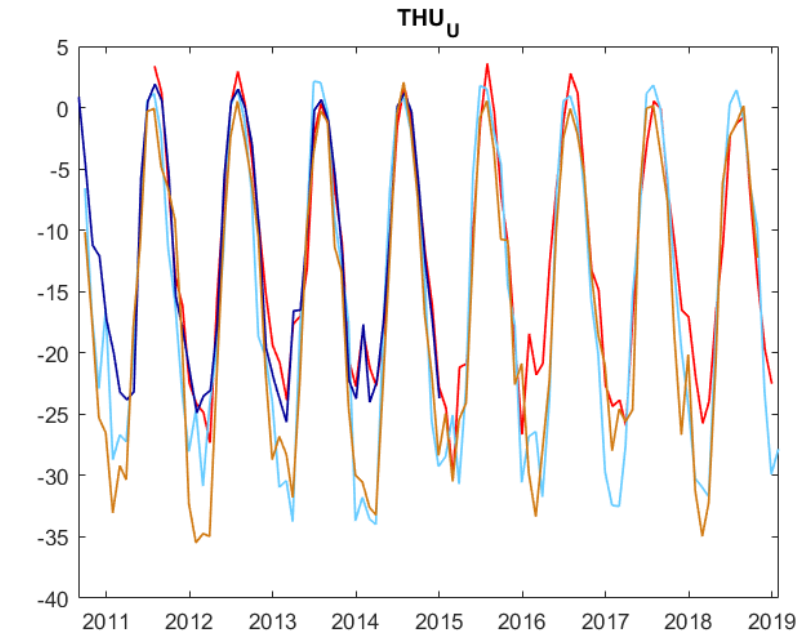
THU U
5
0
-5
-10
-15
-20
-25
-30
-35
-40
2011
2012
2013
2014
2015
2016
2017
2018
2019

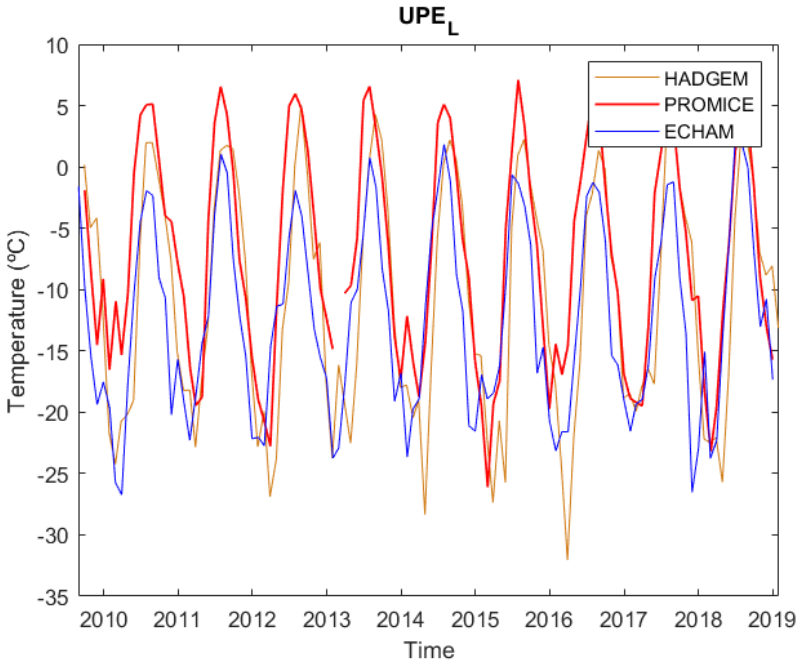
UPE_L
HADGEM
PROMICE
ECHAM
Temperature (ºC)
Time
10
5
0
-5
-10
-15
-20
-25
-30
-35
2010
2011
2012
2013
2014
2015
2016
2017
2018
2019

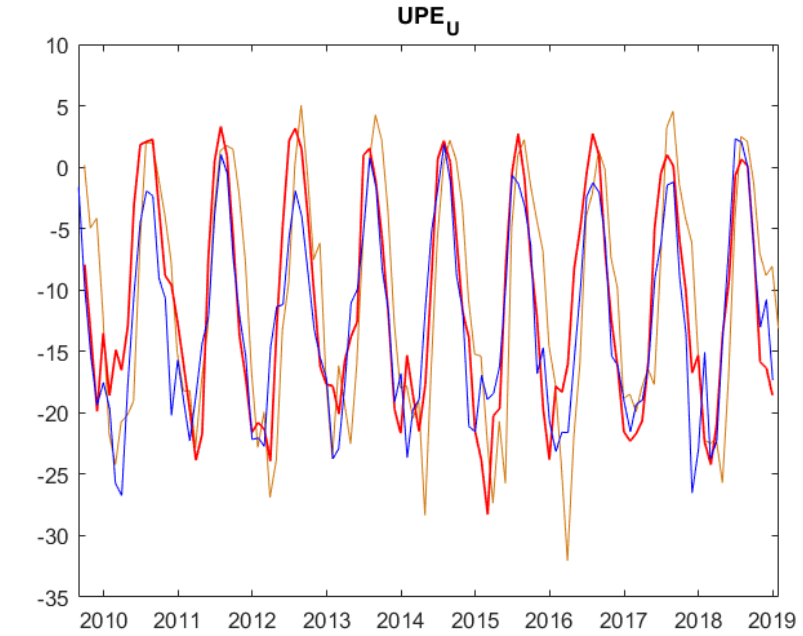
UPE_U
10
5
0
-5
-10
-15
-20
-25
-30
-35
2010
2011
2012
2013
2014
2015
2016
2017
2018
2019

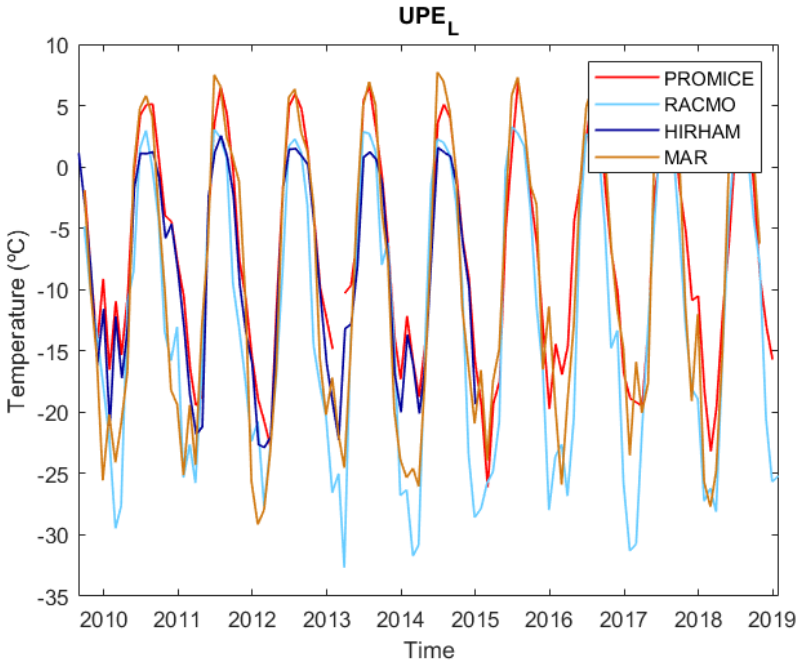
UPE_L
PROMICE
RACMO
HIRHAM
MAR
Temperature (ºC)
Time
10
5
0
-5
-10
-15
-20
-25
-30
-35
2010
2011
2012
2013
2014
2015
2016
2017
2018
2019

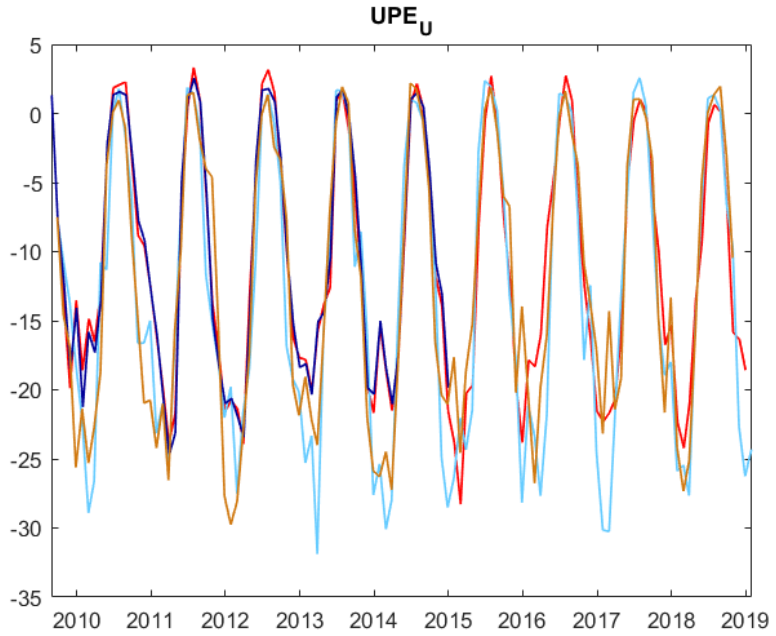
UPE_U
5
0
-5
-10
-15
-20
-25
-30
-35
2010
2011
2012
2013
2014
2015
2016
2017
2018
2019

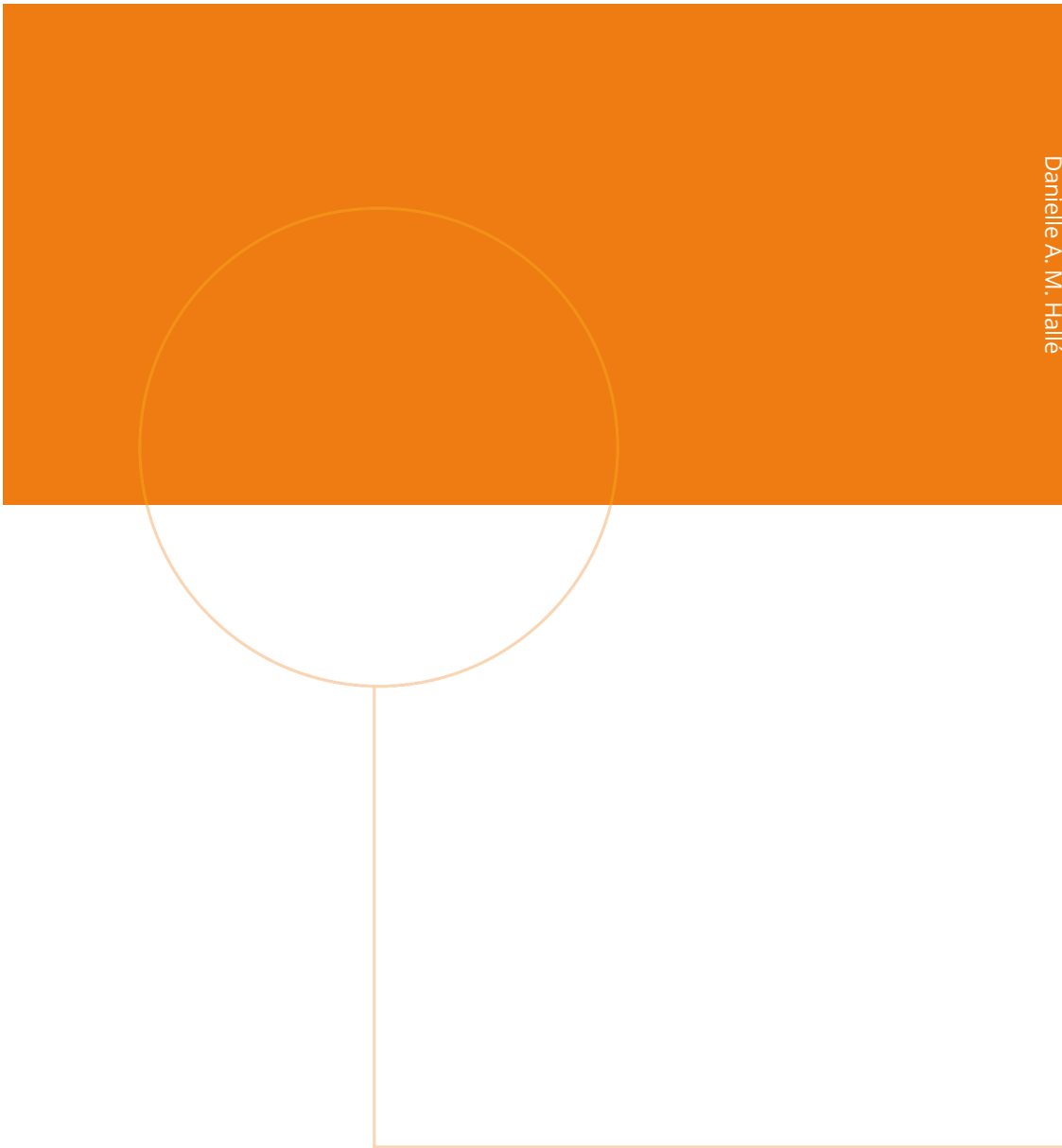

Danielle A. M. Hallé

NTNU
Norwegian University of
Science and Technology